UNIVERSITY
INSTITUTE
OF LISBON

ROADM architectures for future high-capacity MB over SDM optical networks

Catarina da Silva Costa Vieira Jara

Master in Telecommunications and Computer Engineering

Supervisor:
PhD Luís Gonçalo Lecoq Vences e Costa Cancela, Associate Professor,
Iscte – Instituto Universitário de Lisboa

Supervisor:
PhD João Lopes Rebola, Associate Professor,
Iscte – Instituto Universitário de Lisboa

June, 2026

[This page is intentionally left blank.]

TECHNOLOGY
AND ARCHITECTURE

Department of Information Science and Technology

ROADM architectures for future high-capacity MB over SDM optical networks

Catarina da Silva Costa Vieira Jara

Master in Telecommunications and Computer Engineering

Supervisor:
PhD Luís Gonçalo Lecoq Vences e Costa Cancela, Associate Professor,
Iscte – Instituto Universitário de Lisboa

Supervisor:
PhD João Lopes Rebola, Associate Professor,
Iscte – Instituto Universitário de Lisboa

June, 2026

[This page is intentionally left blank.]

Family, Friends and Myself

[This page is intentionally left blank.]

Acknowledgment

As I conclude this dissertation, I would like to express my sincere gratitude to all those who supported me throughout this journey. Firstly, I would like to thank Instituto de telecomunicações (IT) and Iscte - Instituto Universitário de Lisboa for these remarkable years filled with unforgettable memories that now come to an end. Secondly, I would like to express my gratitude to my supervisors Luís Cancela and João Rebola for their huge support, guidance and patience throughout all of these months.

I would also like to thank my friends and family, particularly my mum, dad and sister Joana for their help, motivation and unconditional support always, but mainly in the most challenging moments.

Lastly, I want to especially thank my ETI friends Mariana Marques, Gonçalo Cavalheiro, Gonçalo Carrasco, Gonçalo Cardoso, Guilherme Aleixo, Manuel Inácio, Bernardo Assunção and Afonso Miguel. Without them these years would not have been the same.

[This page is intentionally left blank.]

Resumo

Prevê-se que o aumento de novos serviços baseados na inteligência artificial contribua de forma decisiva para uma falta de capacidade de transporte na actual rede ótica. As tecnologias de multiplexagem por divisão espacial (SDM) e multi-banda (MB) têm sido estudadas como possíveis soluções para aumentar a capacidade da rede. Esta dissertação analisa a granularidade, o custo por bit e o consumo de potência por bit de várias arquiteturas de nós para redes óticas baseadas nas tecnologias SDM e MB - normalmente referidas como MBoSDM.

Analisaram-se duas arquiteturas MB — MB *Baseline* e MB *Common band*, duas arquiteturas SDM — SDM *Space* e SDM *Space-wavelength*, e três arquiteturas MBoSDM — *Baseline*, MBoSDM com um único comutador de cruzamento espacial e MBoSDM FLEX-SCALE — para dois cenários de largura de banda por direção de nó: 16 e 32 THz. A FLEX-SCALE tem a capacidade de adicionar e retirar bandas de canais, em vez de canais óticos individuais, como acontece tipicamente nas estruturas convencionais de inserção/extracção (A/D), o que será uma característica importante nas futuras redes de núcleo.

De todas as arquiteturas, a FLEX-SCALE é a que apresenta o menor custo por bit (80% a 94% mais barata), uma vez que utiliza transcetores de banda na sua estrutura de A/D, ao contrário das outras, que utilizam apenas transcetores de canal. Relativamente ao consumo de potência por bit, a FLEX-SCALE apresenta um consumo de potência semelhante ao das outras arquiteturas. Estas conclusões mantêm-se inalteradas à medida que o grau da arquitetura ou a capacidade dos nós aumentam.

Palavras Chave: arquiteturas do nó óptico, consumo de potência por bit, custo por bit, multiplexagem por divisão espacial, multi-banda, redes óticas

[This page is intentionally left blank.]

Abstract

An optical network capacity crunch is foreseen as new and more demanding services based on artificial intelligence are appearing. Spatial division multiplexing (SDM) and multi-band (MB) technologies have been investigated as potential solutions for this capacity crunch. This dissertation studies the granularity, the cost per bit and the power consumption per bit of several node architectures for optical networks based on both SDM and MB technologies - usually called MB over SDM (MBoSDM).

We analyzed two MB architectures - MB Baseline and MB Common Band, two SDM architectures - SDM Space and SDM Space-wavelength, and three MBoSDM architectures - Baseline, MBoSDM with a single spatial optical cross-connect and MBoSDM FLEX-SCALE – for two scenarios: 16 THz and 32 THz bandwidth per node direction. The FLEX-SCALE architecture has the capability of adding and dropping bands of channels, instead of individual channels as is performed in conventional add/drop (A/D) structures, which will be an important feature in future core networks.

Of all architectures, the FLEX-SCALE architecture is the one with the lowest cost per bit (80% to 94% less expensive), as it uses band transceivers in its A/D structure, unlike the others that use only wavelength channel transceivers. Regarding power consumption per bit, the FLEX-SCALE has a similar power consumption in comparison with the other architectures. Moreover, these conclusions are unaffected as the node degree or the node capacity increases.

Keywords: Cost per bit, multi-band, optical networks, optical node architectures, power consumption per bit, spatial-division multiplexing

[This page is intentionally left blank.]

Contents

Acknowledgment iii

Resumo v

Abstract vii

List of Figures xi

List of Tables xv

List of Acronyms xvii

Chapter 1. Introduction 1
1.1. Motivation 1
1.2. Goals 3
1.3. Dissertation organization 3
1.4. Main contributions 3

Chapter 2. Literature review on node architectures for MB and SDM networks 5
2.1. Introduction 5
2.2. ROADMs fundamental concepts 5
2.3. MB node architectures 9
2.3.1. Baseline architecture 10
2.3.2. Architecture with AO-WCs 11
2.3.3. Common band architecture 12
2.3.4. Compact architecture 13
2.3.5. SOA-based architecture 14
2.3.6. MB node architecture comparison 15
2.4. SDM node architectures 15
2.4.1. Space granularity architecture 17
2.4.2. Space-wavelength granularity architecture 20
2.4.3. Wavelength granularity architecture 22
2.4.4. Fractional space-full wavelength granularity architecture 25
2.4.5. SDM node architecture comparison 26
2.5. Comparison between MB and SDM node architectures 27
2.6. Conclusions 31

Chapter 3. Node architectures for MBoSDM networks 33
3.1. Introduction 33
3.2. Switching granularity 33
3.3. MBoSDM node architectures 34
3.3.1. Baseline architecture for MBoSDM 34
3.3.2. MBoSDM architecture with one S-OXC per band 35
3.3.3. MBoSDM architecture with a single S-OXC 35
3.3.4. MBoSDM architecture without a S-OXC 36
3.3.5. FLEX-SCALE architecture 37
3.4. MBoSDM node architectures comparison 39
3.5. Conclusions 52

Chapter 4. Cost and power consumption comparison of MB, SDM and MBoSDM node architectures 55
4.1. Introduction 55
4.2. Cost analysis 55
4.2.1. Scenario 1: 16 THz per node direction 55
4.2.2. Scenario 2: 32 THz per node direction 63
4.3. Power consumption analysis 67
4.3.1. Scenario 1: 16 THz per node direction 67
4.3.2. Scenario 2: 32 THz per node direction 69
4.4. Conclusions 71

Chapter 5. Conclusions and future work 73
5.1. Final conclusions 73
5.2. Future work 74

References 77

Appendix A. Validation of the parameters used in the FLEX-SCALE architecture 83

Appendix B. Validation of the network throughput computation for the FLEX-SCALE architecture 85

Appendix C. Implementation details of large-scale WSSs for MBoSDM architectures 87

List of Figures

Figure 2.1 Generic D-degree ROADM structure. 6

Figure 2.2 Drop structure with CD capability. 6

Figure 2.3 Three possible implementations of CDC A/D structures. 7

Figure 2.4 Internal structure of a $D \times N$ WSS. 7

Figure 2.5 Spectrum of the C-, L- and S-bands and corresponding ITU-T grid frequencies. 9

Figure 2.6 Switching strategies for MB switching. 10

Figure 2.7 Baseline D-degree R&S MB ROADM architecture. 11

Figure 2.8 D-Degree R&S MB ROADM architecture with AO-WCs. 12

Figure 2.9 D-degree R&S MB ROADM common band architecture. 13

Figure 2.10 D-degree MB ROADM compact architecture. 13

Figure 2.11 D-degree MB SOA-based architecture. 14

Figure 2.12 Switching strategies for SDM switching. 17

Figure 2.13 Spatial granularity architecture without lane changes with three directions (D=3) and four spatial channels (M=4). 19

Figure 2.14 Spatial granularity architecture with lane changes with three directions (D=3) and four spatial channels (M=4). 19

Figure 2.15 Spatial wavelength granularity R&S architecture without lane changes with three directions (D=3) and four spatial channels (M=4). 21

Figure 2.16 Spatial wavelength granularity R&S architecture with lane changes with three directions (D=3) and four spatial channels (M=4). 22

Figure 2.17 Example of a 1×2 conventional WSS and JS WSS. 23

Figure 2.18 Wavelength granularity architecture with three directions (D=3) and four spatial channels (M=4). 24

Figure 2.19 Fractional space-full wavelength granularity architecture without lane changes with three directions (D=3) and four spatial channels (M=4). 26

Figure 2.20 Drop structure considered for the SDM architectures. 28

Figure 2.21 Drop structure considered for the MB architectures. 29

Figure 3.1 Space switching strategy in MBoSDM networks. 33

Figure 3.2 Baseline architecture for MBoSDM [14]. 34

Figure 3.3 MBoSDM architecture with S-OXC per band. 35
Figure 3.4 MBoSDM architecture with a single S-OXC. 36
Figure 3.5 MBoSDM architecture without a S-OXC. 36
Figure 3.6 FLEX-SCALE architecture considering a ROADM node with D directions, a 4 core MCF fiber per direction and 3 bands per core (C+L+S). 38
Figure 3.7 Number of components (WSSs and OAs) as a function of N_C for several network dimensions. 39
Figure 3.8 Drop structure considered for MBoSDM Baseline architecture. 43
Figure 3.9 Example of large dimension WSSs built with smaller ones for the drop structure. 43
Figure 3.10 Drop structure considered for the MBoSDM architectures in Figures 3.3 to 3.5 considering $N_C = 6$. 44
Figure 3.11 Example of implementation of a 12×12 WXC. 46
Figure 3.12 Express structure cost for all studied MBoSDM architectures with D=3, D=5 and D=7, considering M=4. 49
Figure 3.13 A/D structure cost for all studied MBoSDM architectures with D=3, D=5 and D=7, considering M=4. 49
Figure 3.14 Power consumption for all studied MBoSDM architectures with D=3, D=5 and D=7, considering M=4. 50
Figure 3.15 Node throughput for the FLEX-SCALE architecture as a function of D, considering M=2, 4 and 8. 51
Figure 3.16 A/D capacity for the Layer 2 of the FLEX-SCALE architecture as a function of D, considering M=2, 4 and 8. 51
Figure 3.17 A/D capacity of Layer 3 a) FLEX-SCALE architecture and of b) the other MBoSDM architectures as a function of D, considering M=2, 4 and 8. 52
Figure 4.1 MBoSDM Baseline architecture with 3 directions considering a 2 core MCF with C+L bands per direction. 56
Figure 4.2 MBoSDM architecture with a single S-OXC with 3 directions considering a 2 core MCF with C+L bands per direction. 56
Figure 4.3 FLEX-SCALE architecture with 3 directions considering a 2 core MCF with C+L bands per direction. 57
Figure 4.4 Drop structure considered for the MBoSDM Baseline architectures with D=3 and M=2. 59
Figure 4.5 Drop structure considered for the MBoSDM architecture shown in Figure 4.2 considering D=3, M=2 and $N_C = 3$. 59

Figure 4.6 Express structure cost for SDM architectures with M=4, MB architectures with B=3 and MBoSDM architectures with M=2 and B=2 considering D=3, 5 and 7 for the 16 THz scenario. 61

Figure 4.7 A/D structure cost for SDM architectures with M=4, MB architectures with B=3 and MBoSDM architectures with M=2 and B=2 considering D=3, 5 and 7 for the 16 THz scenario. 61

Figure 4.8 Node throughput for architectures as a function of D. 62

Figure 4.9 Cost per bit normalized to the MBoSDM Baseline architecture (Fig. 4.1) for SDM, MB and MBoSDM architectures considering D=3, 5 and 7 for the 16 THz scenario. 62

Figure 4.10 Express structure cost for SDM architectures with M=8, MBoSDM architectures with M=4 and B=2, and with M=2 and B=3 considering D=3, 5 and 7 directions, for the 32 THz scenario. 66

Figure 4.11 A/D structure cost for SDM architectures with M=8, MBoSDM architectures with M=4 and B=2 and with M=2 and B=3 considering D=3, 5 and 7, for the 32 THz scenario. 66

Figure 4.12 Cost per bit normalized to the MBoSDM Baseline architecture (C+L with 4 cores) for SDM and MBoSDM architectures considering D=3, 5 and 7, for the 32 THz scenario. 67

Figure 4.13 Power consumption per bit normalized to the MBoSDM Baseline architecture (Fig. 4.1) power consumption per bit, for SDM architectures with M=4, MB architectures with B=3 and MBoSDM architectures with M=2 and B=2 considering D=3, 5 and 7 for the 16 THz scenario. 69

Figure 4.14 Power consumption per bit normalized to the MBoSDM Baseline architecture (C+L with 4 cores) for SDM and MBoSDM architectures considering D=3, 5 and 7, for the 32 THz scenario. 71

Figure B.1 Node throughput for FLEX-SCALE Layer 1 as a function of D, considering M=2, 4, 8. 85

Figure C.1 MBoSDM Baseline architecture considering $M = 4$, $D = 3$. 88

Figure C.2 MBoSDM architecture with a S-OXC per band considering $M = 4$, $D = 3$ and $N_C = 0$. 88

Figure C.3 MBoSDM architecture with a S-OXC per band considering $M = 4$, $D = 3$ and $N_C = 6$. 89

Figure C.4 MBoSDM architecture with a S-OXC per band considering $M = 4$, $D = 3$ and $N_C = 12$. 89

Figure C.5 Express structure cost for all studied MBoSDM architectures with $D = 3$, $D = 5$ and $D = 7$, considering $M = 4$ and $N_C = 0$. 90
Figure C.6 A/D structure cost for all studied MBoSDM architectures with $D = 3$, $D = 5$ and $D = 7$, considering $M = 4$ and $N_C = 0$. 90

List of Tables

Table 2.1 Dimensions of the WSSs associated with each strategy considering for various values of D and M for the drop structure. 8

Table 2.2 Number and type of components and their size in the express structure for each of the studied MB architectures considering D directions and B bands. 15

Table 2.3 Number and type of components and their size in the express structure for each of the SDM architectures. 27

Table 2.4 Number and type of components in the express structure and their size for each of the SDM architectures with D=3, M=4 and the MB architectures with D=3, B=3. 28

Table 2.5 Cost of components. 28

Table 2.6 Cost of the studied SDM architectures with D=3 and M=4 and the MB architectures with D=3 and B=3. 30

Table 2.7 Power consumption of components. 30

Table 2.8 Power consumption of the studied SDM architectures with D=3 and M=4 and the MB architectures with D=3 and B=3. 31

Table 3.1 Number and type of components and their port count in the express structure for each of the studied MBoSDM architectures considering the C, L, and S bands. 40

Table 3.2 Number and type of components in the express structure and their port count for each of the studied MBoSDM architectures considering D=3, M=4 and B=3. 41

Table 3.3 Cost of the studied MBoSDM architectures with D=3, M=4 and B=3. 45

Table 3.4 Power consumption of the studied MBoSDM architectures with D=3, M=4 and B=3. 48

Table 4.1 Cost of SDM architectures with D=3 and M=4, MB architectures with D=3 and B=3 and MBoSDM architectures with D=3, M=2 and B=2 for the 16 THz bandwidth scenario. 58

Table 4.2 Cost of SDM architectures with D=3 and M=8, MBoSDM architectures with D=3, M=4 and B=2 and MBoSDM architectures with D=3, M=2 and B=3 for the 32 THz bandwidth scenario. 64

Table 4.3 Power consumption of SDM architectures with D=3 and M=4, MB architectures with D=3 and B=3 and MBoSDM architectures with D=3, M=2 and B=2 for the 16 THz scenario. 68

Table 4.4 Power consumption of SDM architectures with D=3 and M=4, MBoSDM architectures with D=3, M=4 and B=2 and MBoSDM architectures with D=3, M=2 and B=3 for the scenario with 32 THz. 70

Table A.1 Component dimensions for the FLEX-SCALE architecture considering D=2, 3, 5, M=4 and $WBSS_{A/D} = 1$. 84

Table A.2 Component dimensions for the FLEX-SCALE architecture considering D=2, 3, 5, M=4 and $WBSS_{A/D} = 2$. 84

List of Acronyms

A/D: add/drop

AO-WC: all-optical wavelength converter

DEMUX: demultiplexer

ICXT: inter-core crosstalk

ISRS: inter-channel stimulated Raman scattering

IoT: Internet of Things

JS: joint switch

MB: multi-band

MCF: multicore fiber

MEMS: micro-electro-mechanical systems

MMF: multimode fiber

MUX: multiplexer

NLI: nonlinear interference

OADM: optical add-drop multiplexer

OA: optical amplifier

OXC: optical cross-connect

PLI: physical layer impairment

QAM: quadrature amplitude modulation

RMSA: routing, modulation format and spectrum assignment

RMSCA: routing, modulation format, spectrum, and core assignment

ROADM: reconfigurable optical add-drop multiplexer

SDM: spatial-division multiplexing

SMF: single-mode fiber

SOA: semiconductor optical amplifier

S-OXC: spatial optical cross-connect

WBSS: waveband selective switch

WXC: wavelength cross-connect

WSS: wavelength selective switch

CHAPTER 1

Introduction

1.1. Motivation

With the exponential growth of data traffic on optical networks, driven by the Internet of Things (IoT), augmented reality and artificial intelligence, among other large demanding bandwidth services and technologies, the need for high-capacity optical networks has become a priority for network and service providers [1]. Nowadays, most single-mode fiber (SMF) optical networks operate in the C-band, that has available a 4.8 THz bandwidth in the extended C-band solution. It is expected that in the upcoming years current SMF-based optical networks will approach their capacity limits. This calls for new technological solutions to enable large-scale, high-speed data transmission, with low energy consumption and low costs [2].

To face these challenges, two important technologies stand out: spatial-division multiplexing (SDM) and multi-band (MB). SDM is a technique that expands network capacity through multiplexing in the space dimension and can be implemented with multicore fibers (MCFs), multimode fibers (MMFs) or a bundle of parallel fibers [3]. The MB solution exploits the spectrum available in the SMF beyond the traditional C-band by resorting to other available bands, O, E, S, C, L and U-bands for optical transmission, paving the way for more efficient use of existing deployed fibers [4] .

The MB solution is considered a short-term promising solution for quickly expanding the capacity of optical networks. Google is already using the C+L band on several of their terrestrial long-haul networks [5]. However, the MB solution must address some challenges before a massive deployment and use [3]. At the physical layer, some physical layer impairments (PLIs) are enhanced when bands other than the C-band are added, like the interaction between the nonlinear interference (NLI) and the inter-channel stimulated Raman scattering (ISRS) and must be accounted for [6]. Also, the MB nodes become more complex compared to exclusively C-band nodes, as they need to integrate components and technologies capable of routing signals in multiple bands efficiently [3]. In addition, network planning tools must be adapted to deal with these specific problems, and so routing, modulation format and spectrum assignment (RMSA) algorithms have to be designed for dealing with this increased number of bands, different PLIs and more complex routing at the reconfigurable optical add-drop multiplexer (ROADM) nodes [6].

On the other hand, SDM is seen as a long-term solution for increasing network capacity since new fibers have to be built and installed [3], [7]. There are already some pioneer experiments and a few commercial systems using MCFs [8], [9]. Once again, specific challenges must be addressed when the MCF technology is used. One of the main issues

at the physical layer when uncoupled MCF are used is the crosstalk between cores, called inter-core crosstalk (ICXT), which can significantly degrade the signal quality [10]. In addition, SDM networks require more complex and larger dimension nodes compared to the ones used in conventional SMF networks, as the former nodes need to handle a greater number of optical spatial channels simultaneously. These nodes typically require wavelength selective switches (WSSs) with dimensions greater than the ones commercially available [11]. Moreover, network planning requires specialized tools to efficiently manage the routing, modulation format, spectrum, and core assignment (RMSCA) aware of the SDM networks PLIs and, so, new and efficient RMSCA algorithms have to be designed. Several works have already proposed several RMSCA algorithms [12].

The integration of MB and SDM (called MB over SDM, or simply MBoSDM) represents a unique opportunity to create next-generation optical networks, combining the advantages of both technologies to meet the growing number of traffic demands and capacity required. This integration can potentially use in a more efficient way, the multiple bands and the number of cores to expand capacity. For example, to achieve a 40 THz bandwidth scenario which is tenfold above the current available bandwidth, we can use the C+L+S bands with a MCF with 2 cores, instead of using only a MB solution with all the bands (also with 40 THz) or a MCF with ten cores (4 THz per core). Some works have already tested MBoSDM transmission scenarios, for example, in [13], a low-loss 125 μm cladding diameter four core fiber using the C+L+S band has been tested. However, this integration brings additional transmission challenges, such as the interaction between the ICXT and the NLI noise. Also, new node structures have to be designed and new planning tools must be developed. There is a recent work that started exploring three MBoSDM node architectures [14], involving different levels of switching granularity. The reference architecture in [14] has the highest granularity, but uses a $M \times M$ WSS per band, whereas the other proposed architectures in [14] use space switches or fixed connections between node inputs and outputs and $M \times M$ WSS in the add/drop (A/D) structure, leading to less granularity. However, the node architectures presented in [14] rely in WSSs or space switches that can potentially lead to larger dimensions, and higher costs. In [15], several directions to build cost effective node architectures with large dimensions are pointed out, for example, by using modular structures.

Our work will be focused on node architectures for these future MBoSDM networks that can be built with modular and hierarchical structures, based on route and select (R&S) or broadcast and select (B&S) architectures. A comparison study in terms of granularity, cost per bit and power consumption per bit will be performed for several MBoSDM architectures.

1.2. Goals

This dissertation focuses on the development and analysis of ROADM architectures for future high-capacity optical networks, exploring the integration of SDM and MB solutions. Specific goals of this dissertation are:

i) Study and compare ROADM node architectures for SDM and MB (C+L+S band) networks in terms of granularity, cost and power consumption.

ii) Study and compare ROADM node architectures for MBoSDM networks in terms of granularity, cost and power consumption.

iii) Compare MBoSDM node architectures with SDM and MB architectures in terms of granularity, cost and power consumption.

1.3. Dissertation organization

This section describes the organization of this dissertation.

In Chapter 2, we begin with a general review of the fundamental concepts of ROADMs and of MB and SDM node architectures already proposed in the literature. We discuss the number and type of components, and compare MB and SDM architectures in terms of granularity, cost and power consumption.

In Chapter 3, we discuss various MBoSDM architectures proposed in the literature. We compare the architectures in terms of granularity, number and type of components, and again analyse their cost, power consumption and throughput, in order to figure out the most effective MBoSDM architectures.

In Chapter 4, we select the most effective and promising MB, SDM and MBoSDM architectures studied in the previous chapters, and compare them, in terms of granularity, cost per bit and power consumption per bit for two bandwidth application scenarios: 16 THz and 32 THz per node degree. We analyse once again all components of each architecture, their hardware count and granularity, costs and power consumption per bit, and conclude which of them are more suitable for the two bandwidth scenarios studied.

In Chapter 5, we present the conclusions of this work and propose possible topics for future research.

1.4. Main contributions

This work has the following main contributions:

- Comparison and analysis of five C+L+S MB architectures in terms of component types, granularity, cost and power consumption.

- Comparison and analysis of four SDM architectures in terms of component types, granularity, cost and power consumption.

- Comparison and analysis of four MBoSDM architectures in terms of component types, granularity, cost and power consumption.

- A comparison study between the MBoSDM, MB and SDM architectures in terms of cost and power consumption.

[This page is intentionally left blank.]

CHAPTER 2

Literature review on node architectures for MB and SDM networks

2.1. Introduction

In this chapter, we begin with a general review of the fundamental concepts of ROADMs in section 2.2. In section 2.3, we present the MB architectures already proposed in the literature and the respective granularity: baseline architecture [16], architecture with all-optical wavelength converters (AO-WCs), common band architecture [16]–[19], compact architecture [20] and SOA-based architecture [21]. A comparison of the number of components and their dimensions in the different MB architectures is also performed in this section. Likewise, in section 2.4, we present the SDM architectures proposed in the literature with the respective switching granularity. Lastly, in this section, a comparison of the number of components and their dimensions in the different SDM architectures is performed. Section 2.5 presents a comparison between MB architectures and SDM architectures in a transmission scenario with a 16 THz available bandwidth regarding the cost and power consumption. Lastly, section 2.6 draws the main conclusions of this chapter.

2.2. ROADMs fundamental concepts

ROADMs have a very important role in optical networks, providing connectivity between network clients. ROADMs allow channels (wavelengths) to be switched from any input to any output, in the optical domain, and they allow also channels to be added and dropped to/from the optical network.

A ROADM architecture is generically composed of the express structure and the A/D structure, as shown in Figure 2.1. The express structure is responsible for routing wavelengths that don't need to be added or dropped in that node. The A/D structure allows specific wavelengths to be added or dropped. Both structures can use WSSs, which have the capability for selecting and routing the wavelengths.

Nowadays, a ROADM node has two possible architectures: B&S and R&S. In the B&S architecture, the input optical signals are broadcasted to every ROADM direction using splitters (component A in Figure 2.1), and the selection of the wavelengths to be transmitted is done in the output WSSs (see Figure 2.1).

In the R&S architecture, we use input and output WSSs (i.e. the component A in Figure 2.1 is a WSS). The input WSSs identify the incoming wavelengths and route them in the right direction, represented by D in Figure 2.1, while the output WSSs select the specific wavelengths that should be routed to the corresponding output ports.

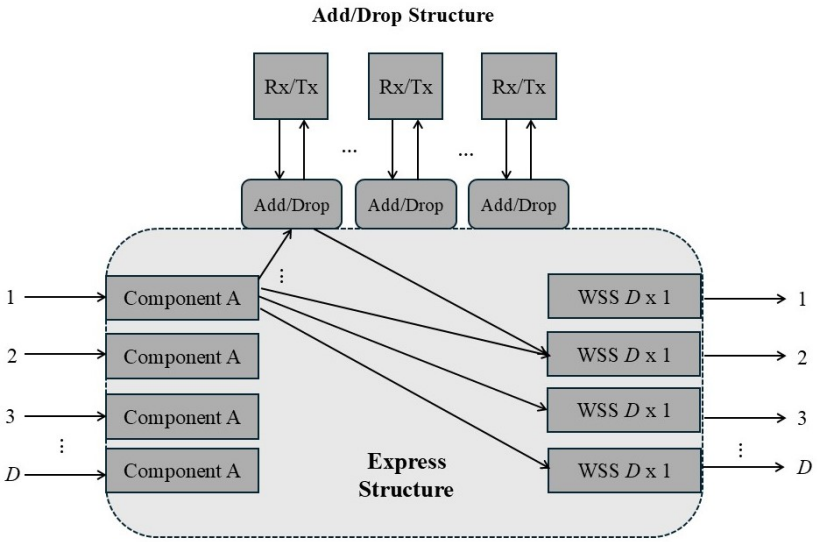


FIGURE 2.1. Generic D-degree ROADM structure.

Both architectures have advantages and disadvantages. The R&S architecture is designed to eliminate the insertion losses of the splitter in the B&S architecture, in particular for large ROADM dimensions (typically higher than 8×8 [22]). The R&S architecture also offers more flexibility [23]. The B&S architecture has typically a lower cost and less power consumption [23].

ROADMs have three properties that describe their flexibility: colorless, directionless and contentionless. A colorless ROADM allows any wavelength to be added/dropped from any ROADM port. The directionless property allows that an add signal can be routed to any direction of the ROADM. In a contentionless ROADM, multiple signals with the same wavelength are allowed to exist in the same A/D structure [24], [25].

A colorless A/D structure can be implemented with a $1 \times W$ WSS on the drop side and an $W \times 1$ coupler on the add side, where W represents the number of wavelengths to be added or dropped by the node, typically obtained from a pre-defined A/D ratio ($W = N_W \times A/D_{ratio}$, where N_W is the number of wavelength channels considered in each core or spatial channel) [23].

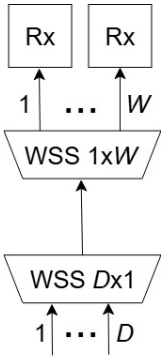
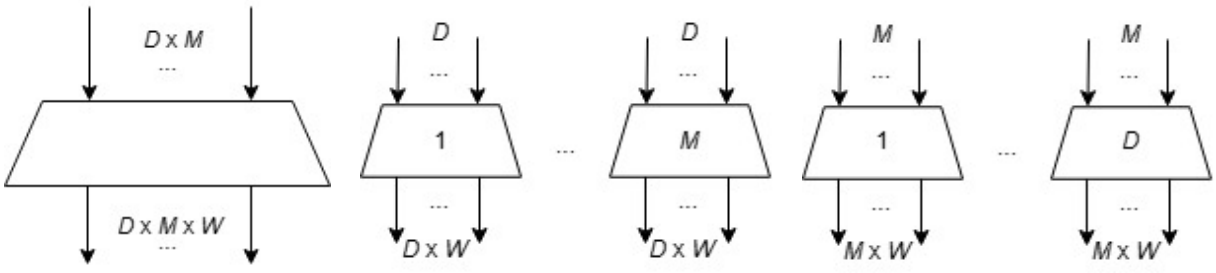


FIGURE 2.2. Drop structure with CD capability.

A CD ROADM can be implemented with a cascade of two WSSs, a WSS $D \times 1$ followed by, a WSS $1 \times W$, as shown in figure 2.2 [26]. In this case, wavelength contention may occur when, for example, two signals with the same wavelength (from two different node directions) are dropped in the same drop structure. A CD ROADM can also be implemented by replacing the WSS $1 \times W$ with a splitter of the same dimension, where the optical receiver must select the corresponding wavelength through the use of coherent detection [26].

To avoid wavelength contention, a CDC A/D structure must be used. This structure can be implemented in three different ways, as shown in Figure 2.3 [27]. These strategies offer different options between flexibility, cost and complexity [27].



(A) A/D structure with Full CDC capability.

(B) A/D structure with CDC capability per spatial channel.

(C) A/D structure with CDC capability per direction.

FIGURE 2.3. Three possible implementations of CDC A/D structures.

The first strategy, Figure 2.3 a), uses a single WSS for all directions and spatial channels, ensuring full CDC capacity. However, due to its size and complexity, it requires a large port count WSS, which can significantly increase cost and energy consumption [27]. This large port count WSS has $D \times M$ inputs, with M representing the number of cores, and $D \times M \times W$ outputs that depend on the A/D ratio considered, and for large ROADM size, may lead to unfeasible WSS dimensions. Internally, a generic $D \times N$ WSS is composed of two stages. A set of $1 \times D$ WSSs, in the first stage, interconnected with a set of $N \times 1$ optical switches in the second stage, as shown in figure 2.4. This strategy with full CDC capability can also be implemented with a multicast switch [24].

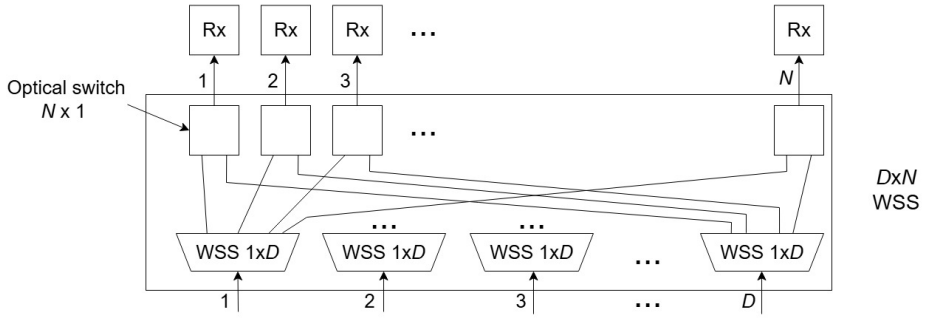


FIGURE 2.4. Internal structure of a $D \times N$ WSS.

In the second strategy, Figure 2.3 b), each spatial channel has its own dedicated WSS, which reduces the complexity of the individual WSSs, but it does not allow the switching between spatial channel in the A/D structure [27]. Although this strategy reduces flexibility, it uses smaller, commercially available WSSs. In this strategy, we have one $D \times (D \times W)$ WSS per spatial channel with D inputs and $(D \times W)$ outputs with a total of M WSSs per A/D structure, so we have CDC capacity for each specific spatial channel [27].

The third strategy, Figure 2.3 c), uses one WSS for each direction of the architecture, allowing independent switching of the spatial channels within each direction. This improves the manageability of the network, but limits the CDC capacity to only exist within each specific direction. Here, we consider one $M \times (M \times W)$ WSS per direction with a total of D WSSs per A/D structure with M inputs and $(M \times W)$ outputs. This strategy is less flexible than the full CDC, but uses smaller, commercially available WSSs [27].

TABLE 2.1. Dimensions of the WSSs associated with each strategy considering for various values of D and M for the drop structure.

Strategy		Full CDC	CDC per spatial channel	CDC per direction
D=2	M=4	8×128 WSS	4 WSSs 2×32	2 WSSs 4×64
	M=7	14×224 WSS	7 WSSs 2×32	2 WSSs 7×112
	M=12	24×384 WSS	12 WSSs 2×32	2 WSSs 12×192
D=3	M=4	12×192 WSS	4 WSSs 3×48	3 WSSs 4×64
	M=7	21×336 WSS	7 WSSs 3×48	3 WSSs 7×112
	M=12	36×576 WSS	12 WSSs 3×48	3 WSSs 12×192
D=4	M=4	16×256 WSS	4 WSSs 4×64	4 WSSs 4×64
	M=7	28×448 WSS	7 WSSs 4×64	4 WSSs 7×112
	M=12	48×768 WSS	12 WSSs 4×64	4 WSSs 12×192
D=8	M=4	32×512 WSS	4 WSSs 8×128	8 WSSs 4×64
	M=7	56×894 WSS	7 WSSs 8×128	8 WSSs 7×112
	M=12	96×1536 WSS	12 WSSs 8×128	8 WSSs 12×192
D=16	M=4	64×1024 WSS	4 WSSs 16×256	16 WSSs 4×64
	M=7	112×1792 WSS	7 WSSs 16×256	16 WSSs 7×112
	M=12	192×3072 WSS	12 WSSs 16×256	16 WSSs 12×192

Table 2.1 shows the dimensions of the WSSs in the drop structure associated with each strategy mentioned in Figure 2.3, with different values of D and M and assuming an A/D ratio of 20% and N_W =80 wavelengths per spatial channel.

From Table 2.1, we can conclude that the dimensions of the WSSs in all the strategies increase when the values of M and D increase. Despite the greater flexibility of the full CDC strategy, WSSs with very large dimensions are required in this strategy, which can not be implemented commercially. For example, for D=2 and M=4, a 8×128 WSS is needed (note that the maximum WSS dimension is 1×64) [28]. CDC per spatial channel and CDC per direction strategies, have less flexibility, but require WSSs with lower dimensions, e.g., for D=2 and M=4, respectively, 4 WSSs 2×32 and 2 WSSs 4×64 are required. In the CDC per spatial channel strategy, we can see that the dimension of the WSSs is constant for the same D and different M, and as M increases, a higher number of WSSs is needed. In the CDC per direction strategy, we conclude that the dimension of a WSS is the same for a particular value of M, independently of D.

These strategies used for CDC to reduce the dimension of the components can also be used for the CD strategy, but in this case, we must use a cascade of two WSS as mentioned above. In the case of a full CD A/D structure, with D=2 and M=4, we have an 8×1 WSS followed by a 1×128 WSS instead of an 8×128 WSS as found in the full CDC A/D structure.

2.3. MB node architectures

In MB networks, several bands, besides the common C-band, are used for transmission and switching. In Figure 2.5, the spectrum considered in this work for the L, C and S bands is represented for a total bandwidth of approximately 16 THz [29]. A band guard is used between bands, with a 600 GHz band gap between the L and C bands and between the C and S bands. The number of channels is calculated considering a channel spacing of 50 GHz [29], so that the total number of channels is 320, comprising a bandwidth of about 16 THz. The L-band has capacity for 130 channels, the C-band can accommodate 87 channels and the S-band 103 channels as indicated in Figure 2.5.

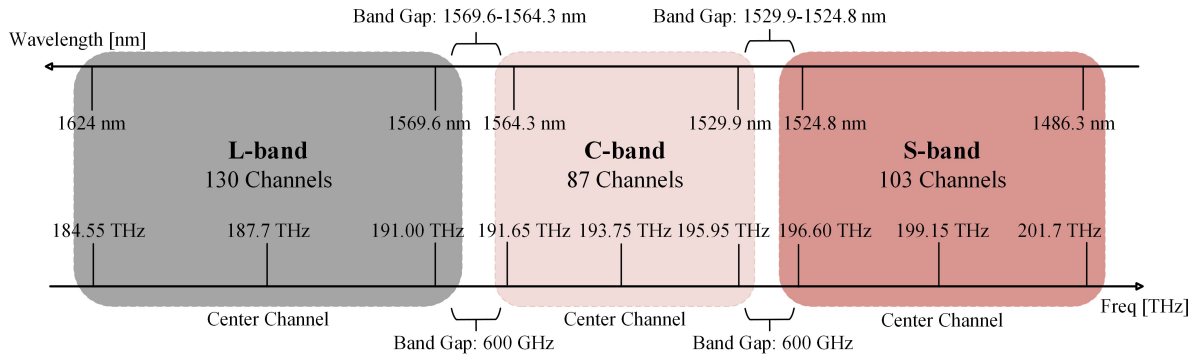
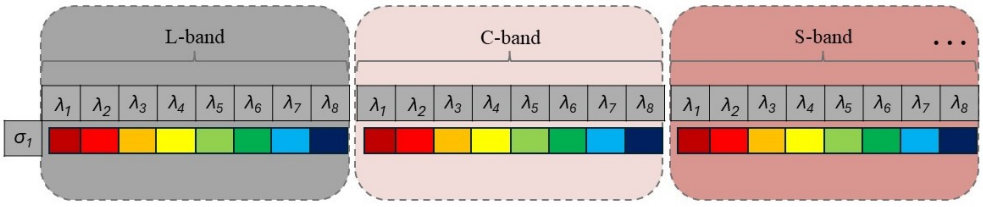
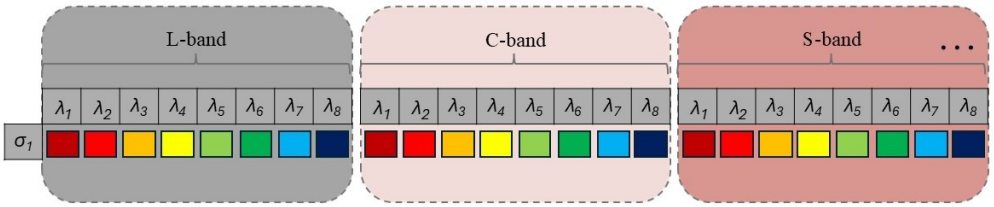


FIGURE 2.5. Spectrum of the C-, L- and S-bands and corresponding ITU-T grid frequencies.

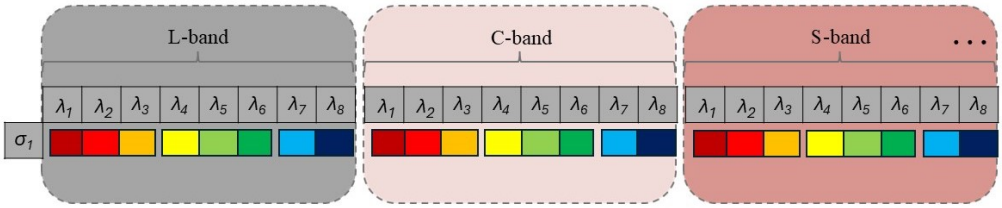
In MB ROADM node architectures, switching can be done in space, in wavelength or between bands (e.g. C, L, S). Hence, these architectures can be classified based on their granularity, resulting in six types of granularities: space granularity, space-wavelength granularity, full space-fractional wavelength granularity, space and band granularity, space-wavelength and band granularity and full space and band-fractional wavelength granularity. Three of these granularities are shown in Figure 2.6. Note that if the new waveband selective switches (WBSS) proposed in [30] were used, we can have fractional band granularity, which means that we can select the bands, in the same way as we can select wavelengths in a WSS.



(A) Spatial granularity strategy.



(B) Spatial-wavelength granularity strategy.



(C) Full space- fractional wavelength granularity strategy.

FIGURE 2.6. Switching strategies for MB switching.

In the context of MB, some architectures have already been proposed in the literature: baseline architecture [16], architecture with AO-WCs, common band architecture [16]–[19], compact architecture [20] and SOA-based architecture [21]. These architectures will be explained in the following sub-sections.

2.3.1. Baseline architecture

The baseline architecture is shown in Figure 2.7 considering a R&S architecture, for the C+L+S band scenario [16]. It consists of a MB multiplexer (MUX), optical amplifiers (OAs), WSSs and a MB demultiplexer (DEMUX). The DEMUXs separate the three bands, and the MUXs join them together. There are also multiple single-band WSSs, at

the input (ingress) and at the node output (egress). Regarding routing flexibility, this architecture allows wavelengths to be switched in any direction within each band. The problem with this architecture is that it is not possible to switch between bands [16].

This architecture has spatial-wavelength granularity, as described in Figure 2.6 (b). No switching between bands is allowed so there is no band granularity.

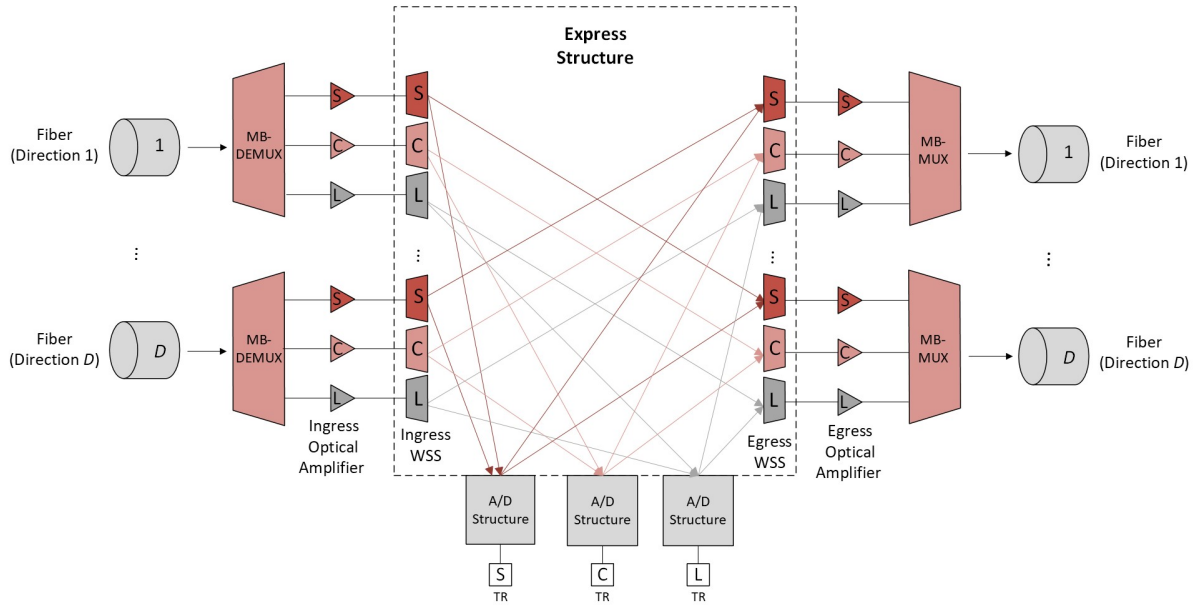


FIGURE 2.7. Baseline D-degree R&S MB ROADM architecture.

2.3.2. Architecture with AO-WCs

To solve the problem of not switching wavelengths between bands, two node architectures have been proposed: the architecture with AO-WCs and the common band architecture [16]–[18]. A R&S MB ROADM architecture with AO-WCs is shown in Figure 2.8, considering the C+L+S band scenario (not all the bands are represented due to simplify the connections representation). In this architecture, AO-WCs have been used after the ingress WSSs, which allow multiple wavelengths to be converted from one band to another, thus increasing the node flexibility. The problem is that the number of AO-WCs required is very high when all the bands are in use, which increases significantly the node cost. Furthermore, as another disadvantage, the AO-WC is also an optical device that is not technologically mature and is far from the commercial phase [18].

In terms of granularity, this architecture has granularity in all the three dimensions, space, wavelength and band.

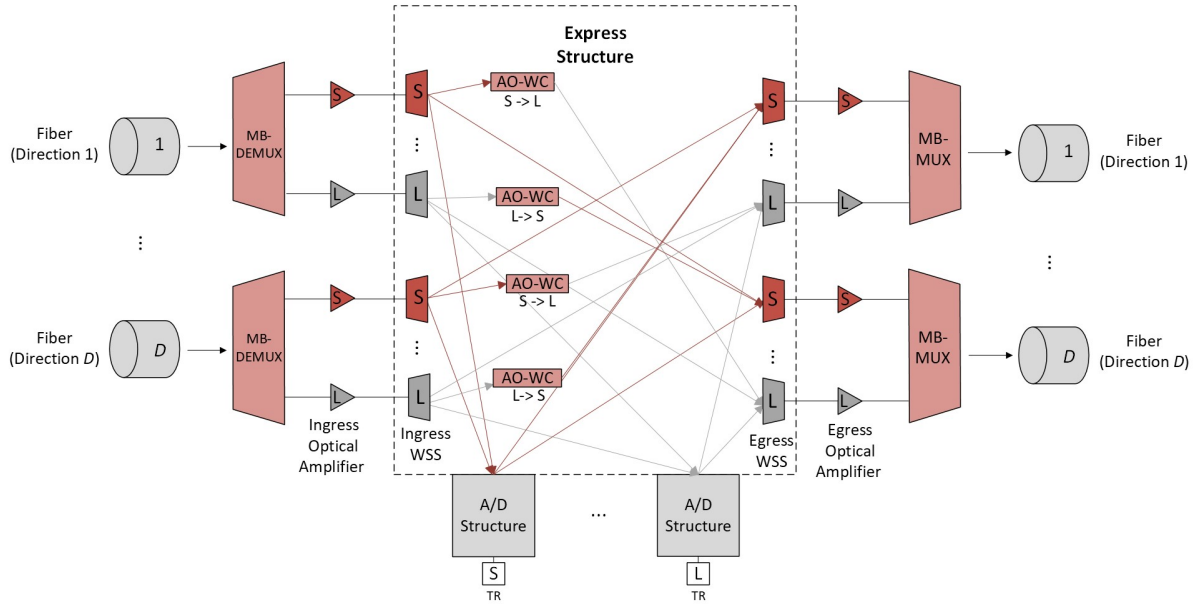


FIGURE 2.8. *D*-Degree R&S MB ROADM architecture with AO-WCs.

2.3.3. Common band architecture

To improve the previous architecture, a R&S MB ROADM architecture that works only on the C-band is proposed, that is called common band architecture [16]–[19]. In this architecture, the incoming signals from other bands are all converted to the C-band at the architecture input. Figure 2.9 shows a R&S common band architecture for the C+L+S band scenario. In this architecture, the optical signal is routed through the MB-DEMUX that separate the bands. The wavelengths in the L and S bands are converted to the C-band by the AO-WCs and then routed to the input C-band WSSs. At the architecture output, they are converted back to the original band by the output AO-WC and, then combined by the MB-MUX at the ROADM output. This architecture has cost advantages over previous ones since C-band WSSs and C-band transponders are the equipments commercially used and technologically mature as opposed to WSSs and transponders for the L and S bands.

This architecture has also granularity in all three dimensions, space, wavelength and band.

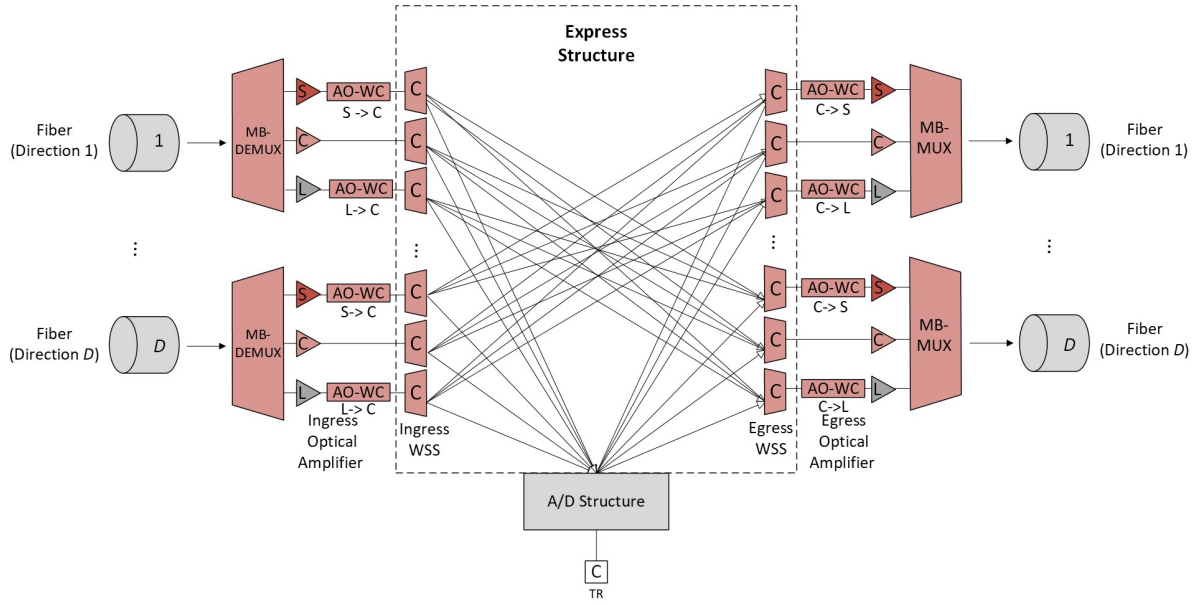


FIGURE 2.9. D-degree R&S MB ROADM common band architecture.

2.3.4. Compact architecture

Figure 2.10 shows a generic D-degree R&S C+L+S MB ROADM architecture that uses WSSs that work simultaneously in the three bands. This architecture is commonly known as compact architecture [20]. As this architecture requires all the MB components at the start of network operation, it is an architecture that leads to high costs in comparison with the previous architectures, where the components can be acquired over time as network traffic demands increase. Its flexibility is similar to the architecture with AO-WCs and to the compact architecture.

This architecture has also granularity in all three dimensions.

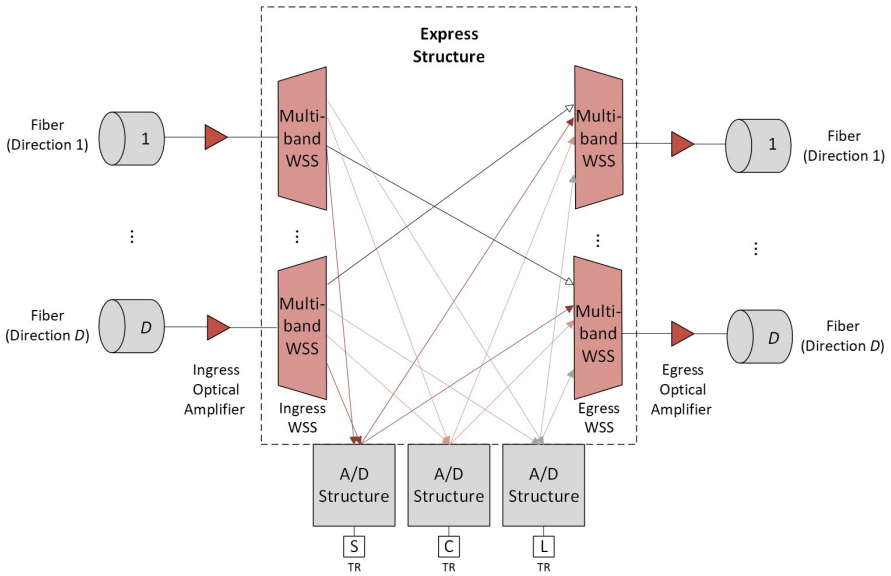


FIGURE 2.10. D-degree MB ROADM compact architecture.

2.3.5. SOA-based architecture

Figure 2.11 shows a C+L+S ROADM SOA-based architecture. This architecture consists of a MB DEMUX and MUX and can support the S, C and L-bands [21]. The input signal is separated into different bands and directed to the respective optical add-drop multiplexer (OADM) that can operate in parallel for the S, C, and L bands. The OADM includes a WDM demultiplexer and an array of semiconductor optical amplifiers (SOAs) that operate as gates and amplifiers for each WDM channel, and a WDM multiplexer, with the opposite functions. The add-drop function is performed with splitters/combiners. When a channel needs to be blocked (dropped), the SOA is switched off to block the transmission of signals within each specific wavelength, otherwise the SOA is switched on allowing the signal to pass and compensating for the losses caused by the MUX/DEMUX and splitters. After processing in the SOAs, the signals pass through the WDM multiplexer and are sent to the MB MUX which gathers the signals together before exiting the node. The main application of this architecture is in MB optical metro-access network to support the 6G era, being a node designed for low cost. In this architecture, wavelengths are not reconfigurable (are fixed wavelengths) and this architecture leads to lower costs due to the SOAs reduced cost, which also consume less energy [21].

In this architecture it is not possible to switch between bands, so it only has spatial and wavelength granularity, as shown in Figure 2.6 (b).

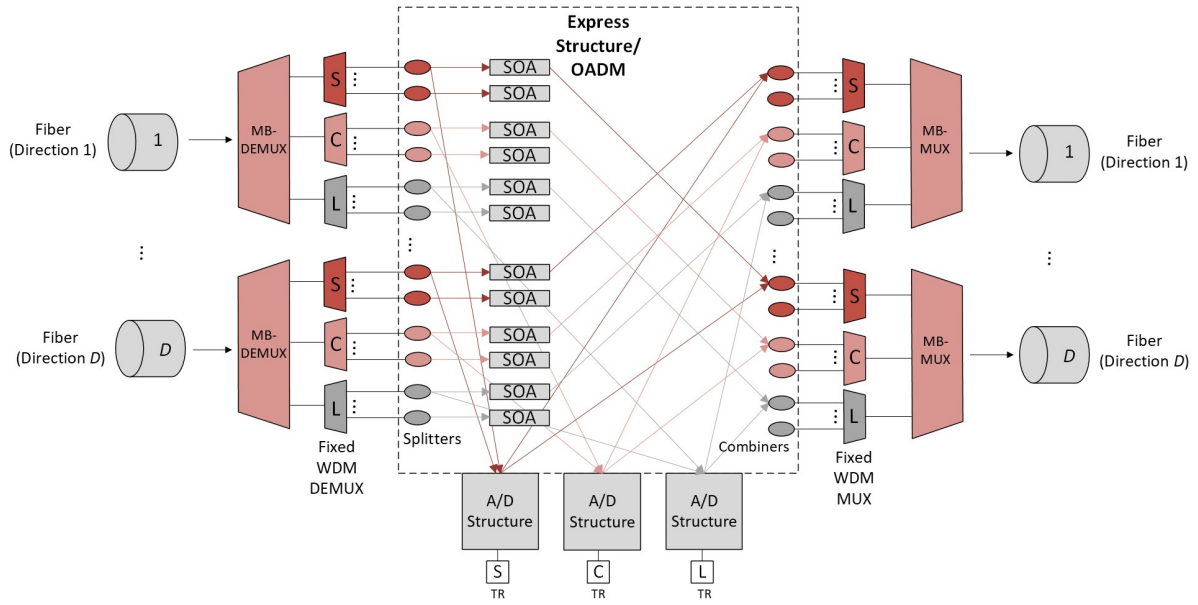


FIGURE 2.11. *D*-degree MB SOA-based architecture.

2.3.6. MB node architecture comparison

Table 2.2 shows the number and type of components and their dimension (number of inputs and outputs) for the MB architectures described in the previous sub-sections. From Table 2.2, we can conclude that the architecture that uses AO-WCs (Figure 2.8) should have the highest cost, because the number of AO-WCs required is very high when all the bands are in use [21]–[23]. The compact architecture (Figure 2.10) may lead also to a high cost, because it requires that all MB components are acquired at the start of network operation [25]. The lowest cost architectures should be the architecture with SOAs (SOAs are cheaper components [31], [32]) and the common band architecture (Figure 2.9), since C-band WSSs and C-band transponders are commercially used and technological mature as opposed to WSSs and transponders for the L and S bands [21]–[24], [31]. In terms of granularity, the SOA-based architecture (Figure 2.11) should be the least flexible, since the wavelengths are fixed, followed by the baseline, which does not allow switching between bands. The architectures with AO-WCs should be the most flexible, as they allow switching between bands [21]–[23], [31]. Finally, in terms of energy consumption, the best option should be the architecture with SOAs, while the architectures that use AO-WCs consume the most energy [31]. Note that to obtain the expressions for the different architectures, it was assumed that we only have one output for the drop and one input for the add per spatial channel, and that each direction does not switch information back to the same direction, for example, incoming information from the north direction is not sent back to the north direction.

TABLE 2.2. Number and type of components and their size in the express structure for each of the studied MB architectures considering D directions and B bands.

Architectures	Type and Number of components	Dimensions of WSS	Dimensions of MB MUX/ DEMUX	Dimensions of splitters/ combiners
Baseline Architecture	D MB DEMUX, D MB MUX, $2 \times D \times B$ Optical Amplifier, $2 \times D \times B$ WSS	$1 \times D$	$1 \times D$	-
Architecture with AO-WCs	D MB DEMUX, D MB MUX, $2 \times D \times B$ Optical Amplifier, $2 \times D \times B$ WSS, $D \times (B-1)$AO-WCs	$1 \times [(B \times (D-1)) + 1]$	$1 \times D$	-
Common band	D MB DEMUX, D MB MUX, $2 \times D \times B$ Optical Amplifier, $2 \times D \times B$ WSS, $2 \times D \times (B-1)$ AO-WCs	$1 \times [(B \times (D-1)) + 1]$	$1 \times D$	-
Compact	$2 \times D$ Optical Amplifier, $2 \times D$ Multi-band WSS	$1 \times (B + D - 1)$	-	-
SOA-based architecture	D MB DEMUX, D MB MUX, $2 \times D \times B$ Fixed WDM DEMUX, $2 \times D \times B$ Fixed WDM MUX, $D \times B \times N_w$ splitters, $D \times B \times N_w$ combiners, $D \times B \times N_w$ SOAs	-	$1 \times D$	$1 \times D$

2.4. SDM node architectures

SDM is a promising solution for increasing the capacity of optical networks. With the exponential growth of data traffic and the imminent data capacity saturation of conventional single-mode fibers, SDM has emerged as an essential approach to ensure the scalability of future telecommunication networks [3], [7].

SDM operates by exploiting different spatial channels within the C-band transmission scenario to increase transmission capacity. These spatial channels can be implemented

with a bundle of parallel fibers that use several fibers in parallel to carry independent signals, with MCFs, which have several cores within the same fiber, where each core can function as an independent channel, and MMFs, which use different propagation modes within a single fiber to transmit simultaneous signals [3].

In SDM ROADM node architectures, switching can be done in two dimensions, space and wavelength, and can be classified based on their granularity, resulting in eight types of switching strategies: space granularity, fractional space granularity, wavelength-space granularity, wavelength granularity, fractional wavelength granularity, fractional space-full wavelength granularity, fractional space-fractional wavelength granularity and full space-fractional wavelength granularity [7]. These types of switching strategies are shown in figure 2.7, considering a MCF with 6 cores (σ_1 to σ_6) and 8 wavelengths per core (λ_1 to λ_8) as represented in Figure 2.12 a).

In the space granularity strategy, shown in Figure 2.12 (b), each spatial channel σ_n (with n=1, ...,6) is switched as a whole inside the ROADM node without the possibility of switching wavelengths.

In the fractional space granularity, shown in Figure 2.12 (c), spatial channels are grouped and switched as a whole, like in the space granularity strategy presented in Figure 2.12 b).

In the space-wavelength granularity strategy, shown in Figure 2.12 (d), spatial and wavelength switching coexist, being this strategy, from the ones shown in Fig. 2.7, the one that leads to the highest granularity, i.e., the highest network flexibility.

In the wavelength granularity strategy, as shown in Figure 2.12 (e), switching is done with groups of channels of the same wavelength (which are known as wavelength channels). These groups of channels are switched independently of the spatial channel. A joint switch (JS) WSS is typically used to perform this operation [7].

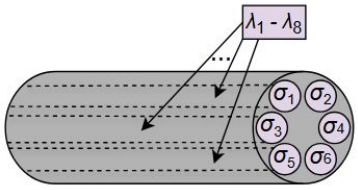
In the fractional wavelength granularity, shown in Figure 2.12 (f), wavelength channels are grouped together and switched as a whole, as in Fig 2.12 e), for a single wavelength channel.

In the fractional space-full wavelength granularity, the switching is done with previously defined groups of the same wavelength channels, as shown in Figure 2.12 (g). In this strategy, unlike in the wavelength granularity strategy where there is only one group with the same wavelength, several groups can be formed within the same wavelength.

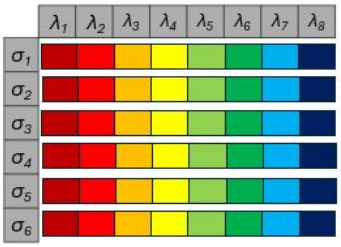
In the full space-fractional wavelength granularity, the switching is done with previously defined groups of the same spatial channel, as shown in Figure 2.12 (h). In this strategy, unlike in the space granularity strategy where there is only one group per spatial channel, several groups per spatial channel can be formed.

In the fractional space-fractional wavelength granularity architecture, spatial channels and wavelengths are grouped together as shown in Figure 2.12 (i). Switching is done with groups that have several spatial channels and several wavelengths.

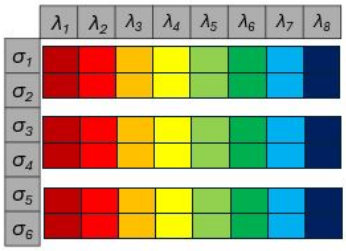
In the following, several examples of implementation of the ROADM architectures with the granularities shown in Figure 2.12 are presented and discussed.



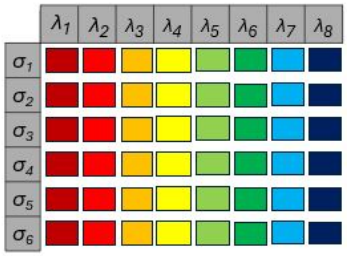
(A) MCF with 6 cores (corresponding to 6 spatial channels) and 8 wavelengths in each core.



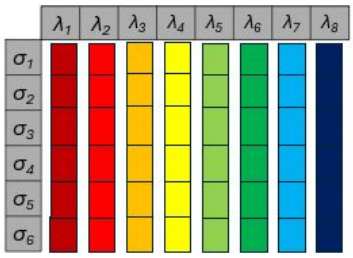
(B) Spatial granularity strategy.



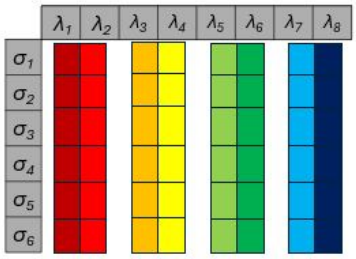
(C) Fractional space granularity strategy.



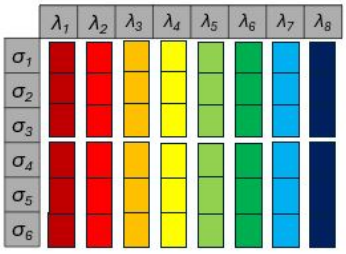
(D) Spatial-wavelength granularity strategy.



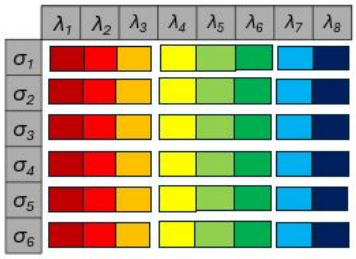
(E) Wavelength granularity strategy.



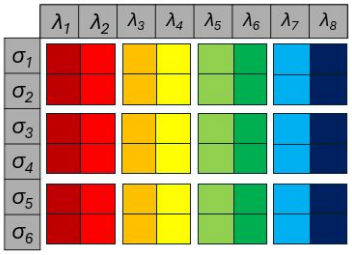
(F) Fractional wavelength granularity strategy.



(G) Fractional space-full wavelength granularity strategy.



(H) Full space-fractional wavelength granularity strategy.



(I) Fractional space- fractional wavelength granularity strategy.

FIGURE 2.12. Switching strategies for SDM switching.

2.4.1. Space granularity architecture

The main feature of the spatial granularity strategy in SDM networks, shown in Figure 2.12 (b), is the use of optical switches to route the full band of each spatial channel to the intended destination. This approach can be implemented with node architectures with or without lane changes.

In the implementation without lane changes, the input spatial channel (fibers, core or mode) transmits the data on the same spatial channel to one of the output fibers. This can be achieved using several low-port count optical cross-connects (OXCs), with one OXC dedicated to each spatial channel. Internally, an OXC is implemented with an optical

switching matrix that can use micro-electro-mechanical systems (MEMS) technology [33]. Each OXC must have at least a number of input and output ports equal to the number of ROADM directions (D). This means that a total of M OXCs with $((D+1) \times (D+1))$ dimension, where M corresponds to the number of spatial channels, is required to ensure a proper switching operation [7].

Figure 2.13 shows a SDM ROADM-based architecture with spatial granularity without lane changes, using three directions (D=3) and four spatial channels (M=4), which are represented by different colors. The fan-ins, fan-outs and optical amplifiers are also represented in Figure 2.13 [34]. Routing is done with four 4×4 OXCs, each responsible for forwarding a particular spatial channel. In this case without lane changes, one spatial channel from one direction cannot be changed to another spatial channel in other node direction.

On the other hand, implementation with lane changes allows spatial channels to be redirected to different spatial channels in other directions. In this case, a single large OXC can be used to manage all traffic on the node, with a port count of $((D+1) \times M) \times ((D+1) \times M)$ [7]. Figure 2.14 shows an SDM ROADM-based architecture with spatial granularity with lane changes with 3 directions and 4 spatial channels per direction, using a single 16×16 OXC, which allows for more flexible routing.

This architecture can be used in core networks, where spatial granularity is sufficient to guarantee the necessary routing flexibility. In addition, spatial granularity switching reduces implementation complexity compared to architectures that involve spatial and wavelength granularity. However, the need for a large OXC in the architecture with lane changes can increase the cost and complexity of the architecture, especially for ROADMs with many directions and spatial channels. In addition, failures in this OXC can impact the entire network performance, requiring additional redundancy and protection measures [7]. The possibility of using several smaller OXCs, as in the architecture without lane changes, can avoid critical failures in a single large switch [7].

In the fractional space granularity, shown in Figure 2.12 (c), the switching is done with previously defined groups of spatial channels. For this granularity, the same architecture used for the space granularity can be used, but the control signals for the space channels that form a group must be the same.

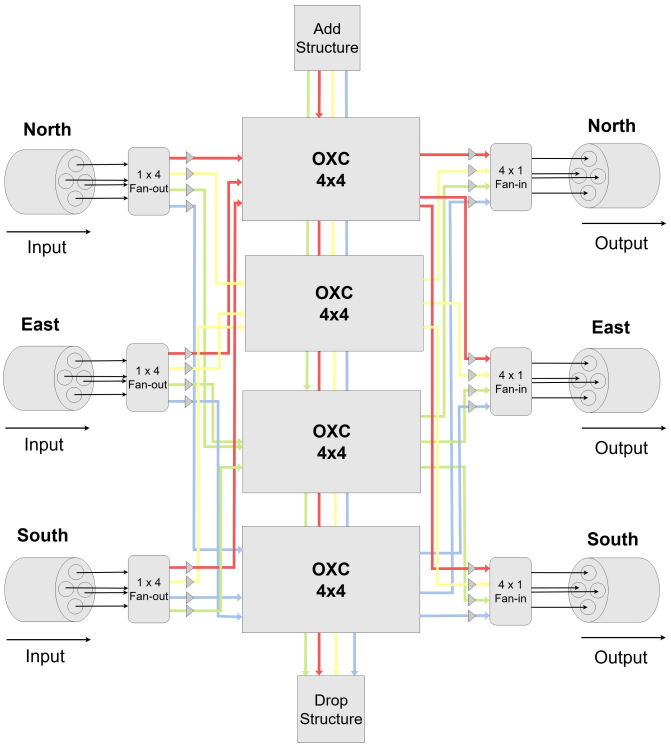


FIGURE 2.13. Spatial granularity architecture without lane changes with three directions (D=3) and four spatial channels (M=4).

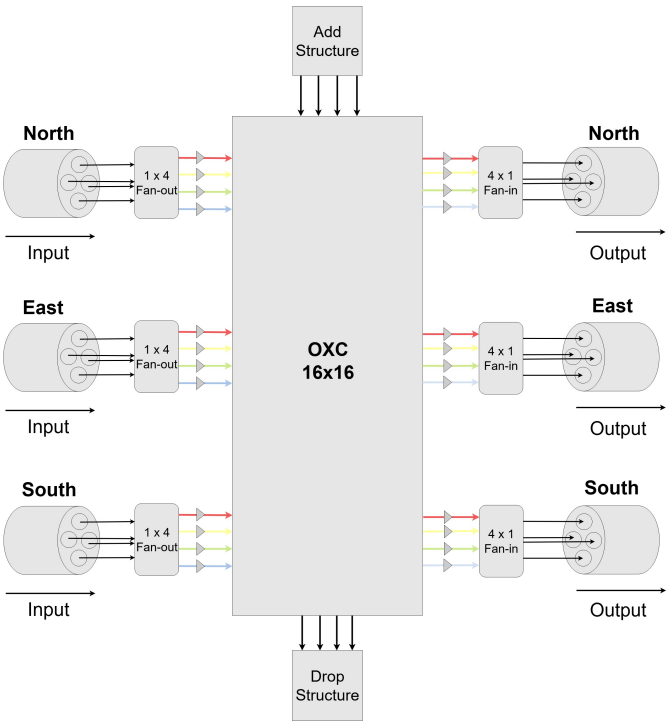


FIGURE 2.14. Spatial granularity architecture with lane changes with three directions (D=3) and four spatial channels (M=4).

2.4.2. Space-wavelength granularity architecture

The space-wavelength granularity strategy, shown in Figure 2.12 (d), allows the wavelengths within each spatial channel to be routed individually. This strategy can be also implemented with or without lane changes.

Figure 2.15 shows an SDM R&S ROADM-based architecture with spatial wavelength granularity without lane changes, where three directions (D=3) and four spatial channels (M=4) are used, being the spatial channels distinguished by four different colors. This configuration, called also core-wise switching [35], does not allow switching between cores within an MCF, hence, reducing the WSSs port count in comparison with the lane changes architecture. This architecture consists of 24 1×3 WSSs. For a generic architecture with space-wavelength granularity without lane changes, $2 \times M \times D$ WSSs with $1 \times [(D-1)+1]$ dimension are required, assuming one additional connection to the A/D structure.

Figure 2.15 only shows the connections in the North direction in order to simplify the connections representation, but all directions follow the same logic. The input WSSs of each direction connect to the output WSSs of the other directions and to the drop structure. The output WSSs are also connected to the add structure.

Figure 2.16 shows an SDM R&S ROADM-based architecture with spatial wavelength granularity with lane changes, where individual wavelengths can be routed to any of the spatial channels and directions of the ROADM. This approach requires 24 1x9 WSSs, which increases the complexity of the ROADM. For a generic ROADM with space-wavelength granularity and lane changes, $2 \times M \times D$ WSSs with $1 \times [(D-1) \times M)+1]$ dimension are required, assuming one connection per spatial channel to the A/D structure.

Despite the greater flexibility of space-wavelength granularity architectures, they require many components, hence leading to a higher cost. A possible solution to build cost effective space-wavelength architectures is to use a modular architecture, as pointed in [15] and analyzed in [36].

In the full space-fractional wavelength granularity, shown in Figure 2.12 (h), the same architecture used for the space-wavelength granularity can be used. In this scenario, the dimension of the WSSs is smaller than in the space-wavelength granularity scenario. Moreover, instead of a single wavelength, we have groups of wavelengths where the inputs WSSs routes those groups. In [37], an alternative architecture with space-fractional wavelength granularity is proposed. This architecture is based on JSs WSS and optical space switches and a comparative cost analysis is done in [36].

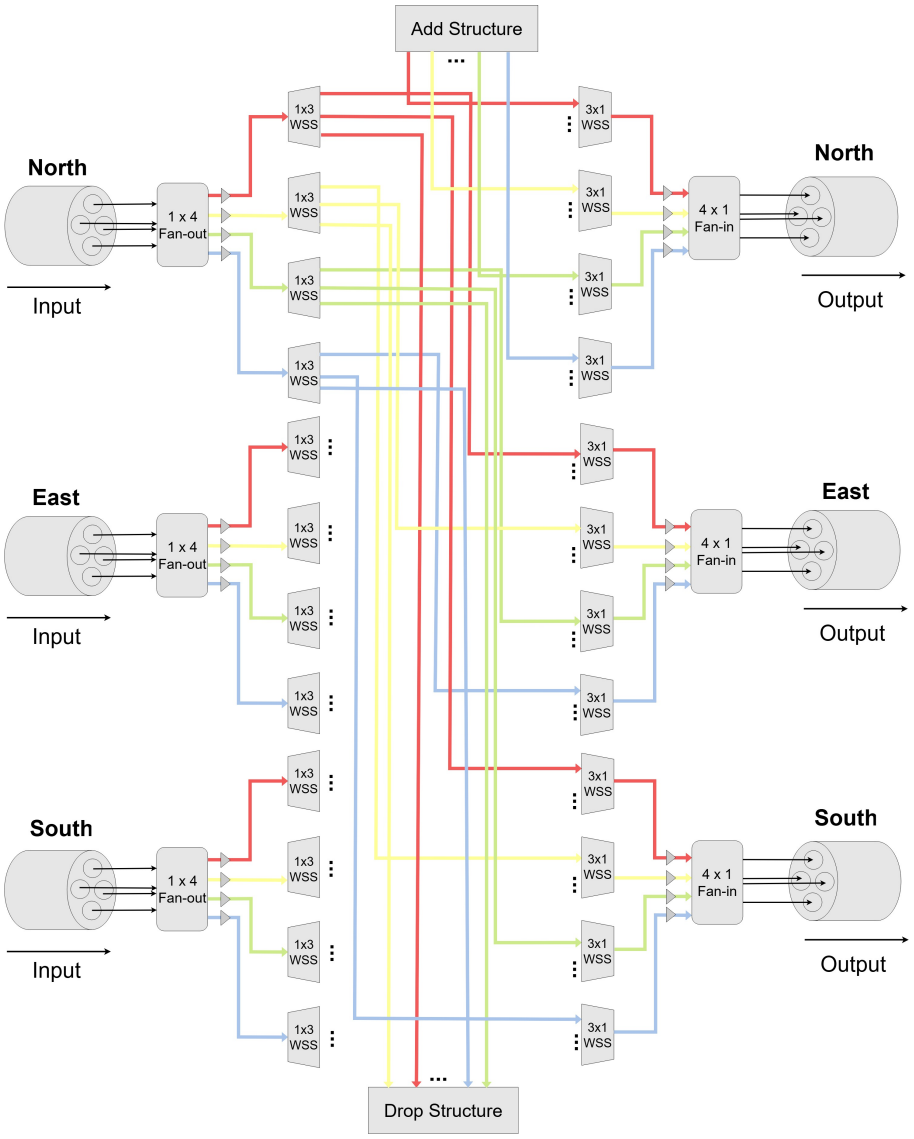


FIGURE 2.15. Spatial wavelength granularity R&S architecture without lane changes with three directions (D=3) and four spatial channels (M=4).

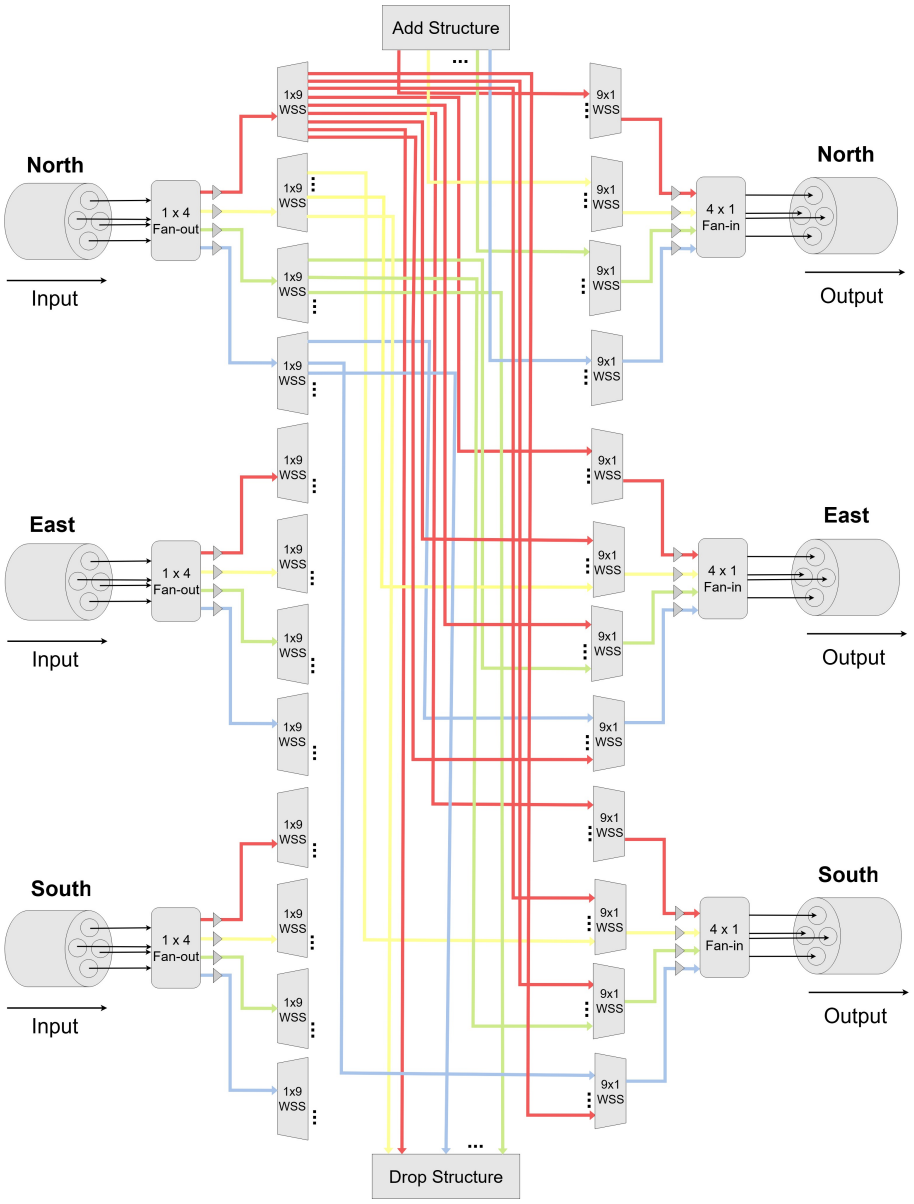


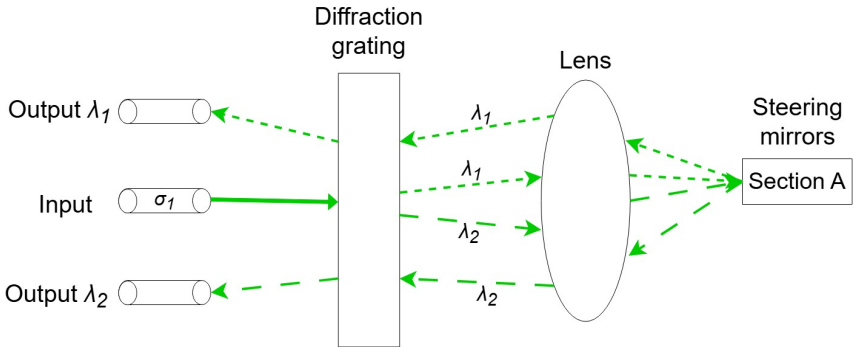
FIGURE 2.16. Spatial wavelength granularity R&S architecture with lane changes with three directions (D=3) and four spatial channels (M=4).

2.4.3. Wavelength granularity architecture

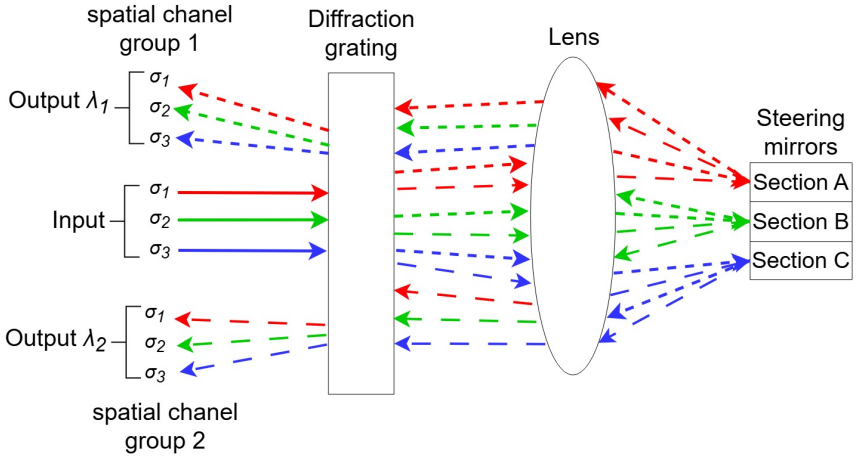
In the wavelength granularity strategy, shown in Figure 2.12 (e), which sacrifices spatial granularity to simplify the switching hardware, instead of routing signals individually per spatial channel and per wavelength, all spatial channels are routed together for each wavelength. This is achieved with a single WSS modified to support joint switching of all the spatial channels that share the same wavelength [15]. The architecture associated with this strategy is known as spatially jointed switching ROADM [35].

Unlike a conventional WSS, which treats each wavelength individually, the JS WSS is a device used for SDM ROADMs, where a specific wavelength from all the spatial

channels is routed as a group [11]. Figure 2.17 a) shows a 1×2 conventional WSS, considering that the input fiber transports two wavelengths, which are represented by green dashed and dotted lines. The diffraction grating demultiplex the two wavelengths, the lens directs the two wavelengths to the respective mirror that forwards the wavelengths to the respective output fiber. Figure 2.17 b) shows a $3 \times (1 \times 2)$ JS WSS, where each input core transports two wavelengths. Each core is represented by a different color, red, blue and green and each one of the two wavelengths by the dashed and dotted lines. Likewise, the diffraction grating separates the two wavelengths from the three cores, while the lens focuses these wavelengths at different spatial positions on the steering mirrors. These mirrors are divided into sections, where each section is responsible for a specific spatial channel, simultaneously deflecting all the beams to the desired output with the same deflection angle. In this way, spatial channels that share the same wavelength are grouped and routed together, reducing the complexity of switching and optimizing the use of the optical spectrum [11].



(A) Conventional 1×2 WSS with 2 wavelength channels.



(B) JS 1×2 WSS with 3 spatial channels with 2 wavelengths each.

FIGURE 2.17. Example of a 1×2 conventional WSS and JS WSS.

Figure 2.18 shows an R&S SDM ROADM-based architecture with wavelength granularity, with three directions (D=3) and four spatial channels (M=4). In this architecture, each group of spatial channels (with channels of the same wavelength) is represented by

a group of colors in the input and output JS WSSs. This architecture consists of three $4 \times (1 \times 3)$ input JS WSSs and three $4 \times (3 \times 1)$ output JS WSSs. The input JS WSSs allow a group of spatial channels with the same wavelength to be switched to a specific direction or to the drop structure. The output JS WSSs of a specific direction receive a group of spatial channels from the other directions or from the add structure. For a generic ROADM with wavelength granularity, D $M \times (1 \times D)$ input JS WSSs and D $M \times (D \times 1)$ output JS WSSs are required.

In the fractional wavelength granularity, shown in Figure 2.12 (f), the same architecture used for the wavelength granularity can be used, since the JS WSSs can select for the same output a group of wavelengths, instead of a single wavelength similarly to what is used in the wavelength granularity scenario.

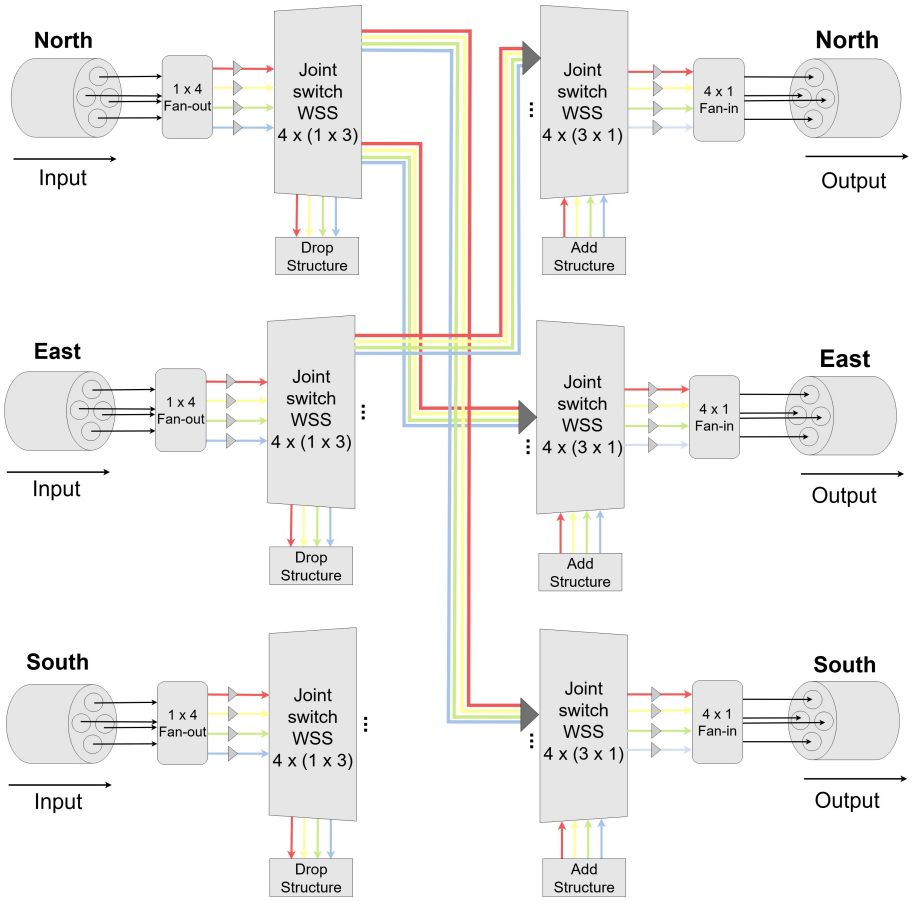


FIGURE 2.18. Wavelength granularity architecture with three directions (D=3) and four spatial channels (M=4).

2.4.4. Fractional space-full wavelength granularity architecture

In the fractional space-full wavelength granularity strategy, shown in Figure 2.12 (g), unlike the wavelength granularity strategy where there is only one spatial group with the same wavelength, several spatial groups can be formed within the same wavelength. This allows for greater flexibility in routing, optimizing the use of optical resources in high-capacity networks [11],[38].

Figure 2.19 shows an SDM R&S ROADM-based architecture with fractional space-full wavelength granularity without lane changes, with three directions (D=3), four space channels (M=4) and two space groups (G=2). The spatial groups are differentiated by color: blue, red, yellow and green. The first spatial group includes the spatial channels represented by the colors red and yellow, while the second group contains the green and blue channels. This architecture consists of 6 input JS WSSs 2×(1×3) and 6 output JS WSSs 2×(3×1). The input JS WSS routes all the wavelengths of a spatial group to the corresponding output JS WSS, ensuring that the signals remain correctly grouped, and to the drop structure. The output JS WSS receives and groups wavelength channels from the input JS WSS that belong to the same space group or add structure. For a generic ROADM with fractional space-full wavelength granularity without lane changes, G×D G×(1×D) input JS WSSs and G×D G×(D×1) output JS WSSs are required.

Likewise, an SDM R&S ROADM-based architecture with fractional space-full wavelength granularity with lane changes, with D=3, M=4 and G=2 consists of 6 input JS WSSs 2 × (1 × 5) and 6 output JS WSSs 2×(5×1). In this architecture, spatial channels can be redirected to different directions within the network, increasing routing flexibility. To allow for the extraction and addition of channels, the architectures A/D structure must be able to manage spatial groups independently. For a generic ROADM with fractional space-full wavelength granularity with lane changes, G×D G×[1×(D+G)] input JS WSSs and G×D G×[(D+G)×1] output JS WSSs are required.

In the fractional space-fractional wavelength granularity, shown in Figure 2.12 (i), the same architecture used for the fractional space-full wavelength granularity can be used since, as in the wavelength granularity scenario, the JS WSSs can select for the same output a group of wavelengths, instead of a single wavelength.

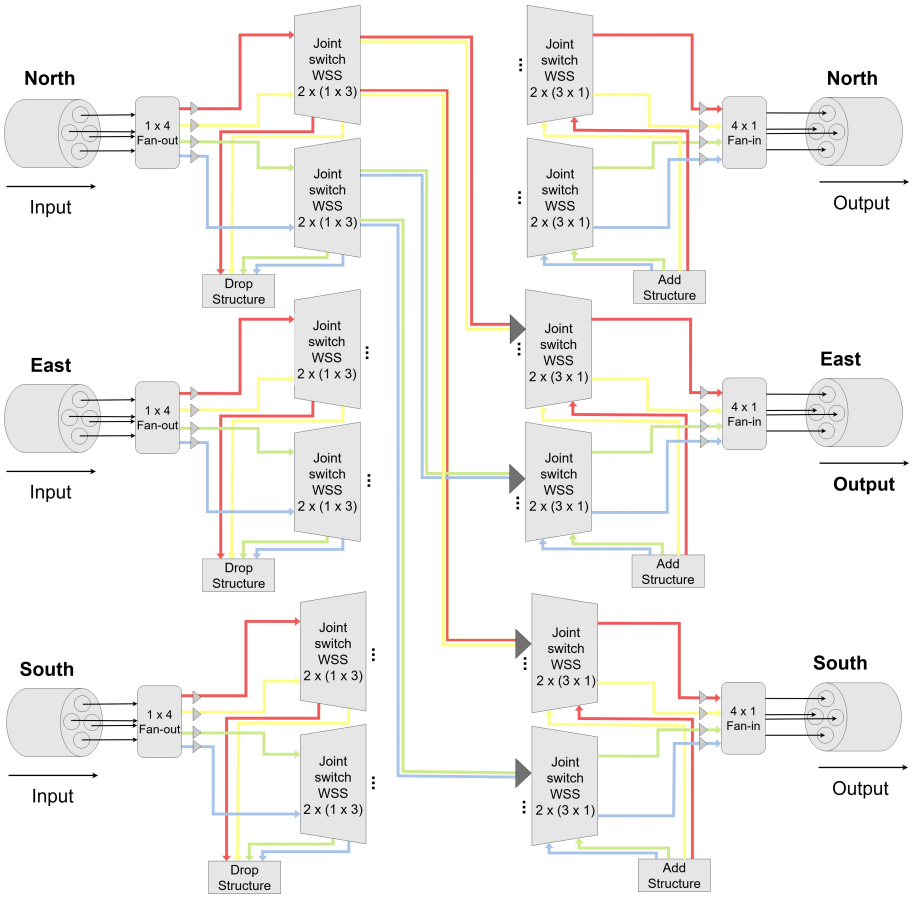


FIGURE 2.19. Fractional space-full wavelength granularity architecture without lane changes with three directions (D=3) and four spatial channels (M=4).

2.4.5. SDM node architecture comparison

Table 2.3 shows the number and type of components (OXCs, WSSs or JS WSSs) and their dimension (number of inputs and outputs) for each one of SDM node architectures studied in the previous sub-sections, with and without lane changes considering only the express structure. Note that to obtain the expressions for the different architectures, it was assumed, as for the MB nodes, that we only have one output for the drop structure and one input for the add structure per spatial channel, and that each direction does not switch information back to the same direction.

From Table 2.3, we can conclude that the architectures that have the higher number of components are the space-wavelength granularity and the full space-fractional wavelength granularity, which are the studied architectures with the highest granularities. Space granularity architectures have less components. We can also conclude that the components with the largest dimensions are the OXCs used in the space granularity architecture with lane changes, and the JS WSSs used in the wavelength granularity. The number of cores, M, does not influence the dimension of the components in the space and space/wavelength architectures without lane changes, whereas for the other architectures both the number of cores and directions impact the components dimension.

TABLE 2.3. Number and type of components and their size in the express structure for each of the SDM architectures.

Granularity	Lane Changes	Type and Number of components	Dimensions of OXC	Dimensions of WSS	Dimensions of WSS JSs
Space/ Fractional Space	without	M OXCs, $2 \times D \times M$ OAs	$(D+1) \times (D+1)$	-	-
	with	1 OXC, $2 \times D \times M$ OAs	$(D \times M + M) \times (D \times M + M)$	-	-
Space-wavelength/ Fractional Wavelength	without	$2 \times D \times M$ WSSs, $2 \times D \times M$ OAs	-	$1 \times D$	-
	with	$2 \times D \times M$ WSSs, $2 \times D \times M$ OAs	-	$1 \times [((D-1) \times M) + 1]$	-
Wavelength/ Fractional Wavelength	not applicable	$2 \times D$ WSS JSs, $2 \times D \times M$ OAs	-	-	$(M \times 1) \times (M \times D)$
Fractional space-full wagevelgth / Fractional space-fractional wavelength	without	$2 \times G \times D$ WSS JSs, $2 \times D \times M$ OAs	-	-	$\frac{M}{G} \times (D \times \frac{M}{G})$
	with	$2 \times G \times D$ WSS JSs, $2 \times D \times M$ OAs	-	-	$\frac{M}{G} \times [\frac{M}{G} \times [(D-1) \times G + 1]]$

2.5. Comparison between MB and SDM node architectures

In this section, we compare the number and type of components, as well as the respective cost for some of the MB and SDM node architectures previously analyzed, considering that each node has the same bandwidth per direction available. We have considered in our study an available bandwidth of 16 THz (which can accomodate 320 channels with 50 GHz spacing). For the SDM node scenario, it means that, for each direction, we must have a MCF fiber with 4 cores, M=4, (assuming that each core uses the C-band with a 4 THz bandwidth), whereas for the MB node scenario, we consider that the C+L+S bands have a total bandwidth of 16 THz, as shown in Fig. 2.5, corresponding to B=3, for each node direction. We also compare those nodes regarding their switching granularity and power consumption. We consider in this comparison study the MB baseline, MB common band and MB SOA-based node architectures, and the SDM space and space-wavelength node architectures, as these are the architectures more readily available, with the highest/lowest granularity and highest/lowest number of components of those analyzed in the previous sections.

Table 2.4 shows the type and number of components and their dimensions for the express structure of the two SDM nodes considered with D=3 and M=4 and the type and number of components and their dimensions for the express structure of the MB nodes considered with D=3 and B=3, according to Tables 2.2 and 2.3. The dimension of the DEMUX and MUX is not shown in the Table 2.4, but a 1×3 dimension is considered. In the case of SOA-based architecture, we consider 80 channels instead of 24 (a 200 GHz channel bandwidth is assumed in [21]) so that the comparison with the other architectures is more fair, even though these values of channels are not practical in a SOA-based architecture.

Table 2.5 shows the cost of each component normalized to the OA cost in band C based on the data provided in [18], [32] and [39]–[41]. The cost of AO-WC depends of the cost of the C-band transponder, with a parameter β that varies between 0.5 and 2. In our case, we chose the worst case, with $\beta = 2$ [41]. The cost of the $N \times N$ OXC is given by $c_{32} \times (N/32)$, where c_{32} is the cost of a 32×32 OXC, whose cost is 3.75 times the cost of a 1×9 WSS that supports 96 wavelengths in the C band ($3.75 \times 5 = 18.75$) [40]. From Table

TABLE 2.4. Number and type of components in the express structure and their size for each of the SDM architectures with D=3, M=4 and the MB architectures with D=3, B=3.

	Granularity	Lane Changes	Type and Number of components	Dimensions of OXC	Dimensions of WSS	Dimensions of splitters/combiners
SDM	Space	without	4 OXCs, 24 OAs	4×4	-	-
		with	1 OXC, 24 OAs	16×16	-	-
	Space-wavelength	without	24WSSs, 24 OAs	-	1×3	-
		with	24WSSs, 24 OAs	-	1×9	-
MB	Space-wavelength (Baseline)	not applicable	3 MB DEMUX, 3 MB MUX, 18 OAs, 18 WSS	-	1×3	-
	Space-wavelength and band (Common band)	not applicable	3 MB DEMUX,3 MB MUX, 18 OAs, 18 WSS, 12 AO-WCs	-	1×7	-
	Space-wavelength (SOA-based architecture)	not applicable	3 MB DEMUX, 3 MB MUX, 18 Fixed WDM DEMUX, 720 splitters, 720 combiners, 720 SOAs	-	-	1×3

2.5, we conclude that the cost of MB MUX/DEMUX and splitters/combiners is very low, unlike transponders and AO-WCs, which are very expensive components. Using these costs, we can calculate the express struture cost of the studied architectures.

TABLE 2.5. Cost of components.

Component	Cost		
	C-band	L-band	S-band
MB MUX/DEMUX [39]	0.04		
Splitter/Combiner, with $N \geq 4$ [41]	$0.0167 \times N/4$		
OA [39]	1	1.2	1.5
AO-WC [18]	72		
SOA [32]	0.2		
$N \times N$ OXC [40]	$18.75 \times N/32$		
1×4 WSS [18]	2.5	3	3.75
1×9 WSS [18]	5	6	7.5
1×80 WSS [18]	30	36	45
Transponder [39]	36	43.2	54

For the A/D structure, we consider an A/D structure with CD per spatial channel, as discussed in section 2.2. Accordingly with Table 2.1, where N_w=80 wavelengths per direction and an A/D ratio of 20% have been considered (W=16), for the SDM architectures (with D=3, M=4) and for the MB architectures (with D=3 and B=3), we can use the A/D structure in Figure 2.20 and Figure 2.21, respectively.

The SDM drop structure, shown in Figure 2.20, has 4 parallel WSSs 3×1 in cascade with 4 parallel WSSs 1×48. Each parallel drop structure corresponds to one spatial channel. In this A/D structure, a total of 192 C-band transponders is required.

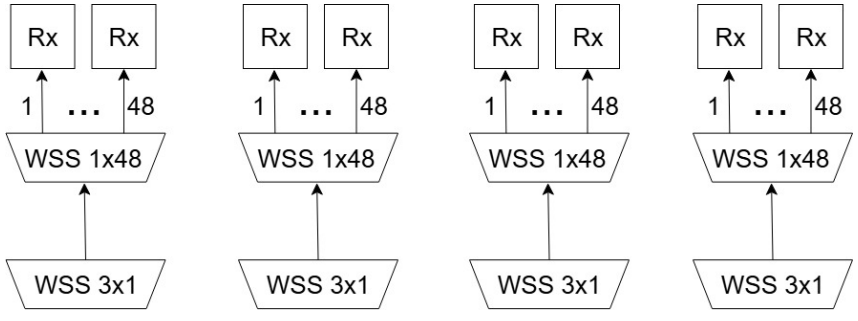


FIGURE 2.20. Drop structure considered for the SDM architectures.

The MB drop structure, shown in Figure 2.21, has 3 parallel WSS 3×1, each working in its own band. For the C-band, we have one WSS 3×1 in cascade with one WSS 1×52. For the S-band, we have one WSS 3×1 cascaded with one WSS 1×62 and for the L-band, we have one WSS 3×1 in cascade with one WSS 1×78 (giving a total of $52 + 62 + 78 = 192$ transponders, the same as for the SDM solution). This A/D structure only works for the Baseline and SOA-based architectures, because in the Common band architecture, we must have 192 transponders, all in the C band. For the Common band architecture, we use an A/D structure similar to the structure shown in Figure 2.21, but all transponders refer to the C band, since the S and L band channels are converted to the C band.

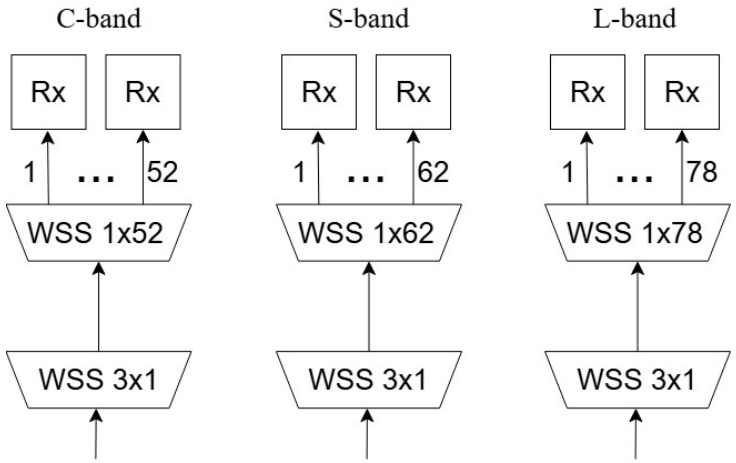


FIGURE 2.21. Drop structure considered for the MB architectures.

Table 2.6 shows the total cost (express cost plus A/D cost) of the SDM (space and space-wavelength) and MB (Baseline, common band and SOA-based) architectures presented in this case study, as well as the express and A/D costs. As for the cost of the express structure, from Table 2.6, we conclude that the Common Band is the most expensive architecture due to the cost of AO-WCs, and SDM Space is the least expensive architecture. In terms of the cost of the A/D structure, it is higher in MB than in SDM since the transponders for other bands than C-band are more expensive. So we conclude that MB architectures have a higher cost than SDM architectures, with the SDM space granularity architecture being the least expensive architecture (total cost of 7075) and MB SOA-based architecture being the most expensive (total cost of 8880). Another interesting conclusion comes from the fact that the transponder cost represents approximately 96% of the total cost for all architectures considered.

Table 2.7 shows the power consumption of each component based in [42]–[46]. The power consumption of the AO-WC was calculated having in mind that each channel (a total of 96 channels is considered) consumes 0.5 W [45]. The power consumption of an OXC is typically three times lower than that of a ROADM. For example, a 4×4 ROADM has 8 WSSs 1×3, so the consumption is 15 W $\times 8 = 120$ W. The consumption of a 4×4

TABLE 2.6. Cost of the studied SDM architectures with D=3 and M=4 and the MB architectures with D=3 and B=3.

	Granularity	Lane Changes	Type and Number of components	Cost of components	Express structure cost	A/D structure cost	Total cost
SDM	Space	without	4 OXCs 4×4	18.75	42.75	7042	7085
			24 OAs	24			
			8 WSSs	130			
			192 Transponders	6912			
		with	1 OXC 16×16	9.38	33.38	7042	7075
			24 OAs	24			
			8 WSSs	130			
			192 Transponders	6912			
	Space-wavelength	without	32 WSSs	190	84	7042	7126
			24 OAs	24			
			192 Transponders	6912			
		with	32 WSSs	250	144	7042	7186
			24 OAs	24			
			192 Transponders	6912			
MB	Baseline	not applicable	3 MB DEMUX, 3 MB MUX	0.24	77.94	8710	8788
			24 WSSs	175.75			
			18 OAs	22.2			
			192 Transponders	8589.6			
	Common band	not applicable	3 MB DEMUX, 3 MB MUX	0.24	997.44	7010	8007
			24 WSSs	208.5			
			18 OAs	22.2			
			12 AO-WCs	864			
			192 Transponders	6912			
	SOA-based architecture	not applicable	3 MB DEMUX, 3 MB MUX	0.24	169.73	8710	8880
			18 Fixed WDM DEMUX and MUX	1.44			
			720 splitters, 720 combiners	24.05			
			720 SOAs	144			
			6 WSSs	120.25			
			192 Transponders	8589.6			

OXC will be $120/3 = 40$ W [43]. To calculate the power consumption of the architectures, we consider a 1×9 WSS [42], [46].

TABLE 2.7. Power consumption of components.

Component	Power Consumption		
	C-band	L-band	S-band
Optical Amplifier [42]	15 W	15 W	20 W
AO-WC [44]	48 W		
Transponder [46]	16 W	20 W	24 W
1×9 WSS [46]	15 W	20 W	25 W
SOA [45]	10 W		
4×4 OXC [43]	40 W		
32×32 OXC [43]	320 W		

Table 2.8 shows the total power consumptions of the studied architectures. From Table 2.8, we can conclude that, in general, transponders are the components that consume the highest power, contributing significantly to the total power of each architecture. The architecture that consumes the most power is the MB SOA-based architecture (power consumption of 11180 W), due to the high number of SOAs used and their power consumption (7200 W), followed by the MB baseline, due to the higher power consumption of the transceivers in L and S-bands in comparison with the C-band. We also concluded that the other architectures have a similar power consumption, with SDM space without

lane changes and SDM space with lane changes having the lowest power consumption (3712 W and 3872 W, respectively).

TABLE 2.8. Power consumption of the studied SDM architectures with D=3 and M=4 and the MB architectures with D=3 and B=3.

	Granularity	Lane Changes	Type and Number of components	Power Consumption of components	Power Consumption of architectures
SDM	Space	without	4 OXCs 4×4	160 W	3712 W
			24 OAs	360 W	
			192 Transponders	3072 W	
			8 WSSs	120 W	
		with	1 OXC 16×16	320 W	3872 W
			24 OAs	360 W	
			192 Transponders	3072 W	
			8 WSSs	120 W	
	Space-wavelength	without	32 WSSs	480 W	3912 W
			24 OAs	360 W	
			192 Transponders	3072 W	
		with	32 WSSs	480 W	3912 W
			24 OAs	360 W	
			192 Transponders	3072 W	
MB	Baseline	not applicable	24 WSSs	412 W	4562 W
			18 OAs	270 W	
			192 Transponders	3880 W	
	Common band	not applicable	18 OAs	270 W	4278 W
			24 WSSs	360 W	
			12 AO-WCs	576 W	
			192 Transponders	3072 W	
	SOA-based architecture	not applicable	720 SOAs	7200 W	11180 W
			192 Transponders	3880 W	
			6 WSSs	100 W	

The cost and power consumption studied previously are two important factors, but the switching granularity of the architectures is also important. We concluded that SDM Space architecture is the architecture with the lowest cost and lowest power consumption, but it is also the architecture with the lowest switching granularity (space), unlike MB Common band architecture, which is the architecture with one of the highest costs and highest power consumption, but with a higher granularity- switching is possible in all three dimensions, space, wavelength and band.

2.6. Conclusions

In this chapter, we reviewed the fundamental concepts of ROADMs, where we also discussed different possible A/D structures implementations. We studied several MB and SDM architectures, presented their granularities and analysed all their components, the dimension of the components and their power consumption.

In terms of architecture costs, we analysed the cost of the express structure, the A/D structure and the total cost of the ROADM architectures. Regarding the express structure cost, we concluded that the most expensive architecture is the MB Common band architecture due to the cost of AO-WCs, while the least expensive is the SDM Space architecture. As for the A/D structure, we concluded that MB architectures have a higher

cost than SDM due to the use of transponders not only in the C band, but also in the S and L bands, which have a higher cost. In terms of total cost (express and A/D), we have concluded that the most expensive architecture is the MB SOA-based architecture (with space and wavelength granularity) and the lowest cost is the SDM space architecture (only with spacial granularity), with MB SOA-based architecture being approximately 25% more expensive than SDM space architecture.

We also studied the ROADM architectures in terms of their power consumption. We concluded that the components that consume the most power in all architectures are the transponders, representing approximately 73% of the total power consumption for all architectures. In terms of total power consumption, we concluded that the architecture that consumes the most is the MB SOA-based architecture due to the number of SOAs used and their consumption. The other architectures all have similar power consumption, with the MB common band architecture (with space, wavelength and band granularity) also being one of the most power consuming and the SDM space architecture being the architecture with the lowest power consumption, at the expense of reduced granularity.

CHAPTER 3

Node architectures for MBoSDM networks

3.1. Introduction

In this chapter, we discuss the functionalities of several MBoSDM ROADM node architectures presented in the literature [14], [30], [47], and analyse their cost and power consumption. In section 3.2, we begin by discussing the granularity type of MBoSDM ROADM node architectures. In section 3.3, we present the MBoSDM architectures already proposed in the literature: Baseline architecture for MBoSDM [14], MBoSDM architecture with one S-OXC per band [14], MBoSDM architecture with a single S-OXC [14], MBoSDM architecture without a S-OXC [14] and the FLEX-SCALE architecture [30], [47]. In section 3.4, we compare the number of components and their dimensions, as well as the power consumption of the different MBoSDM architectures. Finally, in section 3.5, we present the conclusions of this chapter.

3.2. Switching granularity

In MBoSDM ROADM node architectures, switching can be done in three dimensions, space, wavelength and between bands (e.g, C, L, S). Figure 3.1 shows the spatial granularity strategy considering a MBoSDM scenario with 6 spatial channels, 3 bands in each spatial channel and 8 wavelengths in each band. This is a combination of the MB and SDM switching strategies shown previously, respectively, in Figures 2.6(a) and 2.12(b). All the other granularities mentioned in the previous sections (see Figure 2.12) follow the same reasoning in combining granularities to achieve MBoSDM switching as the one shown in Figure 3.1.

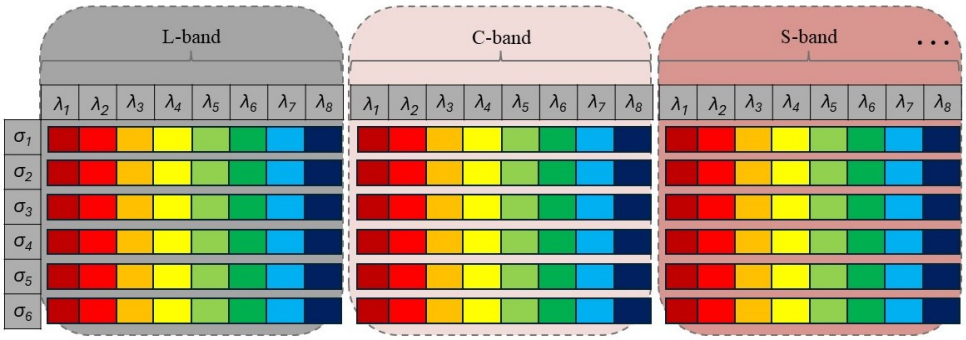


FIGURE 3.1. Space switching strategy in MBoSDM networks.

3.3. MBoSDM node architectures

In [14], four different node architectures for MB and SDM-based optical networks are presented, known as MBoSDM ROADM nodes. Three of the four architectures follow a hierarchical approach, where the switching functionalities are distributed over different levels: spatial, band and wavelength. This hierarchical structure makes it possible to adapt the complexity of the switching to the type of traffic, favoring scalable solutions for core networks with high capacity and flexibility requirements. Moreover in [30], [47] another hierarchical MBoSDM node architecture is proposed, which uses a new component that adds flexibility to the band switching - the waveband selective switch (WBSS). In the following sub-sections these node architectures are presented and their functionalities explained.

3.3.1. Baseline architecture for MBoSDM

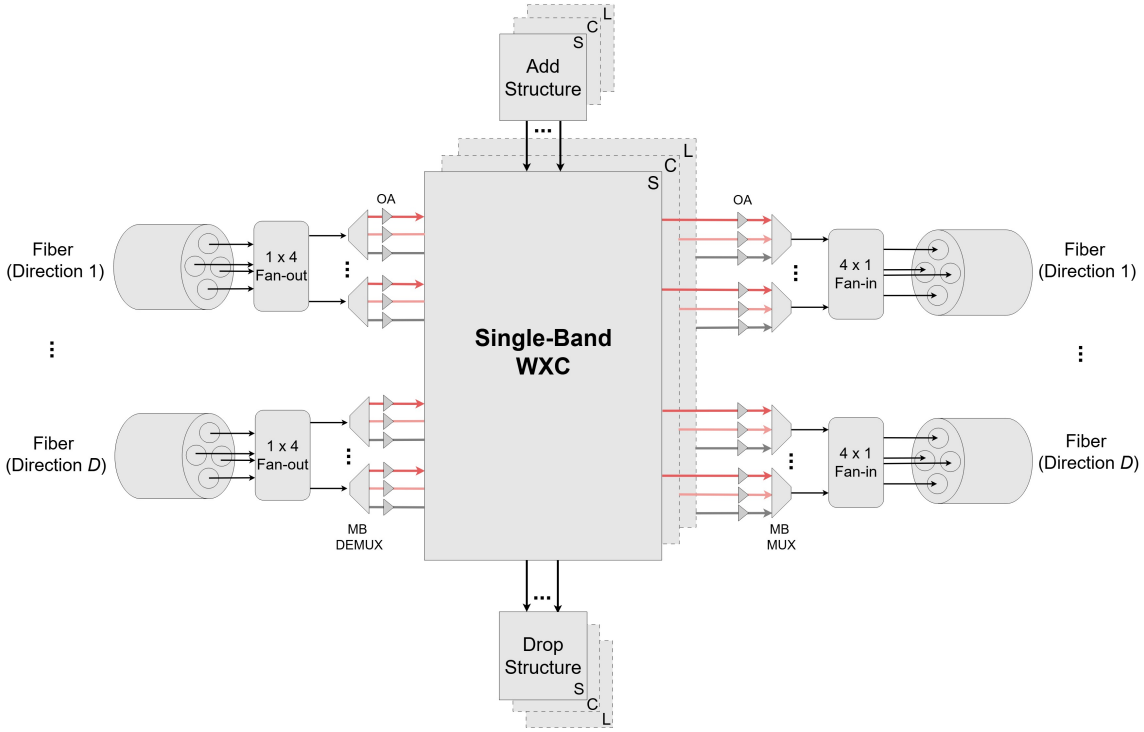


FIGURE 3.2. Baseline architecture for MBoSDM [14].

The baseline architecture in [14] and shown in Figure 3.2, uses a modular structure with several single-band wavelength cross-connects (WXCs). In this architecture, the bands from each core are separated with a MB DEMUXs and amplified with dedicated-band OAs. The single-band WXCs route the input signals to the output cores or to the drop structures. The signals routed to the output are again amplified and the bands are coupled using a MB MUX. In this architecture, one WXC is needed for each band (in our case, as we are considering 3 bands, 3 single-band WXCs will be needed), and each A/D structure works for a specific band. Although this approach is functional, it quickly

becomes complex and difficult to scale as the number of bands and cores increases. To overcome these limitations, three alternative architectures were proposed in [14].

3.3.2. MBoSDM architecture with one S-OXC per band

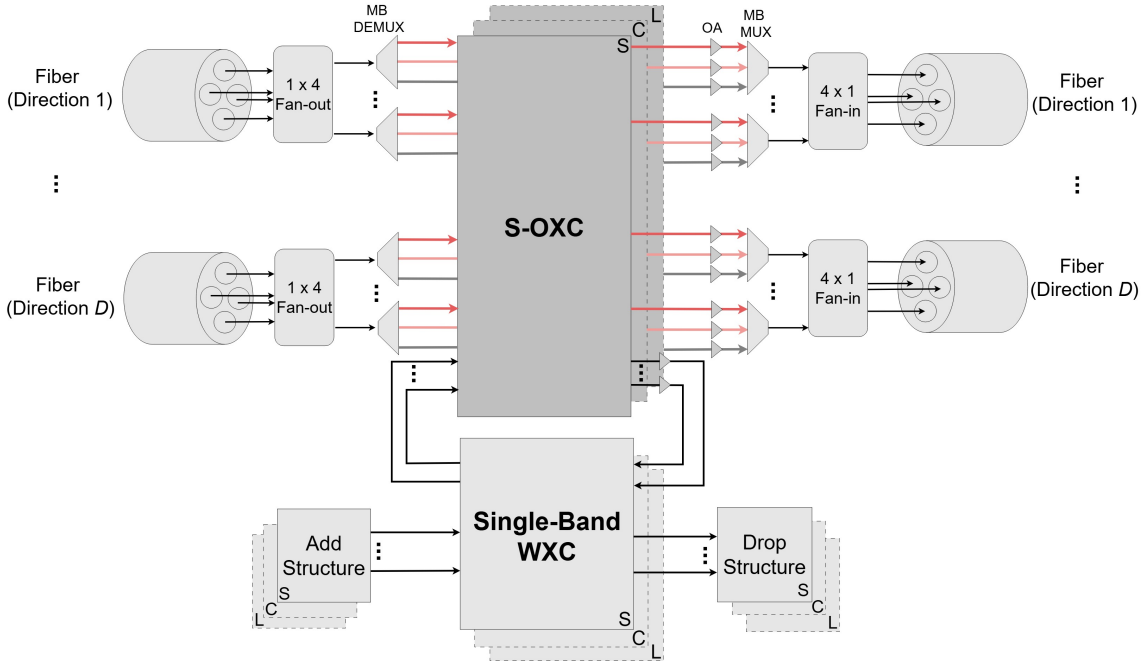


FIGURE 3.3. MBoSDM architecture with S-OXC per band.

The architecture represented in Figure 3.3, also mentioned in [39], uses a spatial optical cross-connect (S-OXC), one for each fiber band, which allows switching between cores without the need to process all signals individually through the express structure. The only difference to the baseline architecture is that we have an S-OXC, which routes each amplification band to an output MB-MUX or to a single-band WXC. These connections depend on N_C, which represents the connections that should pass or do not pass through the single-band WXC (black lines). When a channel needs to be dropped or new channels are added, the single-band WXC is responsible for the processing at the wavelength level.

3.3.3. MBoSDM architecture with a single S-OXC

The architecture represented in Figure 3.4 uses a multi-band WXC to implement the processing at the band and wavelength level, which means that in this architecture only one S-OXC is required for all bands, without the need of using several S-OXCs in parallel, as in the previous architecture. To perform the amplification, the bands must be separated at the output of the S-OXC for each node direction. This architecture has less flexibility than the previous architecture because core switching is simultaneously performed in all bands by the S-OXC [14].

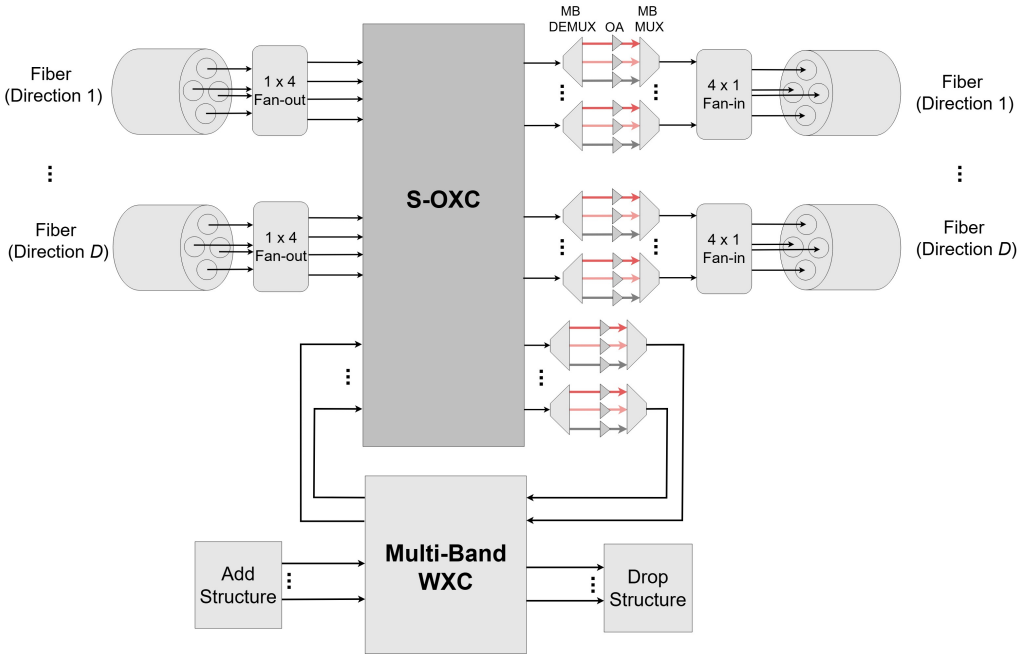


FIGURE 3.4. MBoSDM architecture with a single S-OXC.

3.3.4. MBoSDM architecture without a S-OXC

The two previous architectures shown in Figures 3.3 and 3.4 can be affected by failures in the S-OXC, leading to a complete failure of the node. So, to avoid a single point of failure, a new architecture has been proposed in [14]. Figure 3.5 is a simplified version of Figure 3.3, using fixed connections between cores instead of an S-OXC, which reduces costs and losses, but leading to a architecture that is much less flexible than the previous architectures.

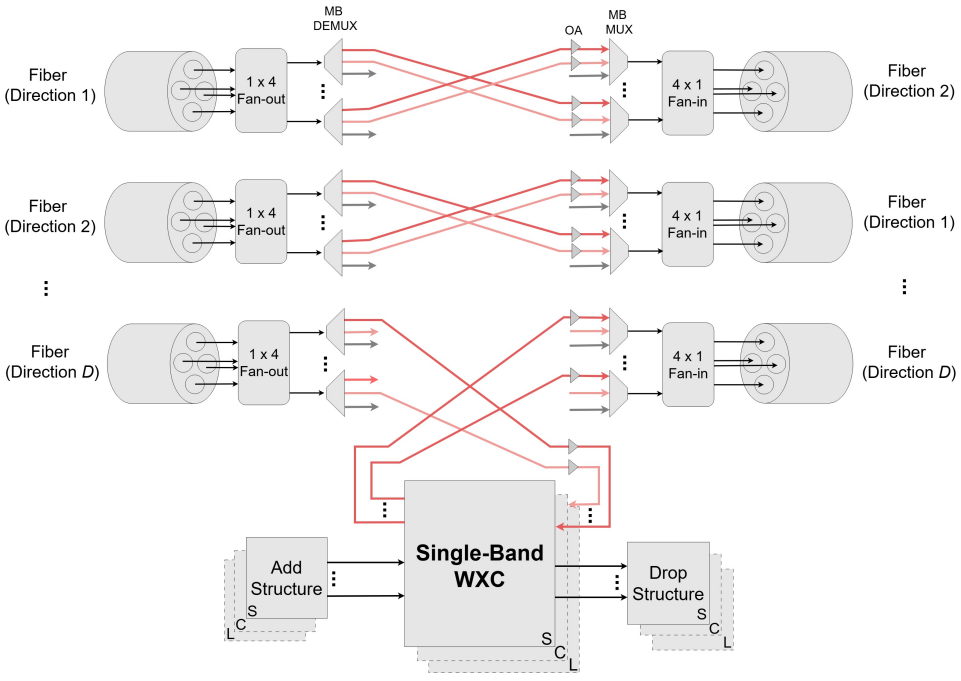


FIGURE 3.5. MBoSDM architecture without a S-OXC.

3.3.5. FLEX-SCALE architecture

In [30] and [47], another MBoSDM node architecture is proposed, named FLEX-SCALE architecture. Before presenting this architecture with detail, three previous architectures were analysed in [47]. In the first one, depicted in Figure 3 of [47], the express structure has the same functionality as the architecture of Figure 3.3, having the capacity of band and wavelength switching. Nevertheless, the architecture of Figure 3 of [47] has the capacity of band A/D alongside wavelength A/D, whereas the architecture of Figure 3.3 has only wavelength A/D capacity. The second architecture, depicted in Figure 4 of [47], can be compared to the architecture of Figure 3.4, with some differences. Both architectures have only one S-OXC for core switching, but the architecture in Figure 4 of [47] has the capacity of switching both bands and wavelenghts, whereas in the architecture of Figure 3.4 only wavelength switching is allowed. The third architecture, depicted in Figure 5 of [47], has more flexibility regarding band switching, since a WBSS is used, which allows to select and build a band with an arbitrary group of wavelengths. Nevertheless, this architecture has a single S-OXC that is viewed as a single point of failure. This shortcoming is resolved with the FLEX-SCALE architecture.

The FLEX-SCALE architecture is presented in Figure 3.6 in which a hierarchical structure with three layers (core, band, and wavelength) represented by the three different colors is shown. The first layer (in grey color in Figure 3.6) responsible for switching fibers and bands uses WBSSs, which are used to select the bands, and can select an entire core or just some bands of a particular core. The WBSS can switch individual bands, in the same way a WSS can switch individual wavelenghts, and can also switch groups of bands, also in the same way a WSS can switch groups of wavelenghts, adapting to network real-time needs and providing better spectral flexibility [47]. The WBSS is developed using silicon photonic technology, allowing fast and flexible switching of spectral bands through tunable network filters integrated into a photonic integrated circuit (PIC) [47]. In Figure 3.6, fibers with 4 cores are used in all directions, but this architecture can be used also with fibers with different number of cores per direction [30], [47].

At the WBSS output, the grey lines can switch the entire core or only some bands of that core. On the other side, the red lines transport only one band and are directed to the second layer (in blue color in Figure 3.6), which has an inter-band OXC, that can extract an entire band through the band receiver or insert a band with the band transmitter, or switch the bands that has received from the first layer. Also, stages of OAs (i.e. composed of one OA for each band) are placed at the input of the input WBSSs and at the output of the output WBSSs. In [48] it is referred that when the WBSSs are used for core switching, the insertion losses are negligible, whereas when the WBSSs are used to switch bands, the insertion losses depend on the adaptive finite-impulse response (FIR) and on the number of junctions of the crossbar matrix and cannot be neglected (assuming 56 taps per filter with a 0.1 dB IL per tap and $4 \times 13 = 52$ junctions in the crossbar switch with a 0.05 dB IL per junction, the ILs can be computed as in [48], $2 \times 56 \times 0.1 + 4 \times 13 \times 0.05 = 13.8$

dB). The third layer (dark gray color in Figure 3.6) uses a conventional intra-band OXC per band and WSSs for switching at the wavelength level. Figure 3.6 shows three intra-band OXCs, one for C-band, one for S-band and one for L-band. In this architecture for the A/D structure, we do not have a structure with WSSs like the other architectures, since Add and Drop are directly connected to the Intra-band OXCs. In [47], to avoid any points of failure in the intra-band OXCs, the authors consider that there are two intra-band OXCs per band for redundancy purposes. In the following calculations, we will consider only one intra-band OXC per band, as shown in Figure 3.6. The OXCs are based on piezoelectrical actuators, and OXCs dimensions of 384×384 are, nowadays, in a commercial status (576×576 are foreseen in a near future). Note also that, currently, these OXCs only work in the C and L bands [47].

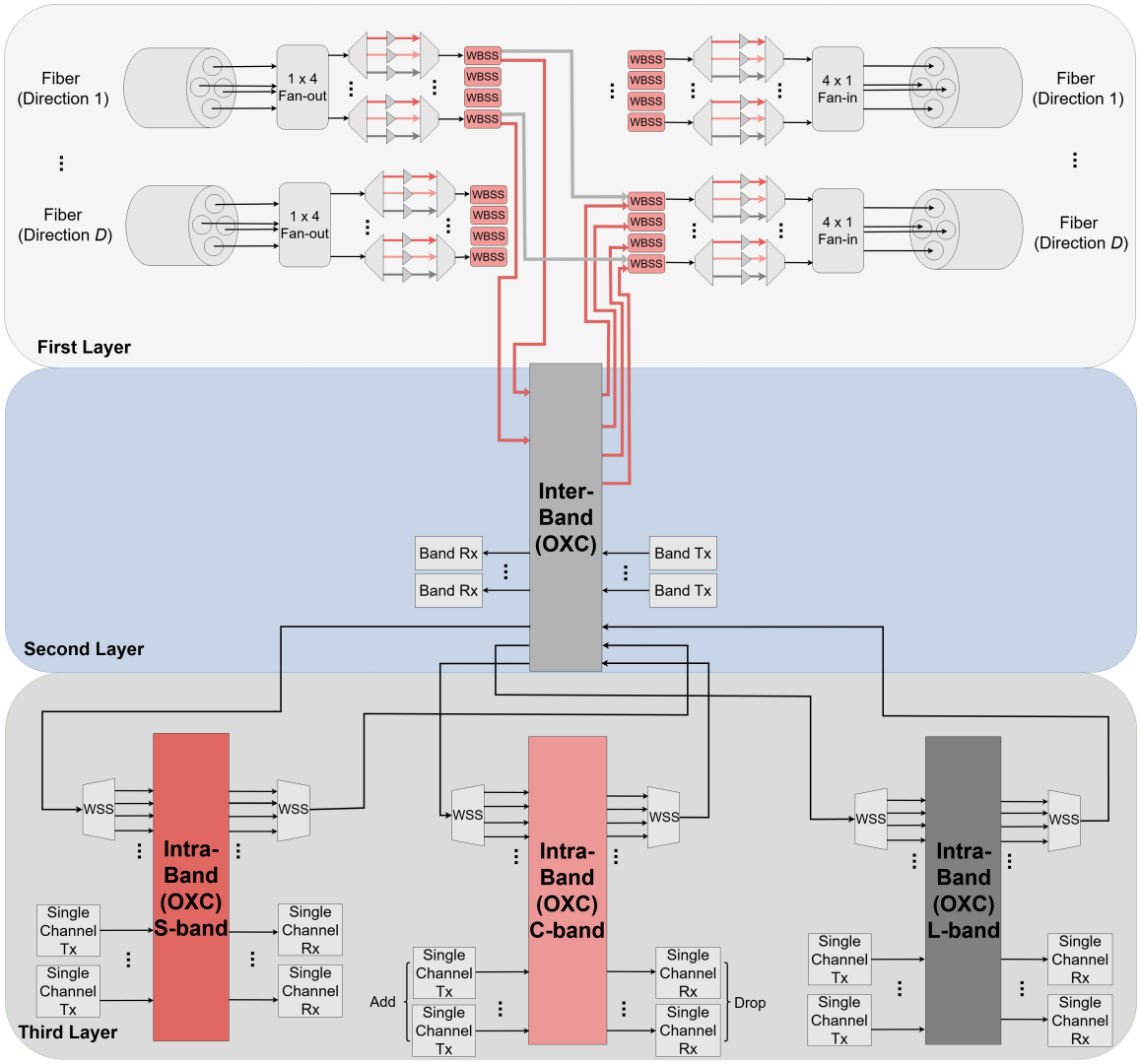


FIGURE 3.6. FLEX-SCALE architecture considering a ROADM node with D directions, a 4 core MCF fiber per direction and 3 bands per core (C+L+S).

3.4. MBoSDM node architectures comparison

In this section, we compare the number and type of components for the MBoSDM architectures presented in section 3.3, analysing their cost and power consumption.

The dimension of the S-OXCs and WSSs presented in the architectures represented in Figures 3.3, 3.4 and 3.5 depends on the number of cores that are directly connected between the input and output of the S-OXC, a variable that is defined by N_C. Note that in the scenario with $N_C = 0$, there are no cores communicating directly to each other (this architecture is functionally equivalent to the baseline architecture), and with $N_C = MD$, all the cores communicate directly between them [14]. Figure 3.7 shows the number of WSSs and OAs, considering a single band (i.e. B=1), as a function of N_C for three different network cases: 1) a small network node with $M = 4$ and D=3; 2) a medium network node with $M = 4$ and $D = 5$; 3) a large network node with $M = 4$ and $D = 7$ and $D = 8$. A similar study has been made in [14] and similar results for $M = 4$ and $D = 8$ have been obtained in Figure 3.7. From Figure 3.7, we can conclude that as N_C increases, the number of WSSs and OAs decreases. In particular, for $M = 4$, $D = 3$ and N_C=10, 4 WSSs 1×20 (2×2 WSS considering $N_{A/D} = 0$) and 14 OAs (10 OAs for the direct links and 4 for the links that cross the WSSs) are needed.

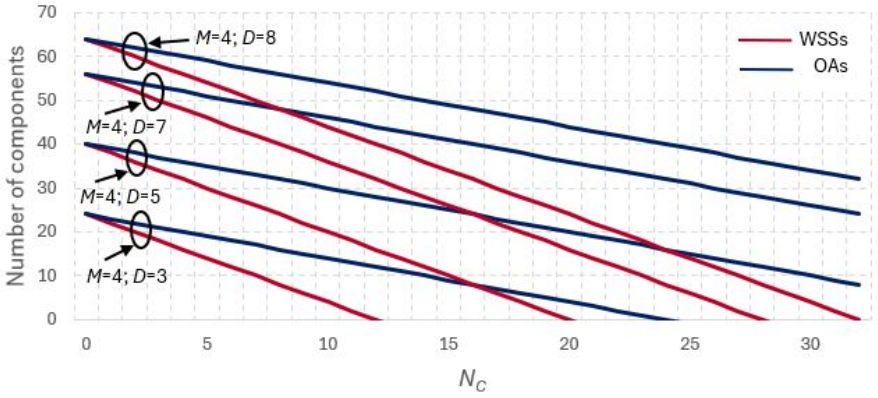


FIGURE 3.7. Number of components (WSSs and OAs) as a function of N_C for several network dimensions.

Table 3.1 shows the number and type of components and their port count (number of inputs and outputs) for the express structure of the MBoSDM architectures described in the previous sub-sections. As observed in Table 3.1, the port count of the WXC, P_{WXC}, depends on M and D and also on $N_{A/D}$, which represents the number of ports of the WSSs connected to the A/D structure [14]. For the scenario with $N_C = MD$, the port count of each WXC in Figures 3.3 to 3.5 is given by $P_{WXC_b} = 2 \times N_{A/D_b}$, with b=C, L, S. For $N_C = 0$, $P_{WXC_b} = 2 \times (M \times D + N_{A/D_b})$, with b=C, L, S. For Figures 3.3 and 3.4, the port count of the S-OXCs with $N_C = MD$ is given by $P_{OXC} = 2 \times M \times D + 2$, whereas with $N_C = 0$, $P_{OXC} = 4 \times M \times D$ (the expression shown in Table 3.1 is generic, except in the case of $N_C = MD$ that includes two A/D ports).

TABLE 3.1. Number and type of components and their port count in the express structure for each of the studied MBoSDM architectures considering the C, L, and S bands.

Architectures	Type and Number of Components	WXC/WSS port count	OXC port count	WBSS port count
Baseline architecture (Figure 3.2)	$M \times D$ MB DEMUXs $M \times D$ MB MUXs $2 \times M \times D \times B$ OAs B single-band WXCs	$P_{WXC_b} =$ $2 \times (M \times D + N_{A/D_b})$, with b = C, L or S	-	-
MBoSDM architecture with an S-OXC per band (Figure 3.3)	$M \times D$ MB DEMUX $M \times D$ MB MUX $2 \times M \times D \times B - N_c$ OAs B single-band WXCs B S-OXCs	$P_{WXC_b} =$ $2 \times (M \times D - N_C + N_{A/D_b})$	$P_{OXC} =$ $4 \times M \times D - 2 \times N_C$	-
MBoSDM architecture with a single S-OXC (Figure 3.4)	$2 \times M \times D \times B - N_c$ MB DEMUX $2 \times M \times D \times B - N_c$ MB MUXs $2 \times M \times D \times B - N_c$ OAs 1 MB WXC 1 S-OXC	$P_{WXC} =$ $2 \times (M \times D - N_C + N_{A/D})$	$P_{OXC} =$ $4 \times M \times D - 2 \times N_C$	-
MBoSDM architecture without a S-OXC (Figure 3.5)	$M \times D$ MB DEMUXs $M \times D$ MB MUXs $2 \times M \times D \times B - N_c$ OAs B single-band WXCs	$P_{WXC_b} =$ $2 \times (M \times D - N_C + N_{A/D_b})$	-	-
FLEX-SCALE architecture (Figure 3.6)	$2 \times M \times D \times B$ OAs $2 \times M \times D$ WBSSs 1 Inter-Band OXC B Intra-Band OXCs $2 \times K_b \times M \times D \times WBSS_{A/D}$ WSSs	$P_{WSS_b} = 1 + WSS_b$	$P_{OXC_{INTER}} =$ $[(M \times D \times WBSS_{A/D}) + N_{B_{Tx}} + K_{WSS}]$ $+ [(M \times D \times WBSS_{A/D}) + N_{B_{Rx}} + K_{WSS}]$ $P_{OXC_{INTRA_b}} =$ $2 \times [(1 + K_{b_{legacy}}) \times N_{WSS_b} \times P_{WSS_b}]$	$P_{WBSS} =$ $M \times (D-1) + WBSS_{A/D} + 1$

For the FLEX-SCALE architecture, based on [30] and [47], we define several variables in order to obtain general expressions for the number and port count of the components presented in Table 3.1. Starting at the first layer, the number of WBSS, N_{WBSS}, is given by $2 \times M \times D$ and the port count of the WBSSs, P_{WBSS}, depends on M and D and also on the number of output ports of each WBSS connected to the inter-band OXC, $WBSS_{A/D}$, a number that is between 1 and 4 (red lines in Fig. 3.6), and should be most likely 1 or 2 [47].

In the second layer, the number of band receivers, $N_{B_{Rx}}$, and band transmitters, $N_{B_{Tx}}$, also depends on $WBSS_{A/D}$. If $WBSS_{A/D} = 1$ (i.e. one dropped band per WBSS), $N_{B_{Rx}} = N_{B_{Tx}} = 1/4 \times M \times D$, meaning that 25% of the bands per WBSS go for add/drop at the node [47], whereas if $WBSS_{A/D} = 2$, it means that there are two dropped bands per WBSS, so, $N_{B_{Rx}} = N_{B_{Tx}} = 1/2 \times M \times D$ [47]. Also in the second layer, the port count of the inter-band OXC, $P_{OXC_{INTER}}$, depends on $WBSS_{A/D}$, on the number of band receivers and band transmitters, and on the number of links routed to the Intra-band OXCs (black lines connecting the third layer in Figure 3.6). The number of links routed to the Intra-band OXCs, which is equal to the number of WSSs of the third layer, is denoted as K_{WSS}. As the third layer includes the number of C, L and S-band WSSs, $K_{WSS} = N_{WSS_C} + N_{WSS_L} + N_{WSS_S}$, where N_{WSS_C} is the number of C-band WSSs, N_{WSS_L} the number of L-band WSSs and N_{WSS_S} the number of S-band WSSs.

In the third layer, the number of C-band WSSs (N_{WSS_C}) depends on K_C, which represents the percentage of Inter-band OXC ports connected to the WBSS that operate in the C band. K_L and K_S represent the same, but for the L and S bands, respectively. The port count of these WSSs, P_{WSS_b} with b=C, L or S, is given by $P_{WSS_b} = 1 + WSS_b$, where WSS_b represents the number of output ports of the WSSs [47]. In this layer, as already referred, we have one intra OXC per band. The percentage of Intra-band OXC ports for the A/D in the C-band is given by $K_{C_{legacy}}$, which is between 20% and 25% of

the number of wavelengths in C-band ($K_{L_{legacy}}$ and $K_{S_{legacy}}$ have the same meaning for the L and S bands) [47].

TABLE 3.2. Number and type of components in the express structure and their port count for each of the studied MBoSDM architectures considering D=3, M=4 and B=3.

Architectures	Type and Number of Components	WXC/WSS port count	OXC port count	WBSS port count
Baseline architecture (Figure 3.2)	12 MB DEMUXs 12 MB MUXs 72 OAs 3 single-band WXCs	$P_{WXC_C} = 48$ $P_{WXC_L} = 48$ $P_{WXC_S} = 48$	-	-
MBoSDM architecture with an S-OXC per band (Figure 3.3)	12 MB DEMUXs 12 MB MUXs 72 OAs (with $N_C = 0$) 66 OAs (with $N_C = 6$) 60 OAs (with $N_C = 12$) 3 single-band WXCs 3 S-OXC	with $N_C = 0$, $P_{WXC_C} = 48$ $P_{WXC_L} = 48$ $P_{WXC_S} = 48$ with $N_C = 6$, $P_{WXC_C} = 24$ $P_{WXC_L} = 24$ $P_{WXC_S} = 24$ with $N_C = 12$, $P_{WXC_C} = 0$ $P_{WXC_L} = 0$ $P_{WXC_S} = 0$	with $N_C = 0$, $P_{OXC} = 48$ with $N_C = 6$, $P_{OXC} = 36$ with $N_C = 12$, $P_{OXC} = 26$	-
MBoSDM architecture with a single S-OXC (Figure 3.4)	72 MB DEMUXs, 72 MB MUXs (with $N_C = 0$) 66 MB DEMUXs, 66 MB MUXs (with $N_C = 6$) 60 MB DEMUXs, 60 MB MUX (with $N_C = 12$) 72 OAs (with $N_C = 0$) 66 OAs (with $N_C = 6$) 60 OAs (with $N_C = 12$) 1 MB WXC 1 S-OXC	with $N_C = 0$, $P_{WXC} = 48$ with $N_C = 6$, $P_{WXC} = 24$ with $N_C = 12$, $P_{WXC} = 0$	with $N_C = 0$, $P_{OXC} = 48$ with $N_C = 6$, $P_{OXC} = 36$ with $N_C = 12$, $P_{OXC} = 26$	-
MBoSDM architecture without a S-OXC (Figure 3.5)	12 MB DEMUXs 12 MB MUXs 72 OAs (with $N_C = 0$) 66 OAs (with $N_C = 6$) 60 OAs (with $N_C = 12$) 3 single-band WXCs	with $N_C = 0$, $P_{WXC_C} = 48$ $P_{WXC_L} = 48$ $P_{WXC_S} = 48$ with $N_C = 6$, $P_{WXC_C} = 24$ $P_{WXC_L} = 24$ $P_{WXC_S} = 24$ with $N_C = 12$, $P_{WXC_C} = 0$ $P_{WXC_L} = 0$ $P_{WXC_S} = 0$	-	-
FLEX-SCALE architecture (Figure 3.6)	72 OAs 24 WBSSs 1 Inter-Band OXC 3 Intra-Band OXCs 9 WSSs for C band 6 WSSs for L band 4 WSSs for S band	$P_{WSS_C} = 11$ $P_{WSS_L} = 11$ $P_{WSS_S} = 11$	$P_{OXC_{INTER}} = 68$, $P_{OXC_{INTRA_C}} = 238$ $P_{OXC_{INTRA_L}} = 159$ $P_{OXC_{INTRA_S}} = 106$	10

Table 3.2 shows the type and number of components and their port count for the express structure of the studied MBoSDM architectures considering D=3, M=4 and B=3, calculated using the formulas shown in Table 3.1. We have considered the following assumptions: 1) to calculate the number of A/D ports per band, $N_{A/D}$, we considered an A/D ratio of 20% for all architectures; 2) the port count of the MB MUX and MB DEMUX of the architectures in Figures 3.2 to 3.5 is not shown in Table 3.2, but a port count of 4 is considered; 3) for the architectures in Figures 3.2 to 3.5, we studied three scenarios,

$N_C = 0$, $N_C = 6$, and $N_C = 12$ and considered the following number of A/Ds per band for the architectures in Figures 3.2, 3.3 and 3.5 (as shown in Figure 3.8), 209 channels for the C band ($N_{A/D_C} = 87 \times 4 \times 3 \times 0.2$), 248 for the S band ($N_{A/D_S} = 103 \times 4 \times 3 \times 0.2$) and 312 for the L band ($N_{A/D_L} = 130 \times 4 \times 3 \times 0.2$) (note that for the architecture in Figure 3.4, we only have 1 WSS for all bands, so $N_{A/D} = N_{A/D_C} + N_{A/D_L} + N_{A/D_S}$); 4) for the FLEX-SCALE architecture (Figure 3.6), we have assumed that: i) $WBSS_{A/D} = 1$ [47], so $N_{B_{Tx}} = N_{B_{Rx}} = 3$ and $P_{WBSS} = 10$; ii) $K_C = 0.35$, $K_L = 0.25$ and $K_S = 0.15$ so that $K_C + K_L + K_S = 0.75$ and $K_{WSS} = 19$ [47]; iii) the port count of the WSSs of the different bands is 11 [47].

From Table 3.2, we can conclude that the higher the parameter N_C, the lower the port count of the WSSs and OXCs. The number of OAs also becomes lower. This is due to the fact that, when N_C increases, there are more connections that are directly linked, and consequently less connections are directed to the single-band WXCs. It was also observed that the results obtained in Table 3.2 for all architectures are consistent with the results obtained in [14], Figure 3, and in [47], Figure 9. In Figure 9 of [47], for the FLEX-SCALE architecture considering D=3 and M=4, the port count of the WBSSs is 14 (note that in [47], the WBSS port count is given by $(D \times M + 1 + 1) = 14$, and in our work we consider $((D-1) \times M + 1 + 1) = 10$ as in [48]) and the port count of the inter-OXC is 68, as shown in Table 3.2. In Figure 3 of [14], for D=4, M=4 and N_C=10, we have confirmed that the port count of the OAs is 22 (there are 10 directed connections and 6 connections that go through the WSSs, so $6 \times 2 + 10 = 22$) and the port count of the WSSs is 12, considering 1×20 WSS, confirming the accuracy of our analysis.

An example of a drop structure for the MBoSDM Baseline architecture studied (Figure 3.2) is shown in Figure 3.8. This drop structure is composed of three WSSs, each one operating in its own band: for the C-band, we have a 12×209 WSS, for the S-band, a 12×248 WSS, and for the L-band, a 12×312 WSS. These WSSs can be implemented, as shown in Figure 3.8, by cascading two WSSs. For example, for the C-band, we can obtain a 12×209 WSS by cascading a 12×1 and 1×209 WSSs. As the drop structure of these architectures is composed of large WSSs, a way to build a 1×209 WSS for C-band, 1×248 WSS for S-band and 1×312 WSS for L-band with smaller WSSs is shown in Figure 3.9 [49]. In this A/D structure, 769 transponders are required (209 for the C-band, 248 for the S-band and 312 for the L-band).

For the other MBoSDM architectures (Figures 3.3 to 3.5), the drop structure is influenced by N_C, and so the drop structures have different dimensions from the one presented in Figure 3.8. For Figures 3.3 and 3.5, considering $N_C = 6$, the drop structure, shown in Figure 3.10 a), is composed of three WSSs, each operating in its own band: for the C-band, we have a 6×105 WSS ($87 \times 6 \times 0.2 = 105$), for the S-band, a 6×124 WSS ($103 \times 6 \times 0.2 = 124$) and for the L-band, a 6×156 WSS ($130 \times 6 \times 0.2 = 156$). In this drop structure a total of 385 transponders is required (105 for the C-band, 124 for the S-band and 156 for the L-band). Figure 3.10 b) shows the drop structure considered for

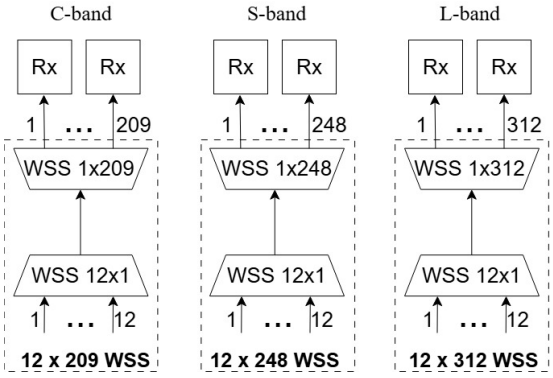


FIGURE 3.8. Drop structure considered for MBoSDM Baseline architecture.

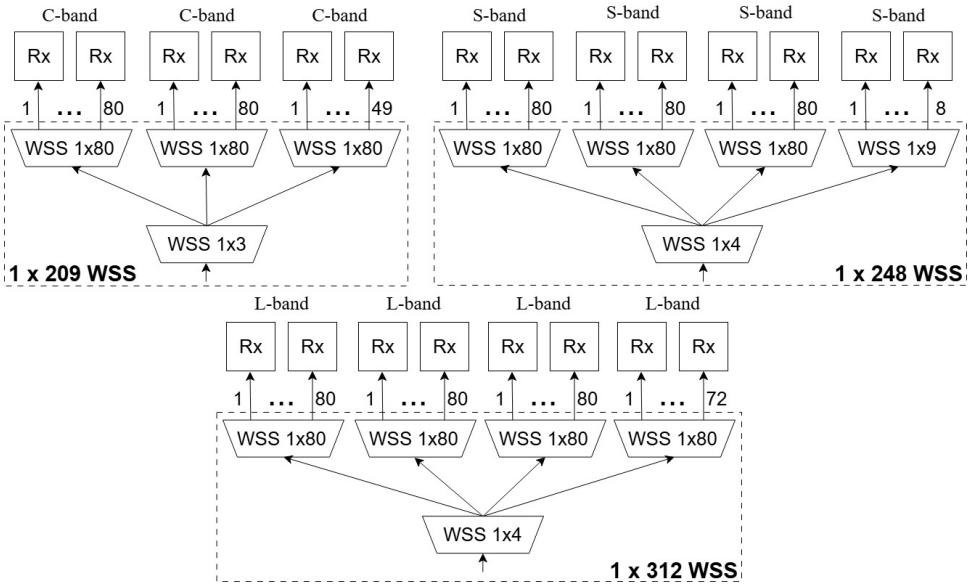
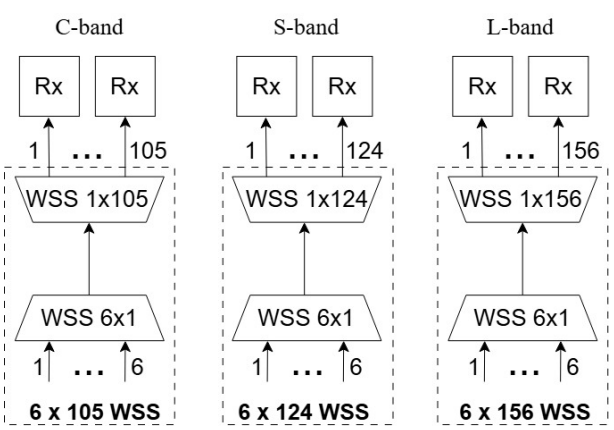


FIGURE 3.9. Example of large dimension WSSs built with smaller ones for the drop structure.

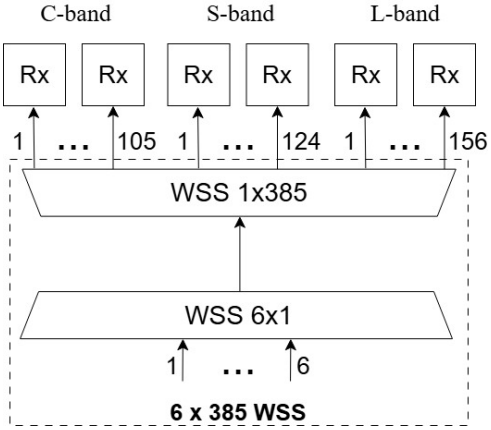
the MBoSDM architecture with a single S-OXC (Figure 3.4). This drop structure consists of a 6×385 WSS MB. In this case, we have a MB WSS, i.e., that operates in the three bands, with 385 transponders.

Table 3.3 shows the total cost (cost of the express structure plus A/D structure) of the studied MBoSDM architectures considering D=3, M=4, and B=3 based on the components cost shown in Table 2.5, in [36] and in [18]. Note that Table 2.5 shows the unit cost of each component, while Table 3.3 shows the total cost of the various components and the total cost of each architecture.

The following assumptions were used to compute the costs in Table 3.3: 1) for the architectures in Figures 3.3, 3.4 and 3.5, we consider $N_C = 6$, since an architecture with this value can represent an architecture with a reasonable cost and flexibility. Note that an architecture with $N_C = 0$ has full flexibility (i.e., it has no core switching, and only wavelength switching is used) and the highest cost; 2) we consider the A/D structure shown in Figure 3.8 to compute the cost of the A/D structure of the Baseline architecture



(A) Drop structure considered for the MBoSDM architectures in Figures 3.3 and 3.5 considering $N_C = 6$.



(B) Drop structure considered for the MBoSDM architectures in Figure 3.4 considering $N_C = 6$.

FIGURE 3.10. Drop structure considered for the MBoSDM architectures in Figures 3.3 to 3.5 considering $N_C = 6$.

shown in Figures 3.2, the A/D structure shown in Figure 3.10 a) for the architectures in Figures 3.3 and 3.5 and the A/D structure shown in Figure 3.10 b) for the MBoSDM architecture in Figure 3.4; 3) we consider that the number of transponders, to calculate the cost of the A/D structure of the FLEX-SCALE architecture, is $N_{Rxs} = N_{Txs} = K_{b_{legacy}} \times (N_{WSS_b}/2 \times P_{WSS_b})$ [47], so we have 10 transponders for the C-band, 7 transponders for the L-band, and 5 transponders for the S-band; 4) we consider that the cost of band transmitters and receivers, B_{Txs} and B_{Rxs}, is similar to that of transponders, as these components are based on a comb-based laser/receiver [48]. The cost of B_{Txs} and B_{Rxs} is calculated by $\beta \times Cost_{BTRxs}$, with β between 1 (best case) and 1.5 (worst case); 5) we consider that the cost of WBSSs is calculated by $\gamma \times Cost_{WSS}$, with γ between 0.5 (best case) and 1 (worst case); 6) to calculate the cost of the single-band and MB WXCs, we consider a R&S architecture [14]. In Figure 3.2, each single-band WXC needs 12 1×12 WSSs and 12 12×1 WSSs, where one output of the input WSSs is going to the drop structure and one input of the output WSSs comes from the add structure. Figure 3.11 shows an example of a 12×12 WXC; 7) to calculate the cost of the MBoSDM architecture shown in Figure 3.4, we considered that the cost of MB WSS is higher than the cost of a single band WSS. Therefore, the cost of MB WSS is, respectively, approximately 2, 1.7, and 1.3 times higher than the WSSs of the C, L, and S bands [18], [50]. So, we consider a cost of 10.5 for a 1×9 MB WSS, 15 for a 1×20 MB WSS and 30 for a 1×40 MB WSS [18], [50].

As observed in Table 3.3, we conclude that the MBoSDM Baseline architecture (Figure 3.2) is the most expensive architecture and the FLEX-SCALE is the least expensive architecture. The Baseline architecture has a higher cost due to the cost of A/D structure, which has a higher number of transponders than the other architectures, and consequently, a higher cost. The FLEX-SCALE architecture is the least expensive - about twenty times

TABLE 3.3. Cost of the studied MBoSDM architectures with D=3, M=4 and B=3.

Architectures	Type and Number of components	Total components cost	Express structure cost	A/D structure cost	Total cost
Baseline architecture (Figure 3.2)	12 MB MUX, 12 MB DEMUX	0.96	756	34808	35564
	72 OAs	88.8			
	3 WXCs (Express structure)	666			
	17 WSSs (A/D structure)	413.5			
	769 Transponders	34394.4			
MBoSDM architecture with an S-OXC per band (Figure 3.3)	12 MB MUX, 12 MB DEMUX	0.96	338	17429	17767
	66 OAs	81.4			
	3 WXCs (Express structure)	222			
	3 S-OXCs	33.4			
	14 WSSs (A/D structure)	213.5			
	385 Transponders	17215			
MBoSDM architecture with a single S-OXC (Figure 3.4)	66 MB MUX, 66 MB DEMUX	5.28	224	17517	17741
	66 OAs	81.4			
	1 WXC (Express structure)	126			
	1 S-OXC	11.13			
	9 WSSs (A/D structure)	301.5			
	385 Transponders	17215			
MBoSDM architecture without a S-OXC (Figure 3.5)	12 MB MUX, 12 MB DEMUX	0.96	304	17429	17733
	66 OAs	81.4			
	3 WXCs (Express structure)	222			
	14 WSSs (A/D structure)	213.5			
	385 Transponders	17215			
FLEX-SCALE architecture (Figure 3.6)	72 OAs	88.8	$\gamma = 1$, 517 $\gamma = 0.5$, 445	$\beta = 1.5$, 1134 $\beta = 1$, 1067	$\gamma = 1, \beta = 1.5$, 1651 $\gamma = 0.5, \beta = 1$, 1512
	24 WBSSs	($\gamma = 1$) 144 ($\gamma = 0.5$) 72			
	3 B_{Tx}, 3 B_{Rx}	($\beta = 1.5$) 201.15 ($\beta = 1$) 134.1			
	19 WSSs (Express structure)	117			
	1 OXC_{INTER}	19.92			
	3 OXC_{INTRA}	147.66			
	22 Transponders	932.4			

less expensive than the Baseline architecture. This is because the A/D structure cost of the FLEX-SCALE architecture is much lower, since it has less A/D capacity, although providing A/D capacity both at the band and wavelength levels, and the cost of the band transmitters/receivers is similar to the transponders cost. In particular, the FLEX-SCALE architecture has 3 B_{Txs} and B_{Rxs} in the second layer that correspond to 320 transponders (87 + 103 + 130 = 320) and 22 transponders in the third layer, giving a total of 342 transponders, which represents less than half of the transponders used in the Baseline architecture (a total of 769 transponders are used, as can be seen in Table 3.3).

From Table 3.3, we conclude that the cost of the A/D structure in all architectures is more significant than the cost of the express structure, with transponders being the component with the largest contribution to the total cost. Therefore, the cost of the A/D structure is approximately 46 times higher than the express structure cost for the Baseline architecture (Figure 3.2), about 58 times higher for the architectures shown in Figures 3.3 to 3.5, and for the FLEX-SCALE architecture, the cost of the A/D structure is approximately the double of the express structure cost.

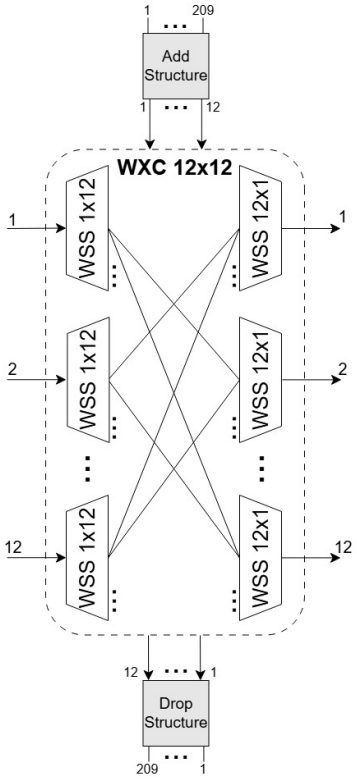


FIGURE 3.11. Example of implementation of a 12×12 WXC.

In [51], a more simplified cost analysis was performed, considering that the cost of the FLEX-SCALE architecture is only the sum of the cost of the WBSSs and the inter-band OXC, i.e., only the first and second layers are considered. From [51], in Figure 3 a), for M=4 and D=3, it is possible to conclude that the relative cost between the WBSSs and the inter-band OXC is 3.6 (18/5), which is in agreement with our assumption for $\gamma = 0.5$, as can be confirmed in Table 3.3 (the cost of the WBSSs varies between 144 and 72 and the cost of the inter-band OXC is 20, which gives a relative cost between 7.2 and 3.6). Also, from Figure 3 a) of [51], it is possible to compute the relative cost between the B_{Txs} and B_{Rxs} and the WBSSs, 18/30=0.6, which is in agreement with the values presented in Table 3.3 (the cost of the B_{Txs} and B_{Rxs} is 134, giving a relative cost between 1.07 and 0.54). Moreover, in [51], Figure 3 b), for M=4 and D=3, it is observed that the cost of the express structure in a conventional architecture is approximately the double of the FLEX-SCALE architecture cost, which is in agreement with the results presented in Table 3.3 (between 1.33 and 1.7).

In [52], Table 2, slightly different values for component costs are considered. In particular, the cost of a conventional 1×9 WSS is considered four times more expensive than an OA, whereas in our case, we consider that a WSS is five times more expensive than an OA. Also, in [52], the cost of the transponder is considered four times more expensive than a conventional 1×9 WSS, whereas in our case, we consider that the cost of the WSS is seven times more expensive. The reason for these differences is attributed to the

fact that in [52] PIC-based components are considered, which are more cost effective than non-PIC based components, considered in our work.

Table 3.4 shows the power consumption of the studied MBoSDM architectures with D=3, M=4 and B=3. The power consumption of each component is taken from Table 2.7. The following assumptions were made to compute the power consumption of the architectures in Table 3.4: 1) for the architectures in Figures 3.3 to 3.5, $N_C = 6$ is considered; 2) the WSSs power consumption corresponds to the power consumption of a 1×9 WSS; 3) the power consumption of the B_{Txs} and B_{Rxs} is calculated with $\alpha \times P_{W_{TRx_b}} \times N_W$, where α is between 0.5 (best case) and 1 (worst case), $P_{W_{TRx_b}}$ represents the power consumption of a transponder and N_W represents the number of channels per band b; 4) the power consumption of the WBSS is assumed to be the same as the one of the WSS [51].

Observing Table 3.4, we can conclude that the Baseline architecture has an higher power consumption, since this architecture has a higher number of transponders than the other architectures. We also observe that the other architectures lead to similar power consumption (about 10000 W). Analysing all components, we can conclude that the components with the highest power consumption are the transponders, followed by B_{Txs} and B_{Rxs}, which are based on integrated comb sources/receivers [48].

In [52], different power consumption values have been considered. In particular, for a small-scale node (D=3, M=2), 12 WBSSs are required with a consumption of 18 W, whereas in our case, for D=3 and M=2, and for the same number of WBSSs a power consumption of 180 W is required, which is ten times than the one reported in [52]. Regarding band transceivers, in [52], for D=3 and M=4, 6 B_{TRxs} are required, leading to a total power consumption of 824 W, whereas in our case, for the same conditions, 120 W are required. Also in [52], with D=3 and M=4, a 112×112 inter-band OXC is required with an power consumption of 60.5 W, whereas in our case, a 112×112 inter-band OXC consumes 597 W. The justification for these power consumption differences, regarding the WBSSs and inter-band OXC, relies on the fact that, in [52], PIC-based technology is used, which results in lower power consumption. One possible reason for the difference in power consumption between $B_{TR_{xs}}$ is that, in [52], the $B_{TR_{xs}}$ have fewer channels (15 channels with a 150 GHz bandwidth) and 13.81 W per channel is required. In our case, we use many more channels per band (87 channels for the C-band, 130 channels for L-band and 103 channels for the S-band) with a 50 GHz channel bandwidth and with about 20 W per channel.

Figure 3.12 shows the express structure cost for all studied MBoSDM architectures considering three different scenarios: small network node (M=4 and D=3); medium network node (M=4 and D=5); and large network node (M=4 and D=7). From Figure 3.12, we conclude that the express structure cost of the Baseline architecture (Figure 3.2) is higher than the other architectures for the three scenarios considered, as already seen in Table 3.3 for the M=4 and D=3 scenario with $N_C = 6$ (a more detailed study of how

TABLE 3.4. Power consumption of the studied MBoSDM architectures with D=3, M=4 and B=3.

Architectures	Type and Number of components	Total components power consumption	Total power consumption
Baseline architecture (Figure 3.2)	72 OAs	1200 W	18521 W
	3 WXCs (Express structure)	1440 W	
	17 WSSs (A/D structure)	345 W	
	769 Transponders	15536 W	
MBoSDM architecture with an S-OXC per band (Figure 3.3)	66 OAs	1100 W	10416 W
	3 WXCs (Express structure)	720 W	
	3 S-OXCs	540 W	
	14 WSSs (A/D structure)	280 W	
	385 Transponders	7776 W	
MBoSDM architecture with a single S-OXC (Figure 3.4)	66 OAs	1100 W	9581 W
	1 WXC (Express structure)	300 W	
	1 S-OXC	180 W	
	9 WSSs (A/D structure)	225 W	
	385 Transponders	7776 W	
MBoSDM architecture without a S-OXC (Figure 3.5)	66 OAs	1100 W	9876 W
	3 WXCs (Express structure)	720 W	
	14 WSSs (A/D structure)	280 W	
	385 Transponders	7776 W	
FLEX-SCALE architecture (Figure 3.6)	72 OAs	1200 W	$\alpha = 1$, 11604 W $\alpha = 0.5$, 8372 W
	24 WBSSs	360 W	
	3 B_{Tx}, 3 B_{Rx}	($\alpha = 1$) 6464 W ($\alpha = 0.5$) 3232 W	
	19 WSSs (Express structure)	305 W	
	1 OXC_{INTER}	340 W	
	3 OXC_{INTRA}	2515 W	
	22 Transponders	420 W	

the value of N_C influences the architectures costs is provided in Appendix C). We can also observe that the cost of the architectures shown in Figures 3.3 and 3.5 is similar, and that the cost of the MBoSDM architecture with a single S-OXC (Figure 3.4) is lower. This is because this architecture has a single MB WSS instead of three single-band WSSs (one for each band) like the other architectures, which reduces its cost, as shown in Table 3.3. We also see that as D increases, the cost of FLEX-SCALE becomes lower compared to the other architectures. This is because the WSSs cost for the MBoSDM architectures shown in Figures 3.2 to 3.5 become much higher than for the FLEX-SCALE architecture, due to their higher port count.

Figure 3.13 shows the A/D structure cost (in logarithmic scale) for the same scenarios as in Figure 3.12. From Figure 3.13, we conclude that the cost of the FLEX-SCALE A/D structure is much lower than that of the other architectures in all scenarios, due to the same reason explained for the M=4 and D=3 scenario presented in Table 3.3. Furthermore, we see that the cost of the other architectures is similar, as already concluded from Table 3.3, for the M=4 and D=3 scenario.

Figure 3.14 shows the power consumption for all studied architectures in the three scenarios considered previously. Looking at Figure 3.14, we see that the power consumption

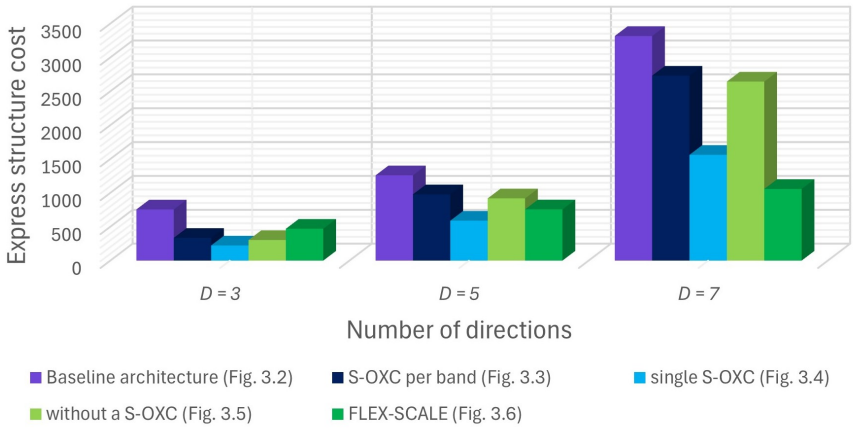


FIGURE 3.12. Express structure cost for all studied MBoSDM architectures with D=3, D=5 and D=7, considering M=4.

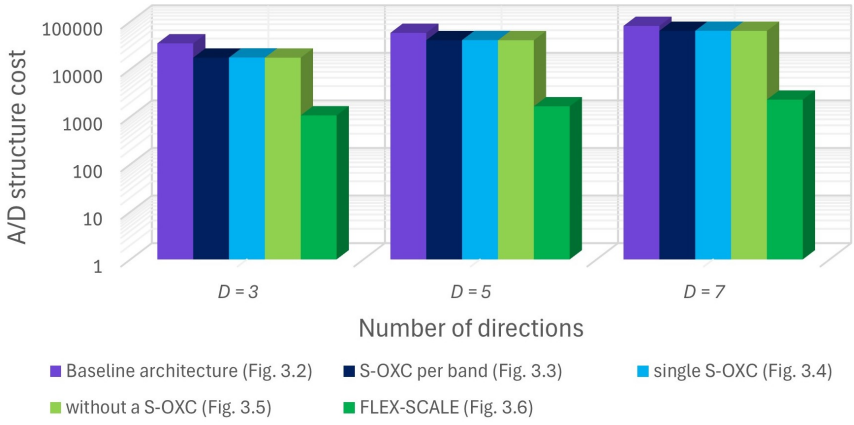


FIGURE 3.13. A/D structure cost for all studied MBoSDM architectures with D=3, D=5 and D=7, considering M=4.

of the MBoSDM Baseline architecture (Figure 3.2), when D=3, is much higher compared to the other MBoSDM architectures, but as the number of directions increases, we see that the power consumption of the other MBoSDM architectures becomes similar to the Baseline architecture power consumption, except for the FLEX-SCALE architecture, which has the lowest power consumption for any number of directions. This happens, once again, because the WSSs of the other architectures have a higher port count as D increases, increasing their power consumption and also because of the higher number of transponders. Furthermore, since the power consumption considered for all WSSs is equal to the power consumption of a 1×9 WSS, the total power consumption of all MBoSDM architectures, except for FLEX-SCALE, tends to be similar - although it is expected that larger WSSs consume more, this is not considered in this work.

After analysing all architectures, we conclude that the FLEX-SCALE is the architecture with the lowest cost and power consumption, which makes this architecture a

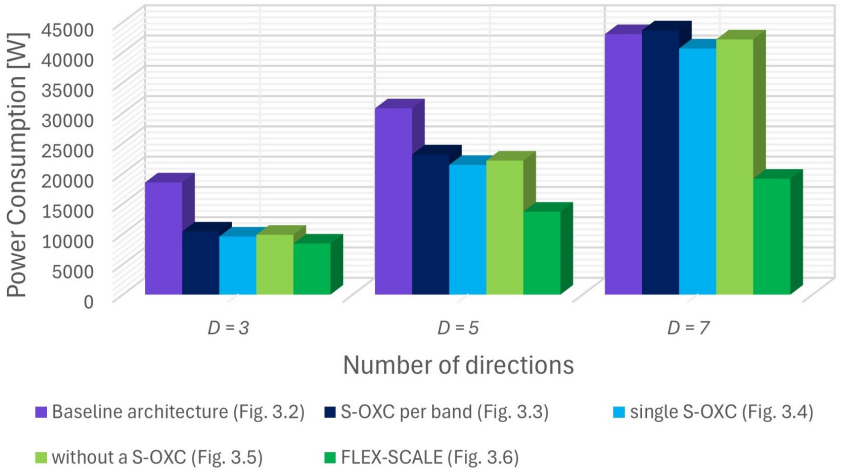


FIGURE 3.14. Power consumption for all studied MBoSDM architectures with D=3, D=5 and D=7, considering M=4.

potential candidate for future high capacity MBoSDM nodes. As disadvantage, this architecture has more layers, leading to a potentially more complex node management and control.

Next, we will analyze the throughput of the studied node architectures. The node throughput, or node capacity, Thr_{Node}, for FLEX-SCALE is defined as [47], [48]:

$$Thr_{Node} = M \times D \times BW \times SE \tag{3.1}$$

where BW represents the C+L+S bandwidth (16 THz, as mentioned in Chapter 2) and SE is the spectral efficiency. The SE, calculated by $SE = p \times R_S \times \log_2 M/BW_{Ch}$, is computed assuming 32 quadrature amplitude modulation (QAM) signals, a channel bandwidth ($BW_{Channel}$) of 50 GHz, two polarizations (p) and a symbol rate (R_S) of 32 GBaud, so that the $SE = 2 \times 32 \times 5/50 = 6.4$b/s/Hz without a band guard (a higher SE scenario is analyzed in Appendix B). Considering band guards of 600 GHz between the C and L bands and between the C and S bands, as in Figure 2.5, and considering 320 channels (87 in C band, 130 in the L band and 103 in the S band) the SE with band guard is $320 \times (2 \times 32\text{GBaud} \times 5)/17.2\text{THz} = 5.95$ b/s/Hz.

Figure 3.15 shows the throughput of FLEX-SCALE for different values of D considering $SE = 5.95$ b/s/Hz, $BW = 16$ THz and M=2, 4, and 8. When analysing Figure 3.15, we conclude that the throughput of FLEX-SCALE increases with M and D, as expected. For example, for $M = 2$ and $D = 2$, we see that $Thr_{Node} = 0.38$ Pb/s and, for $M = 2$ and $D = 8$, we obtain $Thr_{Node} = 1.56$ Pb/s, a fourfold increase. When M increases, for example $M = 8$, for $D = 2$, we obtain $Thr_{Node} = 1.52$ Pb/s, and for $D = 8$, we obtain $Thr_{Node} = 6.08$ Pb/s, which is again a fourfold increase. For the remaining MBoSDM architectures studied in this chapter, we conclude that the node throughput is the same and equal to the FLEX-SCALE throughput. The comparison with the architectures throughput given in [48] is studied in Appendix B.

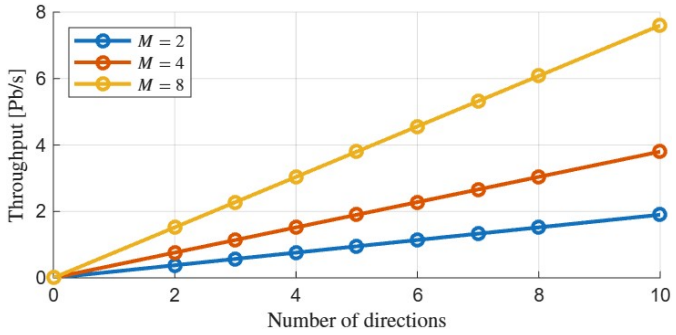


FIGURE 3.15. Node throughput for the FLEX-SCALE architecture as a function of D, considering M=2, 4 and 8.

The A/D capacity, Cap_{A/D_b}, of Layer 2 of the FLEX-SCALE architecture, can be given by,

$$Cap_{A/D_b} = \sum_{b=1}^{B} (N_{BTRxs_b} \times BW_b \times SE) \tag{3.2}$$

where $BW_C = 4.35$ THz, $BW_L = 6.5$ THz, $BW_S = 5.15$ THz , $SE = 6.4$ b/s/Hz and $N_{BTRxs_b} = 1$.

Figure 3.16 shows the A/D capacity of FLEX-SCALE Layer 2 for different values of D considering M=2, 4, and 8. From Figure 3.16, we can conclude that once again, the A/D capacity for FLEX-SCALE layer 2 increases with M and D. For example, for $M = 2$ and $D = 2$, we see that $Cap_{A/D} = 0.034$ Pb/s and for $M = 2$ and $D = 8$ we obtain $Cap_{A/D} = 0.136$ Pb/s, a four times increase. With $M = 8$ and $D = 2$, $Cap_{A/D} = 0.136$ Pb/s and $M = 8$ and $D = 8$, $Cap_{A/D} = 0.546$ Pb/s, which is again a four time increase.

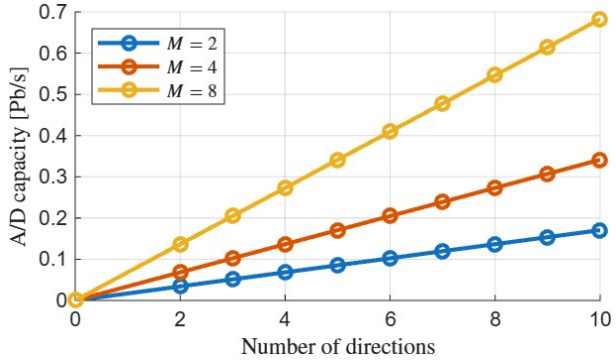


FIGURE 3.16. A/D capacity for the Layer 2 of the FLEX-SCALE architecture as a function of D, considering M=2, 4 and 8.

The A/D capacity of Layer 3 of the FLEX-SCALE architecture is calculated as follows:

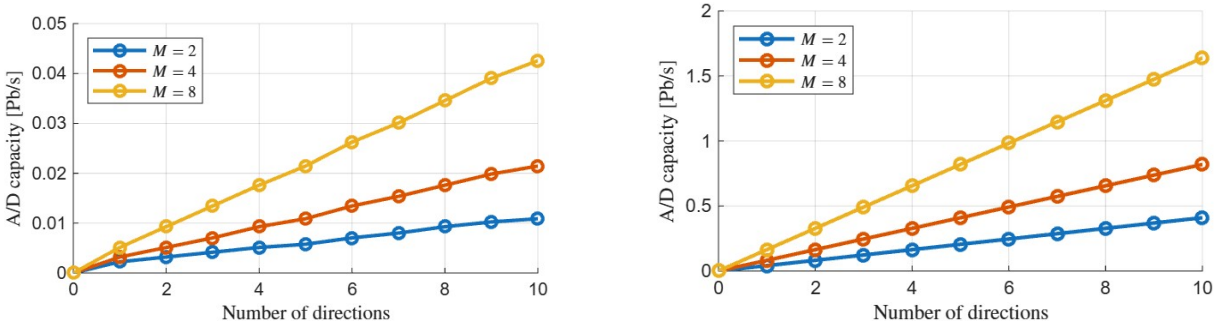
$$Cap_{A/D_b} = \sum_{b=1}^{B} (N_{TXs_b} \times BW_b \times SE) \tag{3.3}$$

where $BW_b = 50$ GHz. For the M=4 and D=3 scenario $N_{TXs_C} = 10$, $N_{TXs_L} = 7$ and $N_{TXs_S} = 5$, as shown in Table 3.3. The A/D capacity of the other MBoSDM architectures studied in this chapter is the same and is calculated in the same way, but considering

different N_{TXs_b}. For the other architectures, we have $N_{TXs_C} = 209$, $N_{TXs_L} = 312$ and $N_{TXs_S} = 248$, for the M=4 and D=3, scenario.

Figure 3.17 a) shows the A/D capacity of Layer 3 for FLEX-SCALE and figure 3.17 b) shows the A/D capacity of the remaining MBoSDM architectures for different values of D considering $SE = 6.4$ b/s/Hz and M=2, 4, and 8.

From Figures 3.17 a) and 3.17 b), we observe that the A/D capacity of the FLEX-SCALE architecture is much lower than the capacity of the other architectures due to its lower wavelength granularity, i.e., its lower number of transponders. In Figure 3.17 a), we obtain, for example, for M=4 and D=3, $Cap_{A/D} = 0.007$ Pb/s. When D increases, we obtain, for M=4 and D=8, $Cap_{A/D} = 0.018$ Pb/s, a threefold increase. In Figure 3.17 b), the A/D capacities obtained are much higher. For example, for M=4 and D=3, we obtain $Cap_{A/D} = 0.24$ Pb/s, and for M=4 and D=8, we obtain $Cap_{A/D} = 0.65$ Pb/s, which again represents a threefold increase.



(A) A/D capacity for FLEX-SCALE Layer 3.

(B) A/D capacity for other MBoSDM architectures Layer 3.

FIGURE 3.17. A/D capacity of Layer 3 a) FLEX-SCALE architecture and of b) the other MBoSDM architectures as a function of D, considering M=2, 4 and 8.

After studying the throughput and the A/D capacity of the several layers of the different MBoSDM architectures, we conclude that the A/D capacity of the FLEX-SCALE architecture is much lower than the other architectures studied in this chapter, although the FLEX-SCALE architecture has also A/D capacity in Layer 2, at the band level, unlike the other architectures, that only have A/D capacity in Layer 3. The FLEX-SCALE architecture reduces significantly the wavelength granularity, while providing band granularity. As indicated in [39], core nodes will progressively reduce wavelength granularity, so that their cost and and power consumption will be reduced.

3.5. Conclusions

In this chapter, we studied and compared different MBoSDM node architectures: Baseline architecture, MBoSDM architecture with S-OXC per band, MBoSDM architecture with a single S-OXC, MBoSDM architecture without a S-OXC and FLEX-SCALE architecture. We studied these architectures in terms of their granularity and analysed the

number and type of hardware components, their cost, power consumption, and throughput.

In terms of architecture cost, we analysed the cost of the express structure and the A/D structure of the MBoSDM architectures. Regarding the cost of the express structure of each architecture, we concluded that the FLEX-SCALE architecture is the least expensive. Regarding the A/D structure cost, we also concluded that the cost of FLEX-SCALE is significantly less expensive. Finally, regarding the total cost, we concluded that, as expected, the FLEX-SCALE architecture is much less expensive than the others (twenty times less expensive), whereas the Baseline MBoSDM architecture has a higher cost. This is because the cost of the A/D structure of the FLEX-SCALE architecture is significantly less expensive (about 30 times less expensive compared to Baseline MBoSDM architecture) since this architecture has fewer transponders than the others, as it sacrifices wavelength level granularity, but provides granularity at the band level.

Regarding the power consumption of the architectures, we concluded that all architectures, except for the MBoSDM Baseline architecture, have similar power consumption when considering D=3. The Baseline architecture has a higher power consumption due to the higher number of transponders required. When D increases, we see that all MBoSDM architectures have similar power consumption, except for FLEX-SCALE, which consumes much less power due to the much lower port count of its WSSs. Furthermore, we see that the power consumption in the remaining MBoSDM architectures is similar because the power consumption for all WSSs, regardless of their port count, is considered equal to the consumption of a 1×9 WSS.

Finally, regarding the throughput of the architectures, we conclude that the node throughput is the same for all architectures and increases with M and D. Regarding the node A/D capacity, we concluded that although the FLEX-SCALE architecture has A/D capacity in both Layers 2 and 3, while the other architectures have only A/D capacity at Layer 3, the A/D capacity of Layer 3 of the FLEX-SCALE architecture is about 34 times lower than the A/D capacities of the other nodes.

In future core node architectures, e.g. FLEX-SCALE, it is expected that wavelength granularity becomes residual, while band granularity will increase, so that cost effective and low power consumption nodes can be built and deployed.

[This page is intentionally left blank.]

CHAPTER 4

Cost and power consumption comparison of MB, SDM and MBoSDM node architectures

4.1. Introduction

In this chapter, some specific MB, SDM and MBoSDM architectures studied in the previous chapters will be compared in terms of the type and number of components, cost, power consumption, cost per bit and power consumption per bit. The chosen architectures from the previous chapters are the ones that are commercially available, that are more cost effective and the ones that lead to a higher granularity. For MB architectures, the chosen architectures are the Baseline (Figure 2.7) and Common band (Figure 2.9) architectures; for SDM, the Space (Figures 2.13 and 2.14) and Space-wavelength (Figures 2.15 and 2.16) architectures with and without lane changes, and for MBoSDM, the Baseline (Figure 3.2), MBoSDM architecture with a single S-OXC (Figure 3.4) and the FLEX-SCALE architecture (Figure 3.6).

In section 4.2, we will analyse the cost per bit of the architectures for two scenarios, the first one considers a 16 THz bandwidth per node direction, while the second one considers 32 THz. In section 4.3, we analyse the power consumption per bit for the same architectures, considering these two scenarios. In section 4.4, we will conclude this chapter.

4.2. Cost analysis

In this section, we will study the cost and cost per bit for some of the architectures studied previously for two scenarios: 16 THz and 32 THz bandwidths per node direction.

4.2.1. Scenario 1: 16 THz per node direction

For the first scenario, 16 THz per node direction, to calculate the cost of the architectures, we considered an equal number of WDM channels in all solutions ($N_W = 320$), to reach the same node throughput. For this scenario, the MB architectures use the C+L+S bands with $N_{W_C} = 87$ channels, $N_{W_L} = 130$ and $N_{W_S} = 103$, the SDM architectures use MCF with 4 cores with 80 channels per core in the C-band, and the MBoSDM architectures use MCF with 2 cores using the C+L bands in each core (in this case, we use 80 channels in each band, so that we have a total of 320 channels in the two cores).

Figure 4.1 shows the Baseline architecture with 3 directions and a MCF with 2 cores using the C+L band per direction, whereas Figure 4.2 shows the MBoSDM architecture with a single S-OXC, and Figure 4.3 shows the FLEX-SCALE architecture for the same scenario.

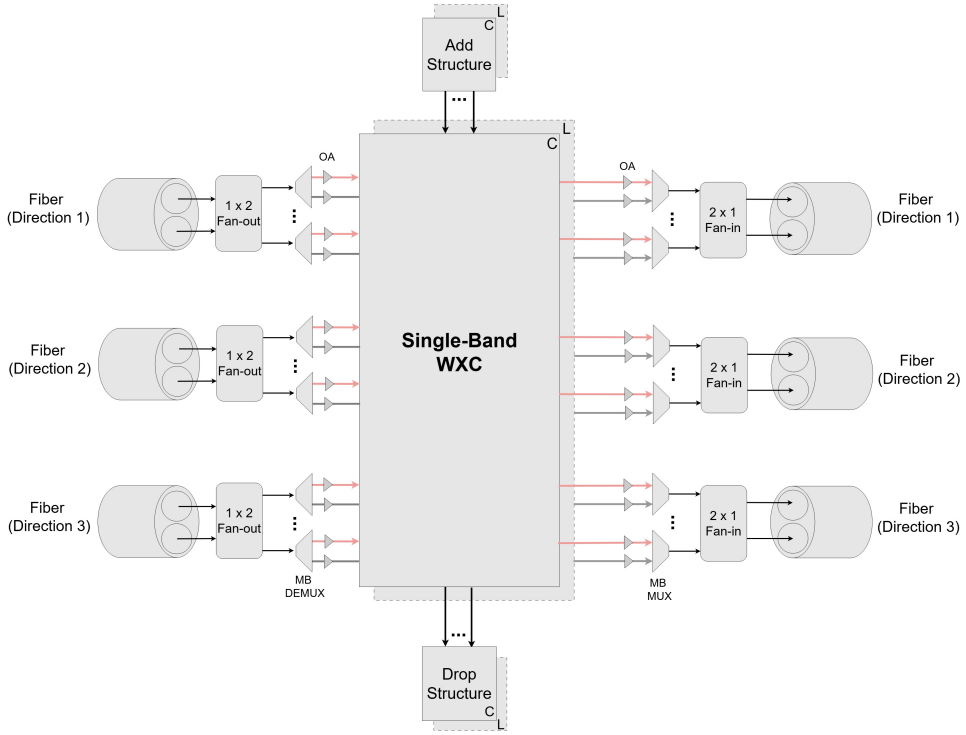


FIGURE 4.1. MBoSDM Baseline architecture with 3 directions considering a 2 core MCF with C+L bands per direction.

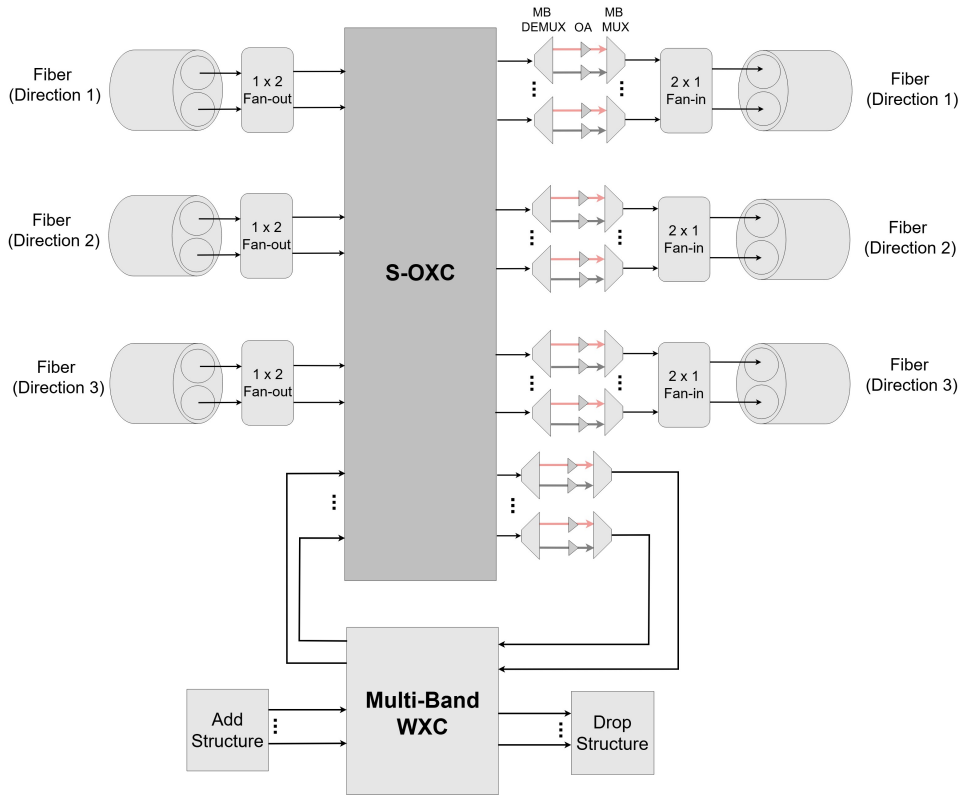


FIGURE 4.2. MBoSDM architecture with a single S-OXC with 3 directions considering a 2 core MCF with C+L bands per direction.

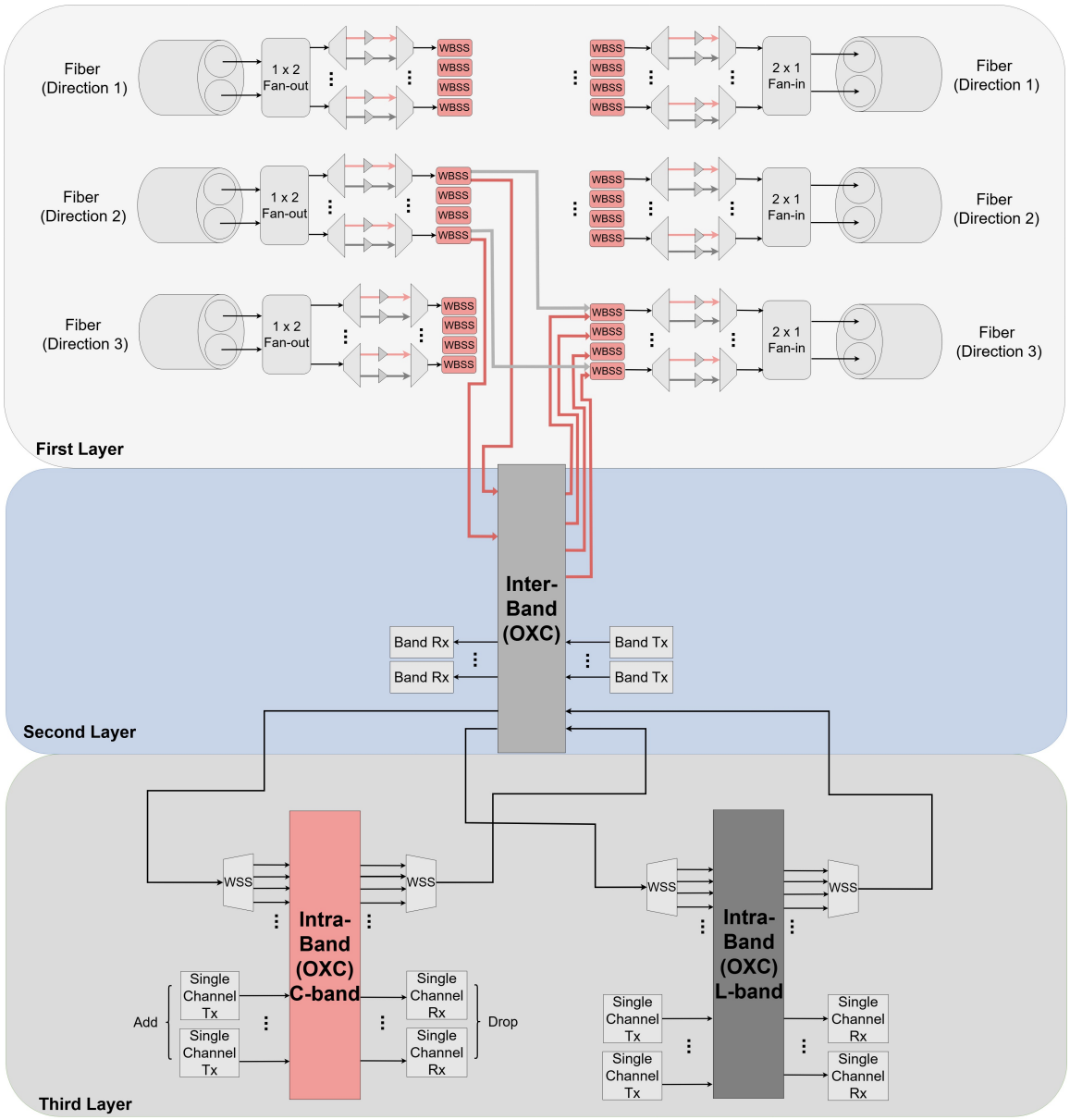


FIGURE 4.3. FLEX-SCALE architecture with 3 directions considering a 2 core MCF with C+L bands per direction.

Table 4.1 shows the costs of the MB, SDM and MBoSDM architectures considering three directions (D=3) and a 16 THz bandwidth per node direction. The cost of the MB architecture with B=3 and SDM architectures with M=4 has been previously calculated in Table 2.6 of Chapter 2. The cost of the MBoSDM architectures with M=2 and B=2 follows the same reasoning as in Chapter 3 (i.e. to calculate the new components dimensions and numbers of components, the expressions in Table 3.1 are used) with the following different features: 1) 80 channels are considered for the C band and 80 channels for the L band, and therefore the A/D structure has 192 transponders. For the MBoSDM Baseline architecture (Figure 4.1), the drop structure is built with two 6×96 WSSs, as shown in Figure 4.4 ($N_{A/D_C} = N_{A/D_L} = 80 \times 2 \times 3 \times 0.20 = 96$ transponders per band and a total of

$N_{A/D_C} + N_{A/D_L} = 192$ transponders). For the MBoSDM architecture shown in Figure 4.2, the drop structure is built with one 3×96 WSS, as shown in Figure 4.5. Note that in this case, $N_C = 3$ was considered, and therefore $N_{A/D_C} = N_{A/D_L} = 80 \times 3 \times 0.2 = 48$ transponders per band and a total of $N_{A/D_C} + N_{A/D_L} = 96$ transponders. In the previous chapter, we saw that N_C varies between 0 (where there are no cores communicating directly with each other) and MD (where all cores are communicating directly with each other). In this case, we have the maximum value of $N_C = 6$, and therefore, as in the previous chapter, we chose an intermediate case, $N_C = 3$; 2) for the FLEX-SCALE architecture, we consider $K_C = 45\%$ and $K_L = 35\%$ to calculate the number of WSSs.

TABLE 4.1. Cost of SDM architectures with D=3 and M=4, MB architectures with D=3 and B=3 and MBoSDM architectures with D=3, M=2 and B=2 for the 16 THz bandwidth scenario.

	Architectures	Lane Changes	Type and Number of components	Total components cost	Express structure cost	A/D structure cost	Total Cost
SDM (4 cores)	Space (Figure 2.13/2.14)	without	4 OXCs 4×4	18.75	43	7042	7085
			24 OAs	24			
			8 WSSs	130			
			192 Transponders	6912			
		with	1 OXC 16×16	9.38	33	7042	7075
			24 OAs	24			
			8 WSSs	130			
			192 Transponders	6912			
	Space-wavelength (Figure 2.15/2.16)	without	32 WSSs	190	84	7042	7126
			24 OAs	24			
			192 Transponders	6912			
		with	32 WSSs	250	144	7042	7186
			24 OAs	24			
			192 Transponders	6912			
MB (C+L+S)	Baseline (Figure 2.7)	not applicable	3 MB DEMUX, 3 MB MUX	0.24	78	8710	8788
			24 WSSs	175.75			
			18 OAs	22.2			
			192 Transponders	8589.6			
	Common band (Figure 2.9)	not applicable	3 MB DEMUX, 3 MB MUX	0.24	997	7010	8007
			24 WSSs	208.5			
			18 OAs	22.2			
			12 AO-WCs	864			
			192 Transponders	6912			
MBoSDM (C+L with 2 cores)	Baseline (Figure 4.1)		6 MB MUX, 6 MB DEMUX	0.48	159	7701	7860
			24 OAs	26.4			
			2 WXCs (Express structure)	132			
			8 WSSs (A/D structure)	97.5			
			192 Transponders	7603			
	MBoSDM architecture with a single S-OXC with $N_C = 3$ (Figure 4.2)		21 MB MUX, 21 MB DEMUX	1.68	63	3884	3947
			21 OAs	23			
			1 WXC (Express Structure)	33			
			1 S-OXC	5.27			
			4 WSSs (A/D structure)	82.5			
			96 Transponders	3801.6			
	FLEX-SCALE architecture (Figure 4.3)		24 OAs	26.4	$\gamma = 1$, 250 $\gamma = 0.5$, 214	$\beta = 1.5$, 630 $\beta = 1$, 590	$\gamma = 1, \beta = 1.5$, 880 $\gamma = 0.5, \beta = 1$, 804
			12 WBSSs	($\gamma = 1$) 72 ($\gamma = 0.5$) 36			
			2 B_{TRxs}	($\beta = 1.5$) 118.8 ($\beta = 1$) 79.2			
			11 WSSs (Express structure)	60			
			1 OXC_{INTER}	11.13			
			2 OXC_{INTRA}	80.86			
			13 Transponders	511.2			

From Table 4.1, we observe that all architectures have a similar cost, with the exception of the FLEX-SCALE architecture, which has a much lower cost (seven times less than the first five other architectures), and the MBoSDM architecture with a single S-OXC (Figure 3.2). In relation to the first five architectures, we observe that the MB Baseline

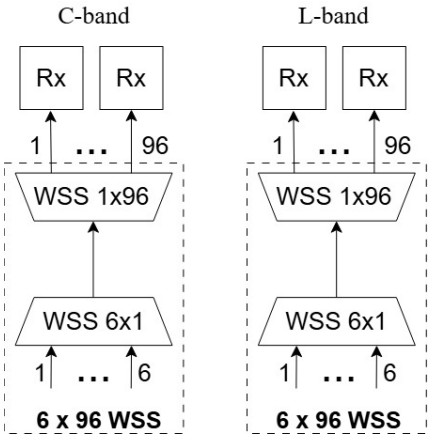


FIGURE 4.4. Drop structure considered for the MBoSDM Baseline architectures with D=3 and M=2.

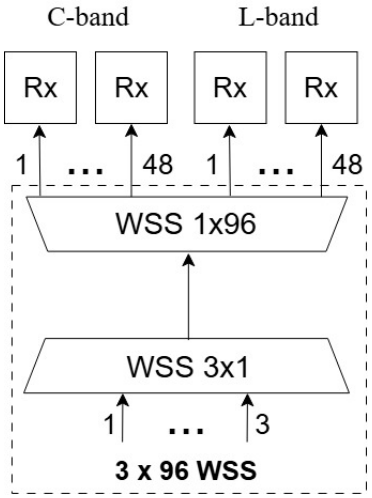


FIGURE 4.5. Drop structure considered for the MBoSDM architecture shown in Figure 4.2 considering D=3, M=2 and $N_C = 3$.

architecture (Figure 2.7) is the most expensive architecture due to the higher cost of the transponders in the L and S bands in comparison with the C-band transponder cost.

Regarding the express structure cost, we see that the MB Common band (Figure 2.9) is the architecture with the highest cost, since this architecture uses AO-WCs, which have a high cost (864 as observe in Table 4.1). On the other hand, the SDM space architectures (Figures 2.13 and 2.14) are the architectures with the lowest express structure cost as they have simpler, smaller and less expensive components compared to other architectures, as shown in Tables 2.3 and 2.5 in Chapter 2.

Regarding the cost of the A/D structure, we see that all architectures have a similar cost, as they have the same number of transponders, except for the FLEX-SCALE, where the cost is ≈ 12 times less than the other architectures cost, and for the MBoSDM architecture with a single S-OXC (Figure 4.2), where the cost is approximately half the cost of the other architectures. This is because, we consider half the number of transponders,

since $N_C = 3$. If $N_C = 0$ was considered, we would have the same number of transponders, and therefore the cost of the A/D structure would be similar (the analysis of how N_C influences architecture costs is similar to that performed in Chapter 3 and Appendix C). In relation to the MB Baseline architecture (Figure 2.7), we see that this architecture has a higher cost than the other architectures. This is because this architecture has transponders for all bands (C+L+S), not just the C band, which increases costs since the cost of L and S band transponders is higher than that of C band transponders, as shown in Table 2.5 (Chapter 2).

In general, we see that the cost of the A/D structure is much higher than the cost of the express structure, 7 to 200 times higher than that of the express structure, except for the FLEX-SCALE, where the cost of the A/D structure is approximately twice the express structure cost.

Figure 4.6 shows the express structure cost for SDM architectures with M=4 (represented by different shades of green), MB architectures with B=3 (represented by different shades of red) and MBoSDM architectures with M=2 and B=2 (represented by different shades of blue), considering different values for the number of directions ($D = 3, 5, 7$). From Figure 4.6, we conclude that as D increases, the architecture with the highest express structure cost is the MB common band (Fig. 2.9). This is due to the fact that this architecture uses AO-WCs, which are very expensive components, as shown in Table 4.1. Furthermore, we observe that the SDM Space-wavelength with lane changes (Fig. 2.16) has a significant increase in cost compared to the other architectures, increasing approximately 6 times from $D = 3$ to $D = 7$, whereas, for example, the SDM Space with lane changes (Fig. 2.14) only increases approximately 2 times. This higher cost increase in SDM Space-wavelength with lane changes (Fig. 2.16) is related with the use of a higher number of WSSs, and as D increases, their dimensions also grow, increasing their cost.

Figure 4.7 shows the A/D structure cost (in logarithmic scale) for the same scenarios considered in Figure 4.6. From Figure 4.7, we conclude that as D increases, the FLEX-SCALE architecture (Fig. 4.3) shows the lowest A/D structure cost, as explained in Chapter 3 and shown in Table 4.1. The remaining architectures have a similar A/D structure cost, with the exception of the MBoSDM architecture with a single S-OXC (Fig. 4.2), which has a slightly lower cost since we are considering $N_C = 3$, which means that this architecture has fewer transponders and therefore a lower cost, and the MB Baseline (Fig. 2.7), which has a higher A/D structure cost, since it uses C+L+S bands transponders.

Next, we will analyze the throughput of the studied node architectures and the cost per bit. The node throughput for the architectures is defined as $D \times BW \times SE$, where BW is 16 THz. The SE is calculated assuming 32 QAM signals with 50 GHz channel spacing and 32 GBaud, so that $SE = 5.95$ b/s/Hz, as calculated in Chapter 3.

Figure 4.8 shows the throughput of the studied architectures as a function of number of directions D, considering $SE = 5.95$b/s/Hz and $BW = 16$ THz. From Figure

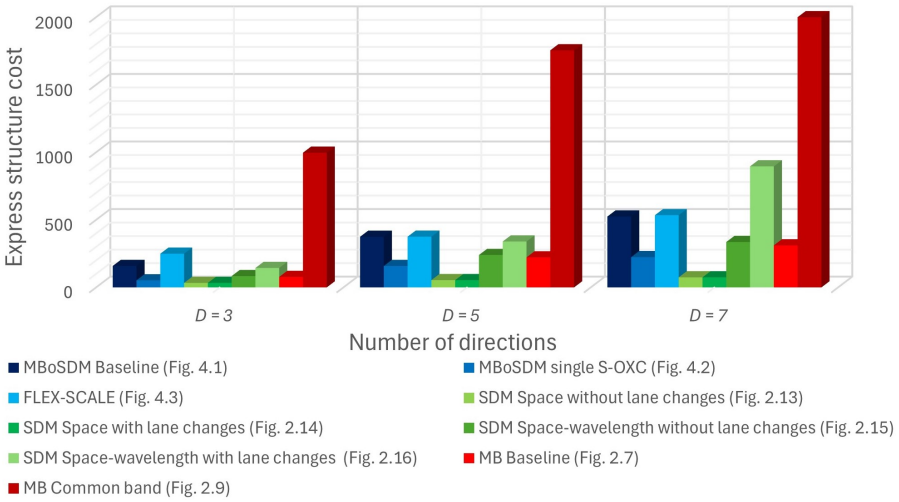


FIGURE 4.6. Express structure cost for SDM architectures with M=4, MB architectures with B=3 and MBoSDM architectures with M=2 and B=2 considering D=3, 5 and 7 for the 16 THz scenario.

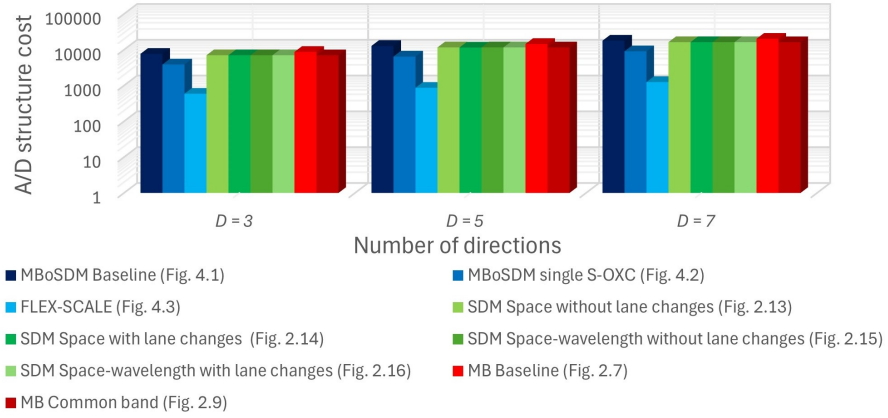


FIGURE 4.7. A/D structure cost for SDM architectures with M=4, MB architectures with B=3 and MBoSDM architectures with M=2 and B=2 considering D=3, 5 and 7 for the 16 THz scenario.

4.8, we observe that capacity increases linearly as D increases, i.e. considering $D = 3$, $Thr_{Node} = 0.28$ Pb/s, and considering $D = 7$, $Thr_{Node} = 0.66$ Pb/s, which correspond to a 2.3 times increase. Note that all studied architectures have the same throughput, since we are assuming that all architectures have the same number of directions and the same number of channels per direction (i.e. the same bandwidth per direction).

Figure 4.9 shows the cost per bit normalized to the cost per bit of the MBoSDM Baseline architecture (Fig 4.1) for the studied MB, SDM and MBoSDM architectures considering D=3, 5 and 7. To calculate the normalized cost per bit, we compute the ratio between the cost per bit of each architecture and the cost per bit of the MBoSDM Baseline architecture (Fig. 4.1) for the different scenarios [18], [41]. The cost per bit of each architecture is obtained by dividing the cost of each architecture by its throughput.

From Figure 4.9, we can conclude that the MB architectures have the highest cost per bit - the MB Baseline, since it uses transponders in three bands, and the MB Common

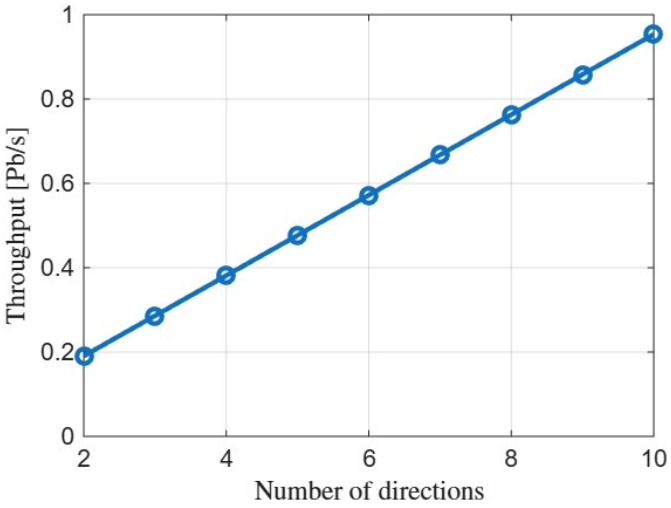


FIGURE 4.8. Node throughput for architectures as a function of D.

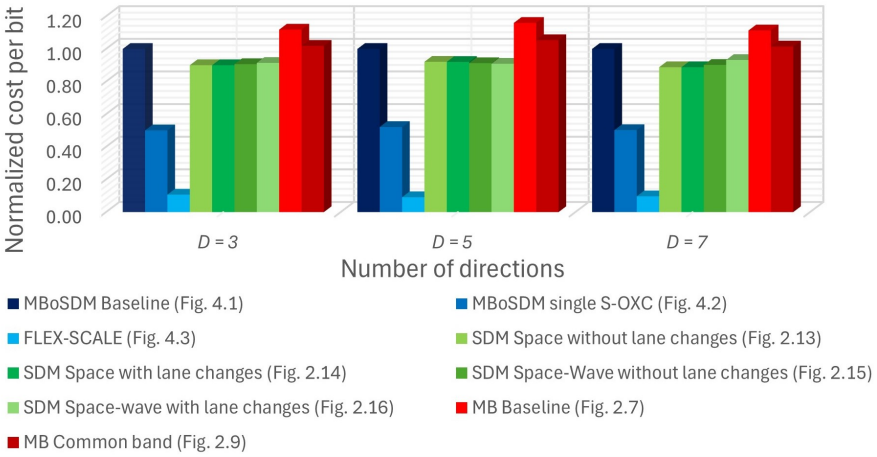


FIGURE 4.9. Cost per bit normalized to the MBoSDM Baseline architecture (Fig. 4.1) for SDM, MB and MBoSDM architectures considering D=3, 5 and 7 for the 16 THz scenario.

band due to the number of AO-WCs it uses, as mentioned previously. Figure 4.9 also shows that MBoSDM architectures, except the MBoSDM Baseline, have a much lower cost per bit compared to all other architectures - the MBoSDM architecture with a single S-OXC, as we considered $N_C = 3$, which reduced costs, and the FLEX-SCALE architecture, which has a much lower cost due to the A/D cost being much lower, as explained earlier. The SDM architectures (simpler architectures with smaller components, as discussed in Chapter 2), also have a lower cost per bit compared to MBoSDM Baseline (Fig. 4.1) and the MB architectures. We can also observe, from Figure 4.9, that the number of directions does not have a visible impact on the normalized cost per bit. So, it can be concluded that node cost and corresponding capacity increase at the same ratio as a function of D and also as a function of the node architecture type.

4.2.2. Scenario 2: 32 THz per node direction

For the second scenario, 32 THz per node direction, we also consider the same number of channels (in this case, $N_W = 640$) for all architectures. For the SDM architectures, we consider 8 cores ($M = 8$) with 80 channels per core in the C band, given a total of 640 channels. For the MBoSDM architectures, two scenarios will be studied: in the first scenario, 4 cores considering the C+L bands in each core with 80 channels per core in C band and 80 in L band; in the second scenario, we consider 2 cores using the C+L+S bands with 87 channels per core in the C band, 130 in L band and 103 in S band (giving a total of 640 channels in both scenarios). Regarding the MB, we decided not to investigate it, since to get 32 THz, we have to use other bands (like the E, O and U bands) than the C+L+S studied in this work. Note, however, that there are already experimental works testing MB transmission in single core fibers using almost 40 THz of bandwidth [13].

Table 4.2 shows the costs of the SDM and MBoSDM architectures considering three directions ($D = 3$), as in Table 4.1, but for a 32 THz bandwidth per node direction. To calculate the number and dimensions of the components, we follow the same reasoning as in the previous section for Table 4.1: 1) for SDM architectures with 8 core fibers, the A/D structure is composed of eight 3×48 WSSs, based on Table 2.1 in Chapter 2, and 384 transponders ($0.2 \times 3 \times 8 \times 80$), for an A/D ratio of 20%; 2) for MBoSDM architectures, using the C+L band with 4 cores, the A/D structure of the MBoSDM Baseline is built with two 12×192 WSSs ($0.2 \times 4 \times 3 \times 80 = 192$ transponders for the C-band and 192 transponders for the L-band); and for the MBoSDM architecture with a single S-OXC, considering $N_C = 6$, the A/D structure consists of a 6×192 MB WSS ($0.2 \times 6 \times 80 = 96$ transponders for the C-band and 96 transponders for the L-band, a total of 192 transponders); 3) for MBoSDM architectures, using the C+L+S band with 2 cores, the A/D structure of the MBoSDM Baseline consists of three 6×96 WSSs, one for each band, giving a total of 288 transponders (96 for the C-band, 96 for the L-band and 96 for the S-band); and for the MBoSDM architecture with a single S-OXC, considering $N_C = 3$, we have one 3×144 MB WSS, and 144 transponders (48 in the C band, 48 in the L band and 48 in the S band); 4) to calculate the cost of the B_{TRxs} in the FLEX-SCALE architecture, we consider that the cost of a B_{TRxs} is similar to the cost of a transponder corresponding to each band, as considered earlier - for MBoSDM architectures, using the C+L bands with 4 cores, the FLEX-SCALE architecture has 3 B_{TRxs} (2 B_{TRxs} for the C band and 1 B_{TRxs} for the L band), whereas in the scenario that considers the C+L+S bands with 2 cores, we have 2 B_{TRxs} (one for the C band and one for the L band).

From Table 4.2, we conclude that all architectures have a similar total cost, with the exception of the FLEX-SCALE architecture, which has a much lower cost, and the MBoSDM architecture with a single S-OXC, which has about half the cost. Regarding the express structure cost, we see that the architectures with the highest cost are the SDM Space-wavelength with lane changes (higher-dimensions WSSs), the MBoSDM Baseline (C+L with 4 cores) and the FLEX-SCALE architecture (C+L with 4 cores). This is due

TABLE 4.2. Cost of SDM architectures with D=3 and M=8, MBoSDM architectures with D=3, M=4 and B=2 and MBoSDM architectures with D=3, M=2 and B=3 for the 32 THz bandwidth scenario.

	Architectures	Lane Changes	Type and Number of components	Total components cost	Express structure cost	A/D structure cost	Total cost
SDM (8 cores)	Space (Figure 2.13/2.14)	without	8 OXCs 4×4	18.75	67	14024	14091
			48 OAs	48			
			16 WSSs	200			
			384 Transponders	13824			
		with	1 OXC 32×32	18.75	67	14024	14091
			48 OAs	48			
			16 WSSs	200			
			384 Transponders	13824			
	Space-wavelength (Figure 2.15/2.16)	without	64 WSSs	320	168	14024	14192
			48 OAs	48			
			384 Transponders	13824			
		with	64 WSSs	560	408	14024	14432
			48 OAs	48			
			384 Transponders	13824			
MBoSDM (C+L with 4 cores)	Baseline		12 MB MUX, 12 MB DEMUX	0.96	450	15393	15843
			48 OAs	52.8			
			2 WXCs (Express structure)	396			
			12 WSSs (A/D structure)	187			
			384 Transponders	15206.4			
	MBoSDM architecture with a single S-OXC with $N_C = 6$		42 MB MUX, 42 MB DEMUX	3.36	186	7767	7953
			42 OAs	46.2			
			1 MB WXC (Express structure)	126			
			1 S-OXC	10.55			
			6 WSSs (A/D structure)	163.5			
			192 Transponders	7603.2			
	FLEX-SCALE architecture		48 OAs	52.8	$\gamma = 1$, 519 $\gamma = 0.5$, 447	$\beta = 1.5$, 994 $\beta = 1$, 936	$\gamma = 1, \beta = 1.5$, 1513 $\gamma = 0.5, \beta = 1$, 1383
			24 WBSSs	($\gamma = 1$) 144 ($\gamma = 0.5$) 72			
			3 B_{TRxs}	($\beta = 1.5$) 172.8 ($\beta = 1$) 115.2			
			19 WSSs (Express structure)	154.5			
			1 OXC_{INTER}	19.92			
			2 OXC_{INTRA}	147.67			
			21 Transponders	820.8			
MBoSDM (C+L+S with 2 cores)	Baseline		6 MB MUX, 6 MB DEMUX	0.48	267	12954	13221
			36 OAs	44.4			
			3 WXCs (Express structure)	222			
			12 WSSs (A/D structure)	166.5			
			288 Transponders	12787.2			
	MBoSDM architecture with a single S-OXC with $N_C = 3$		33 MB MUX, 33 MB DEMUX	2.64	67	6538	6605
			33 OAs	40.7			
			1 MB WXC (Express structure)	18			
			1 S-OXC	5.27			
			6 WSSs (A/D structure)	144			
			144 Transponders	6393.6			
	FLEX-SCALE architecture		36 OAs	44.4	$\gamma = 1$, 276 $\gamma = 0.5$, 240	$\beta = 1.5$, 634 $\beta = 1$, 594	$\gamma = 1, \beta = 1.5$, 910 $\gamma = 0.5, \beta = 1$, 834
			12 WBSSs	($\gamma = 1$) 72 ($\gamma = 0.5$) 36			
			2 B_{TRxs}	($\beta = 1.5$) 118.8 ($\beta = 1$) 79.2			
			9 WSSs (Express structure)	79.5			
			1 OXC_{INTER}	9.96			
			3 OXC_{INTRA}	70.31			
			12 Transponders	514.8			

to the fact that, in these architectures, we consider 4 cores instead of two, which increases the dimensions of the single-band WXCs in the case of the MBoSDM Baseline, and the dimensions of the OXC_{INTRA} in the case of the FLEX-SCALE architecture. Regarding the A/D structure cost, we see that all have a similar cost with the exception of the FLEX-SCALE architecture and the MBoSDM architecture with a single S-OXC, as this architecture has half the number of transponders of the MBoSDM Baseline considering C+L with 4 cores and C+L+S with 2 cores scenarios.

Comparing the costs of the two scenarios, 16 THz and 32 THz, from Tables 4.1 and 4.2, we conclude that the costs of the architectures in Table 4.2 are approximately the

double of those in Table 4.1, with the exception of the FLEX-SCALE architecture. This is because we have considered two times the number of channels in the 32 THz scenario (640 versus 320 channels) – which means twice as many transponders are required, which practically doubles the cost. Regarding the FLEX-SCALE architecture considering the C+L+S band with 2 cores, the costs are similar to those in Table 4.1 that considers the C+L with 2 cores, because although we have different numbers of bands, we have the same number of B_{TRxs} in both scenarios, and a similar number of transponders, as these are the components that most influence the cost of FLEX-SCALE. In the C+L band with 4 cores scenario, the costs are slightly less than double of those shown in Table 4.1.

Figure 4.10 shows the express structure cost for SDM architectures with M=8 (represented by different shades of green) and MBoSDM architectures with M=4 and B=2 and with M=2 and B=3 (represented by different shades of blue), considering different number of directions (D=3, 5 and 7).

From Figure 4.10, we conclude that the architectures with the highest express structure cost are the MBoSDM Baseline (C+L with 4 cores) and the SDM Space-wavelength architecture with lane changes (with 8 cores), as expected and shown in Table 4.2 for $D = 3$. Comparing Figure 4.10 (32 THz scenario) with Figure 4.6 (16 THz scenario), we see that SDM architectures exhibit a similar increase when we increase the number of directions, and that the express structure cost doubles in the 32 THz scenario, since we doubled the number of cores (M=4 in the 16 THz and M=8 in the 32 THz scenarios). In Figure 4.6, we considered MBoSDM architectures C+L with $M = 2$, and when we compare with the MBoSDM architectures C+L+S with $M = 2$ in Figure 4.10, we see that the costs are similar, with the exception of the MBoSDM Baseline C+L+S with 2 cores, which, for $D = 7$, has a much higher cost, as the WSSs used are also for the S band, and not just for the C and L bands. The MBoSDM architectures C+L with $M = 4$ have higher costs than the ones with C+L+S and $M = 2$, although these costs increase in the same way as the number of directions increases, with the exception once again of the MBoSDM Baseline C+L with 4 cores, which shows a significantly higher increase compared to the others, as the number of cores doubles, which results in a higher number of WSSs with larger dimensions.

Figure 4.11 shows the A/D structure cost (in logarithmic scale) for the same scenarios considered in Figure 4.10. From Figure 4.11, we can see that the cost of the A/D structure is similar in all architectures, with the exception of FLEX-SCALE, which is ten times cheaper, and the MBoSDM single S-OXC considering C+L with $M = 4$ and C+L+S with $M = 2$, which is slightly less expensive as expected and shown in Table 4.2 for $D = 3$. Comparing Figure 4.11 (32 THz scenario) with Figure 4.7 (16 THz scenario), we see that the cost increase with the number of directions is similar, although in the 32 THz scenario, the costs are the double since we have doubled the number of transponders (note that this comparison is not very clear in Figures 4.7 and 4.11 because we are using a logarithmic scale).

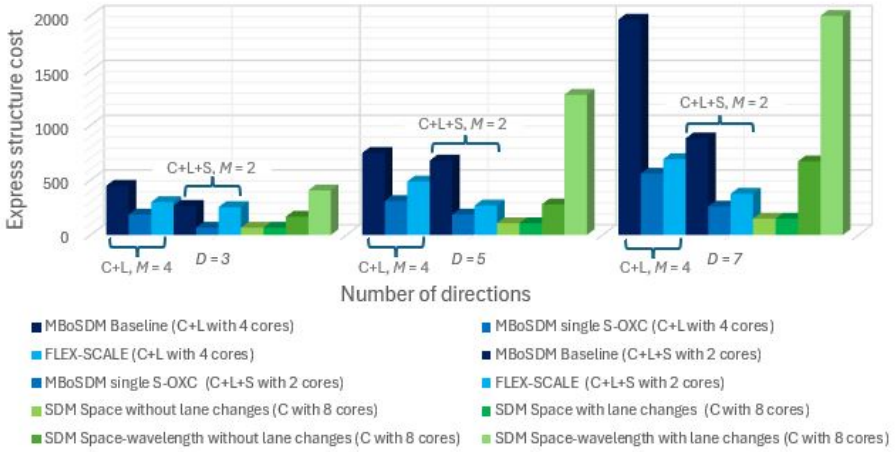


FIGURE 4.10. Express structure cost for SDM architectures with M=8, MBoSDM architectures with M=4 and B=2, and with M=2 and B=3 considering D=3, 5 and 7 directions, for the 32 THz scenario.

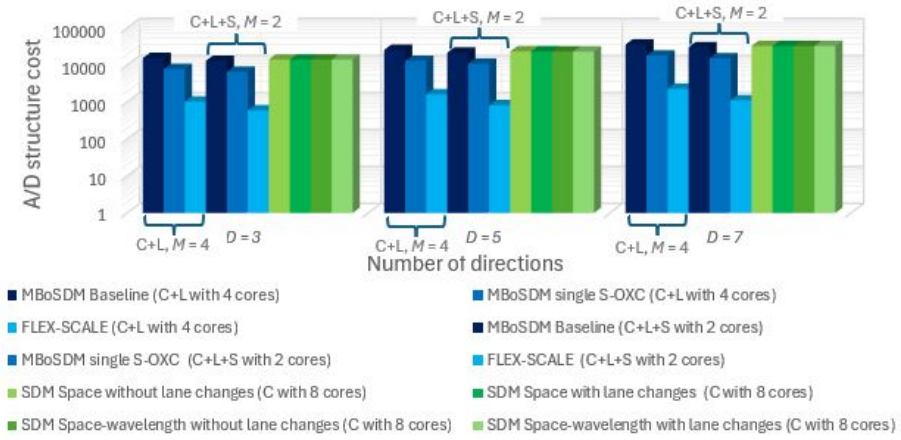


FIGURE 4.11. A/D structure cost for SDM architectures with M=8, MBoSDM architectures with M=4 and B=2 and with M=2 and B=3 considering D=3, 5 and 7, for the 32 THz scenario.

Figure 4.12 shows the cost per bit normalized to the MBoSDM Baseline architecture (C+L with 4 cores) cost per bit for the studied SDM and MBoSDM architectures considering D=3, 5 and 7. The cost per bit was calculated considering $SE = 5.95$ b/s/Hz and $BW = 32$ THz. For $D = 3$, $Thr_{Node} = 0.57$ Pb/s, for $D = 5$, $Thr_{Node} = 0.95$ Pb/s and for $D = 7$, $Thr_{Node} = 1.33$ Pb/s, which is twice the values considered in Figure 4.8.

From Figure 4.12, we conclude that the MBoSDM Baseline architecture considering C+L with $M = 4$ is the architecture with the highest cost per bit, followed by the SDM architectures, the MBoSDM Baseline architecture C+L+S with $M = 2$, and the FLEX-SCALE architecture, which is the architecture with the lowest cost per bit, as expected and shown in Table 4.2 dor $D = 3$. Comparing Figure 4.12 (32 THz scenario) with Figure 4.9 (16 THz scenario), we see that the architectures exhibit a similar cost per bit behavior, meaning that the node capacity increase (from 16 THz per node direction to 32 THz) does not have a visible impact on the relative cost per bit between the studied architectures.

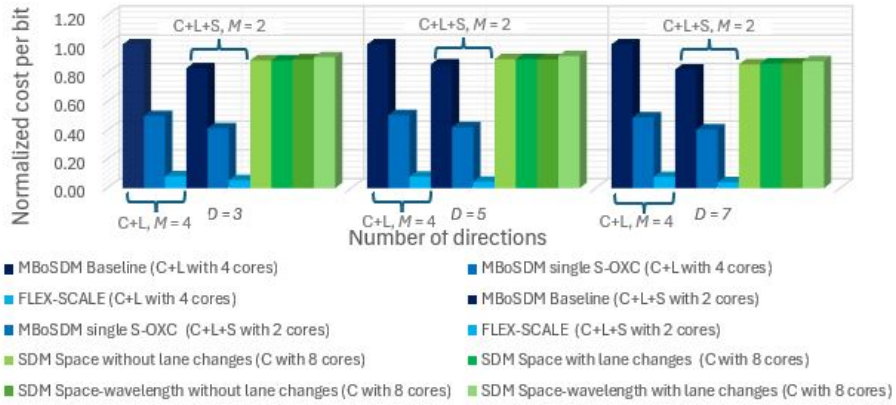


FIGURE 4.12. Cost per bit normalized to the MBoSDM Baseline architecture (C+L with 4 cores) for SDM and MBoSDM architectures considering D=3, 5 and 7, for the 32 THz scenario.

4.3. Power consumption analysis

In this section, we will study the power consumption of all architectures for two scenarios: 16 THz per node direction and 32 THz per node direction.

4.3.1. Scenario 1: 16 THz per node direction

For the first scenario with 16 THz per node, we will calculate and compare the power consumption of the architectures studied previously.

Table 4.3 shows the power consumption of the SDM, MB, and MBoSDM architectures considering three directions (D=3) and 16 THz bandwidth per node direction. From Table 4.3, we conclude that all architectures have a power consumption between 3712 W and 4562 W, with the exception of the MBoSDM architecture with a single S-OXC (Figure 4.2) with a power consumption of 2413 W. This is due, as mentioned earlier when analysing the cost of the architectures (Table 4.1), to the lower number of transponders of these architectures than in the others, since we consider $N_C = 3$, which reduces its cost. Once again, if $N_C = 0$, the number of transponders would be the same, and therefore this architecture would lead to a power consumption similar to the other architectures power consumption. Analysing the remaining architectures, we see that SDM architectures have lower consumption than MB architectures. This is due to the fact that SDM architectures only use C-band transponders, which have lower power consumption, as shown in Table 2.7. Contrarily to what we observe for the architecture costs, where the FLEX-SCALE architecture has a much lower cost, the FLEX-SCALE architecture has similar or even higher power consumption with $\alpha = 1$ when compared to the other architectures. This fact can be explained by noting that band transmitters, B_{TRxs}, when compared to transponders, are components that only cost approximately twice a transponder cost, but their power consumption is approximately 80 times that of a transponder.

Figure 4.13 shows the power consumption per bit normalized to the MBoSDM Baseline architecture (Fig. 4.1) for MB, SDM and MBoSDM architectures considering D=3, 5 and 7 for the 16 THz scenario. The power consumption per bit of the architectures is calculated

TABLE 4.3. Power consumption of SDM architectures with D=3 and M=4, MB architectures with D=3 and B=3 and MBoSDM architectures with D=3, M=2 and B=2 for the 16 THz scenario.

	Architectures	Lane Changes	Type and Number of components	Total components power consumption	Total power consumption
SDM (4 cores)	Space (Figure 2.13/2.14)	without	4 OXCs 4×4	160 W	3712 W
			24 OAs	360 W	
			8 WSSs	120 W	
			192 Transponders	3072 W	
		with	1 OXC 16×16	320 W	3872 W
			24 OAs	360 W	
			8 WSSs	120 W	
			192 Transponders	3072 W	
	Space-wavelength (Figure 2.15/2.16)	without	32 WSSs	480 W	3912 W
			24 OAs	360 W	
			192 Transponders	3072 W	
		with	32 WSSs	480 W	3912 W
			24 OAs	360 W	
			192 Transponders	3072 W	
MB (C+L+S)	Baseline (Figure 2.7)	not applicable	24 WSSs	412 W	4562 W
			18 OAs	270 W	
			192 Transponders	3880 W	
	Common band (Figure 2.9)	not applicable	24 WSSs	360 W	4278 W
			18 OAs	270 W	
			12 AO-WCs	576 W	
			192 Transponders	3072 W	
MBoSDM (C+L with 2 cores)	Baseline (Figure 4.1)		24 OAs	360 W	4376 W
			2 WXCs (Express structure)	420 W	
			8 WSSs (A/D structure)	140 W	
			192 Transponders	3456 W	
	MBoSDM architecture with a single S-OXC with $N_C = 3$ (Figure 4.2)		21 OAs	315 W	2413 W
			1 WXC (Express Structure)	210 W	
			1 S-OXC	60 W	
			4 WSSs (A/D structure)	100 W	
			96 Transponders	1728 W	
	FLEX-SCALE architecture (Figure 4.3)		24 OAs	360 W	$\alpha = 1$, 5482 W $\alpha = 0.5$, 4002 W
			12 WBSSs	180 W	
			2 B_{TRxs}	($\alpha = 1$) 2880 W ($\alpha = 0.5$) 1400 W	
			11 WSSs (Express structure)	190 W	
			1 OXC_{INTER}	190 W	
			2 OXC_{INTRA}	1450 W	
			13 Transponders	232 W	

by dividing the power consumption of each architecture by its throughput, which is shown in Fig. 4.8.

From Figure 4.13, we observe that the MBoSDM Baseline (Fig. 4.1), MB Common band (Fig. 2.9) and MB Baseline (Fig. 2.7) architectures have the highest power consumption per bit for all values of D, as shown also in Table 4.3 for $D = 3$. We also conclude that the SDM architectures have similar power consumption per bit. For the MBoSDM architecture with a single S-OXC (Fig. 4.2), as D increases, the power consumption per bit is about half the power consumption of the SDM architectures (note that $N_C = 3$, leads to smaller WSSs, reducing power consumption). Furthermore, we also observe that the power consumption per bit of the FLEX-SCALE architecture decreases between D=3 and D=5, and slightly increases between D=5 to D=7. This is due to the fact that, although the power consumption increases as a function of D, there is a smaller

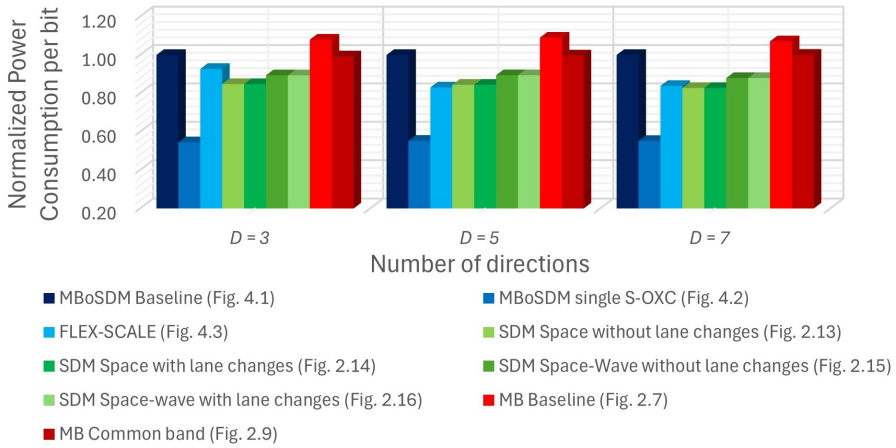


FIGURE 4.13. Power consumption per bit normalized to the MBoSDM Baseline architecture (Fig. 4.1) power consumption per bit, for SDM architectures with M=4, MB architectures with B=3 and MBoSDM architectures with M=2 and B=2 considering D=3, 5 and 7 for the 16 THz scenario.

difference in the power consumption of the FLEX-SCALE architecture between $D = 7$ and $D = 5$ when compared to $D = 3$ and $D = 5$, resulting in lower power consumption per bit since the capacity increases linearly with D.

4.3.2. Scenario 2: 32 THz per node direction

For the second scenario, with 32 THz per node, we will calculate and compare the power consumption of the architectures studied previously in section 4.2.2.

Table 4.4 shows the power consumption of SDM architecture with $M = 8$, MBoSDM architectures considering C+L with 4 cores and considering C+L+S with 2 cores for D=3 and 32 THz bandwidth per node direction. Table 4.4 shows that all architectures have similar power consumption, with the exception of the FLEX-SCALE architecture considering C+L with 4 cores with $\alpha = 1$, which has higher power consumption (approximately 1.4 times more) due to the power consumption of the B_{TRxs}, and the MBoSDM architecture with a single S-OXC, considering C+L with 4 cores and C+L+S with 2 cores that leads to the lowest power consumption (approximately 1.85 times less).

Comparing the two scenarios studied, 16 THz and 32 THz, from Tables 4.3 and 4.4, we see that the power consumption of the architectures studied in Table 4.4 is approximately twice the ones presented in Table 4.3, once again due to the doubling of the number of channels and consequently, the number of transponders.

Figure 4.14 shows the power consumption per bit normalized to the MBoSDM Baseline architecture (C+L with 4 cores) for the SDM and MBoSDM architectures, considering D=3, 5 and 7 for the 32 THz scenario. From Figure 4.14, we can see that the MBoSDM Baseline C+L with $M = 4$ is the architecture with the highest power consumption per bit, followed by the SDM architectures and the MBoSDM Baseline C+L+S with $M = 2$, as shown in Table 4.4 for $D = 3$. When comparing Figure 4.14 (32 THz scenario) with

TABLE 4.4. Power consumption of SDM architectures with D=3 and M=4, MBoSDM architectures with D=3, M=4 and B=2 and MBoSDM architectures with D=3, M=2 and B=3 for the scenario with 32 THz.

	Architectures	Lane Changes	Type and Number of components	Total components power consumption	Total power consumption
SDM (8 cores)	Space (Figure 2.13/2.14)	without	8 OXCs 4×4	320 W	7424 W
			48 OAs	720 W	
			16 WSSs	240 W	
			384 Transponders	6144 W	
		with	1 OXC 32×32	320 W	7424 W
			48 OAs	720 W	
			16 WSSs	240 W	
			384 Transponders	6144 W	
	Space-wavelength (Figure 2.15/2.16)	without	64 WSSs	960 W	7824 W
			48 OAs	720 W	
			384 Transponders	6144 W	
		with	64 WSSs	960 W	7824 W
			48 OAs	720 W	
			384 Transponders	6144 W	
MBoSDM (C+L with 4 cores)	Baseline		48 OAs	720 W	8682 W
			2 WXCs (Express structure)	840 W	
			12 WSSs (A/D structure)	210 W	
			384 Transponders	6912 W	
	MBoSDM architecture with a single S-OXC with $N_C = 6$		42 OAs	630 W	4626 W
			1 MB WXC (Express structure)	240 W	
			1 S-OXC	180 W	
			6 WSSs (A/D structure)	120 W	
			192 Transponders	3456 W	
	FLEX-SCALE architecture		48 OAs	720 W	$\alpha = 1$, 10006 W $\alpha = 0.5$, 7314 W
			24 WBSSs	360 W	
			3 B_{TRxs}	($\alpha = 1$) 5384 W ($\alpha = 0.5$) 2692 W	
			19 WSSs (Express structure)	325 W	
			1 OXC_{INTER}	340 W	
			2 OXC_{INTRA}	2505 W	
			21 Transponders	372 W	
MBoSDM (C+L+S with 2 cores)	Baseline		36 OAs	600 W	7320 W
			3 WXCs (Express structure)	720 W	
			12 WSSs (A/D structure)	240 W	
			288 Transponders	5760 W	
	MBoSDM architecture with a single S-OXC with $N_C = 3$		33 OAs	550 W	3808 W
			1 MB WXC (Express structure)	120 W	
			1 S-OXC	90 W	
			6 WSSs (A/D structure)	120 W	
			144 Transponders	2928 W	
	FLEX-SCALE architecture		36 OAs	600 W	$\alpha = 1$, 6589 W $\alpha = 0.5$, 4593 W
			12 WBSSs	240 W	
			2 B_{TRxs}	($\alpha = 1$) 3992 W ($\alpha = 0.5$) 1996 W	
			9 WSSs (Express structure)	170 W	
			1 OXC_{INTER}	170 W	
			3 OXC_{INTRA}	1185 W	
			12 Transponders	232 W	

Figure 4.13 (16 THz scenario), we see that the normalized power consumption per bit has a similar behavior for both 16 and 32 THz scenarios.

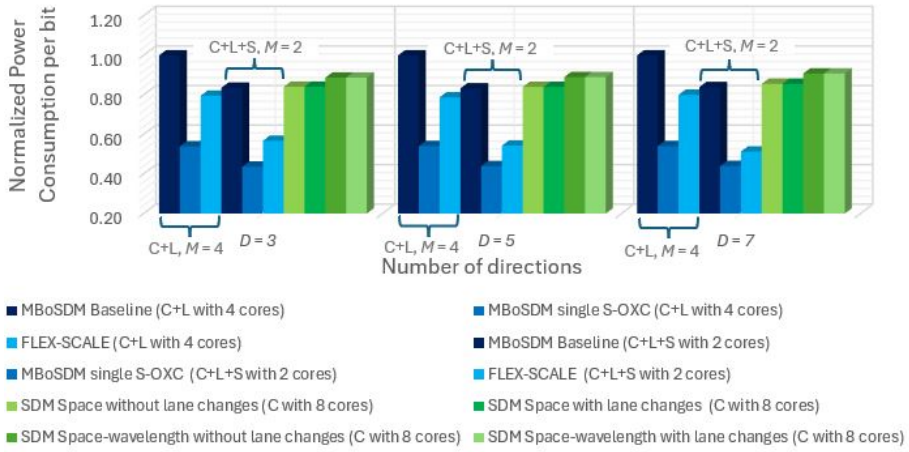


FIGURE 4.14. Power consumption per bit normalized to the MBoSDM Baseline architecture (C+L with 4 cores) for SDM and MBoSDM architectures considering D=3, 5 and 7, for the 32 THz scenario.

4.4. Conclusions

In this chapter, we studied and compared the cost and power consumption of several MB, SDM and MBoSDM architectures, considering two scenarios: 16 THz and 32 THz bandwidths per node direction.

Regarding the node architecture cost per bit, we concluded that the FLEX-SCALE is the lowest-cost architecture in both bandwidth scenarios. This is mainly due to the fact that the FLEX-SCALE architecture uses band transceivers that can add and drop channel bands, which significantly reduces the number of transponders required and, consequently, the cost per bit. We also concluded that the MB architectures using the C+L+S bands are the most expensive - in the Baseline architecture, as S band components are more costly than C and L band components, and in the MB Common band architecture as AO-WCs, which are high-cost components are used. SDM architectures have lower cost per bit than MB architectures since these architectures use only C-band components, which are less expensive, as mentioned earlier. In all studied architectures, the cost of the A/D structure represents between 60% and 99% of the total cost of the architectures, since the transponders and, in the case of FLEX-SCALE, the band transceivers are the components with the highest costs. As the number of node directions increases, we conclude that the cost per bit normalized to the MBoSDM Baseline architecture remains almost constant, for all the architectures studied.

In terms of power consumption per bit, we concluded that the architecture with the lowest power consumption per bit is the MBoSDM architecture with a single S-OXC, assuming $N_C = 3$. The MB architectures have the highest power consumption per bit, once again due to the use of S band components and AO-WCs, which are higher power consuming components. For SDM architectures, we concluded that power consumption per bit is lower than in MB architectures, as these architectures only use C band and simpler components, hence reducing power consumption. Regarding the power consumption

of the MBoSDM architectures, we see that all of them have similar power consumption per bit, with the exception of the MBoSDM with a single S-OXC, and the FLEX-SCALE architecture. In conclusion, regarding power consumption per bit, we see that the FLEX-SCALE architecture does not offer many advantages as it does regarding cost. However, as the FLEX-SCALE architecture allows band channels A/D, a feature that will be important in future networks [47], unlike the other architectures, we can still conclude that the FLEX-SCALE architecture can be considered a good promising choice regarding cost, power consumption and granularity.

CHAPTER 5

Conclusions and future work

5.1. Final conclusions

The main goal of this dissertation was to study architectures for future MBoSDM networks and compare them, in terms of cost and power consumption, with those typically used in MB and SDM networks.

In the second chapter, a literature review on node architectures for MB and SDM networks has been performed. We have studied five MB architectures using the C+L+S band: the Baseline architecture, the architecture with AO-WCs, the common band architecture, the compact architecture and the SOA-based architecture. We have also studied four SDM architectures: the space granularity architecture, the space-wavelength granularity architecture, the wavelength granularity architecture and the fractional space-full wavelength architecture. A comparison of MB and SDM architectures in terms of granularity, number of components, dimensions, costs and power consumption has been done. We have concluded that the most expensive components are the transponders, which represent the largest percentage of the total cost across all architectures, and the AO-WCs, used in the MB common band architecture. With regard to power consumption, we conclude that, once again, transponders are the components that most influence power consumption across all architectures, and that in the MB SOA-based architecture, the SOAs have a significant impact on power consumption. We also concluded that, MB architectures have a higher cost (1.2 times more expensive than SDM architectures) and power consumption (1.15 times higher power consumption, with the exception of the MB SOA-based architecture, which is 2.9 times higher) than SDM architectures, as they operate in the C+L+S bands, unlike SDM architectures which only operate in the C band, where cost and power consumption of the components is lower.

In the third chapter, we studied MBoSDM architectures and, as with MB and SDM architectures, granularity, number of components, dimensions, costs, power consumption and throughput have been analysed. We have studied five MBoSDM architectures operating in the C+L+S bands: the Baseline architecture, the architecture with one S-OXC per band, the architecture with a single S-OXC, the architecture without an S-OXC and the FLEX-SCALE architecture. We concluded that the MBoSDM Baseline architecture is the most expensive architecture, once again due to the number and cost of the transponders. This is due to the fact that in the Baseline MBoSDM architecture, all switching is performed in the WXCs at the wavelength level, which demand more transponders, whereas in the other MBoSDM architectures, some of the signals are switched in the spatial OXC, resulting in fewer transponders and lower cost. We also concluded that the FLEX-SCALE

architecture is the one with significantly lower costs. This can be explained by noting that the FLEX-SCALE architecture, unlike other architectures, has A/D capacity at the wavelength level and also at the band level, due to the new component used in this architecture, the WBSS, hence requiring much less transponders than the other architectures. As band transceiver cost is similar to the transponder cost, the FLEX-SCALE has a considerable cost advantage (approximately 11 times less expensive than the other MBoSDM architectures, and about 22.5 times less expensive than the MBoSDM Baseline architecture). Regarding power consumption, we conclude that all architectures have similar power consumption, with the exception of the MBoSDM Baseline architecture, which is the architecture that consumes the most, once again due to the transponders power consumption. We also concluded that as the number of directions increases, the FLEX-SCALE architecture consumes less power than the other architectures, as the WSSs in this architecture do not have as large dimensions as the WSSs in the other architectures.

In the fourth chapter, we have selected some of the architectures that we consider to have advantages in terms of cost, power consumption, granularity and flexibility within the MB, SDM and MBoSDM types: SDM Space, SDM Space-wavelength, MB Baseline, MB Common band, MBoSDM Baseline, MBoSDM architecture with a single S-OXC and MBoSDM FLEX-SCALE. In this chapter, we compare these architectures in terms of cost per bit and power consumption per bit for two bandwidth scenarios: 16 THz and 32 THz. Regarding the cost per bit, we concluded that the FLEX-SCALE architecture is the least expensive architecture due to the fact that it uses band transceivers and therefore requires fewer transponders. We also concluded that MB architectures are the most expensive due to the fact that they use the three bands. In general, for both bandwidth scenarios, the A/D represents the largest percentage of the total cost of all architectures. Regarding power consumption per bit, we concluded that the MBoSDM architecture with a single S-OXC is the architecture with the lowest consumption. The MB architectures are the architectures with the highest power consumption, while the SDM architectures consume less.

5.2. Future work

In this section, several proposals for future work are presented:

- Include the FLEX-SCALE architecture in a network planning tool and compare the performance of the FLEX-SCALE architecture with the performance of the MBoSDM Baseline architecture.

- Study different A/D structures, different from the one studied in this dissertation - CD per spatial channel - with the goal of reducing the cost of MBoSDM ROADM nodes.

- Perform a quantitative analysis of the architectures studied in this dissertation in in terms of switching capacity, i.e. the total number of possible connection states that a MBoSDM ROADM node can handle in an optical network including the routing of wavelengths for each spatial channel and the ability to add or drop channels, as was done in [53] for SDM ROADM nodes.

- Study MBoSDM node architectures with core selective switches, that switch cores in the same way as WSSs switch wavelengths [54].

[This page is intentionally left blank.]

References

[1] W. Klaus, P. Winzer, and K. Nakajima, "The role of parallelism in the evolution of optical fiber communication systems," *Proceedings of the IEEE*, vol. 110, no. 11, pp. 1619–1654, 2022.

[2] P. Winzer and D. Neilson, "From scaling disparities to integrated parallelism: A decathlon for a decade," *Journal of Lightwave Technology*, vol. 35, no. 5, pp. 1099–1115, 2017.

[3] N. Deng, L. Zong, H. Jiang, Y. Duan, and K. Zhang, "Challenges and enabling technologies for multi-band WDM optical networks," *Journal of Lightwave Technology*, vol. 40, no. 11, pp. 3385–3394, 2022.

[4] D. Uzunidis, E. Kosmatos, C. Matrakidis, A. Stavdas, and A. Lord, "Strategies for upgrading an operator's backbone network beyond the C-band: Towards multi-band optical networks," *IEEE Photonics Journal*, vol. 13, no. 2, pp. 3385–3394, 2021.

[5] M. Cantono, R. Schmogrow, M. Newland, V. Vusirikala, and T. Hofmeister, "Opportunities and challenges of C+L transmission systems," *Journal of Lightwave Technology*, vol. 38, no. 5, pp. 1050–1060, 2019.

[6] M. Mehrabi, H. Beyranvand, and M. J. Emadi, "Multi-band elastic optical networks: Inter-channel stimulated Raman scattering-aware routing, modulation level and spectrum assignment," *Journal of Lightwave Technology*, vol. 39, no. 11, pp. 3360–3370, 2021.

[7] D. Marom and M. Blau, "Switching solutions for WDM-SDM optical networks," *IEEE Communications Magazine*, vol. 53, no. 2, pp. 60–68, 2015.

[8] T. Hayashi, "Multi-core fiber technology from design to deployment," *2022 European Conference on Optical Communication (ECOC)*, Basel, Switzerland, paper Mo4D.1, September 2022.

[9] T. Mori, Y. Yamada, K. Shibahara, T. Matsui, M. Kikuchi, and Y. Sagae, "Applicability of standard cladding diameter multi-core fiber cables for terrestrial field," *Journal of Lightwave Technology*, vol. 42, no. 3, pp. 1044–1055, 2024.

[10] B. Pinheiro, J. Rebola, and A. Cartaxo, "Analysis of inter-core crosstalk in weakly-coupled multi-core fiber coherent systems," *Journal of Lightwave Technology*, vol. 39, no. 1, pp. 42–54, 2021.

[11] D. Marom, P. Colbourne, A. D´Érrico, N. Fontaine, Y. Ikuma, R. Proietti, L. Zong, J. Rivas-Moscoso, and I. Tomkos, "Survey of photonic switching architectures and technologies in support of spatially and spectrally flexible optical networking," *Journal of Optical Communications and Networking*, vol. 9, no. 1, pp. 1–26, 2017.

[12] J. Ravipudi and M. Brandt-Pearce, "Machine-learning-based impairment-aware dynamic RMSCA in multi-core elastic optical networks," *Journal of Optical Communications and Networking*, vol. 16, no. 10, F26–F39, 2024.

[13] B. Puttnam, R. Luis, I. Phillips, M. Tan, A. Donodin, and D. Pratiwi, "402 tb/s GMI data-rate O,E,S,C,L,U-band transmission," *2024 Optical Fiber Communications Conference and Exhibition (OFC)*, San Diego, CA, USA, paper Th4A–3, March 2024.

[14] A. Souza, N. Costa, L. Nadal, R. Casellas, A. Melgar, J. Rivas-Moscoso, M. Quagliotti, E. Riccardi, A. Napoli, and J. Pedro, "Node architectures for high-capacity multi-band over space division multiplexed (MBoSDM) optical networks," *24th International Conference on Transparent Optical Networks (ICTON)*, Bari, Italy, July 2024.

[15] D. Marom, Y. Miyamoto, D. Neilson, and I. Tomkos, "Optical switching in future fiber-optic networks utilizing spectral and spatial degrees of freedom," *Proceedings of the IEEE*, vol. 110, no. 11, pp. 1835–1852, 2022.

[16] H. Kawahara, M. Nakagawa, T. Seki, and T. Miyamura, "Experimental demonstration of wavelength-selective band/direction-switchable multi-band OXC using an inter-band all-optical wavelength converter," *European Conference on Optical Communication (ECOC)*, Brussels, Belgium, December 2020.

[17] M. Nakagawa, H. Kawahara, T. Seki, and T. Miyamura, "Adaptive link-by-link band allocation: A novel adaptation scheme in multi-band optical networks," *International Conference on Optical Network Design and Modeling (ONDM)*, Gothenburg, Sweden, June 2021.

[18] M. Nakagawa, T. Seki, and T. Miyamura, "Techno-economic potential of wavelength-selective band-switchable OXC in S+C+L band optical networks," *Optical Fiber Communications Conference and Exhibition (OFC)*, San Diego, CA, USA, paper W2A.24, March 2022.

[19] S. Yamamoto, H. Taniguchi, Y. Kisaka, S. Camatel, Y. Ma, D. Ogawa, K. Hadama, M. Fukutoku, T. Goh, and K. Suzuki, "First demonstration of a C+L band CDC-ROADM with a simple node configuration using multiband switching devices," *Optics Express*, vol. 29, no. 22, pp. 36 353–36 365, 2021.

[20] N. Deng, L. Zong, H. Jiang, Y. Duan, and K. Zhang, "Challenges and enabling technologies for multi-band WDM optical networks," *Journal of Lightwave Technology*, vol. 40, no. 11, pp. 3385–3394, 2022.

[21] S. Xia, Z. Hu, M. Rombouts, H. Santana, Y. Wang, and A. Zali, "Photonic WDM switches architecture for multi-band optical networks," *Journal of Optical Communications and Networking*, vol. 16, no. 8, pp. D18–D28, 2024.

[22] D. Sequeira, L. Cancela, and J. Rebola, "CDC ROADM design tradeoffs due to physical layer impairments in optical networks," *Optical Fiber Technology*, vol. 62, id. 102 461, 2021.

[23] M. Filer and S. Tibuleac, "N-degree ROADM architecture comparison: Broadcast-and-select versus route-and-select in 120 Gb/s DP-QPSK transmission systems," *Optical Fiber Communications Conference and Exhibition (OFC)*, San Francisco, CA, USA, paper Th1I.2, March 2014.

[24] Y. Li, J. Lin, L. Zong, S. K. Bose, B. Mukherjee, and G. Shen, "Colorless, partially directionless, and contentionless architecture for high-degree ROADMs," *Journal of Optical Communications and Networking*, vol. 14, no. 6, pp. 481–492, 2022.

[25] R. Shankar, M. Florjanczyk, T. Hall, A. Vukovic, and H. Hua, "Multi-degree roadm based on wavelength selective switches: Architectures and scalability," *Optics Communications*, vol. 279, no. 1, pp. 94–100, 2007.

[26] B. Collings, "Advanced ROADM technologies and architectures," *2015 Optical Fiber Communications Conference and Exhibition (OFC)*, Los Angeles, CA, USA, paper Tu3D.3, March 2015.

[27] A. Anchal and D. Marom, "Practical SDM-ROADM designs for uncoupled spatial channels and their switching capacity," *Optical Fiber Communications Conference and Exhibition (OFC)*, San Diego, CA, USA, paper M1A.4, March 2019.

[28] F. Australia, "Flexgrid C+L-band twin 65-port WSS honored by 2025 lightwave BTR innovation reviews," *GlobeNewswire*, March 2025. [Online]. Available: `https://finisarwss.com/`.

[29] I.-T. R. G., "Spectral grids for WDM applications: DWDM frequency grid," *Telecommunication Standardization Sector of ITU*, October 2020.

[30] J. Fabrega, R. Munoz, D. Marom, J. Rivas-Moscoco, M. Enrico, and L. Poti, "Flex-scale: A disruptive approach toward flexibly scalable energy efficient networking," *IEEE Communications Magazine*, vol. 63, no. 9, pp. 86–93, April 2025.

[31] T. Zami, "High degree optical cross-connect based on multicast switch," *Optical Fiber Communications Conference and Exhibition (OFC)*, San Francisco, CA, USA, paper W2A.36, March 2014.

[32] OMCH, "Fiber optic amplifier," January 2023. [Online]. Available: `https://www.rp-photonics.com/fiber_amplifiers.html`.

[33] T. Ye and K. Chen, "Modular WSS-based oxcs for large-scale optical networks," *Journal of Optical Communications and Networking*, vol. 2005, no. 12751, pp. 1–8, 2020.

[34] D. Soma, S. Beppu, Y. Wakayama, S. Sumita, H. Takahashi, N. Yoshikane, I. Morita, T. Tsuritani, and M. Suzuki, "Trans-pacific class transmission over a standard cladding ultralow-loss 4-core fiber," *Optics Express*, vol. 30, no. 6, pp. 9482–9493, March 2022.

[35] R. Yang, L. Liu, S. Yan, and D. Simeonidou, "A programmable ROADM system for SDM/WDM networks," *Applied Sciences*, vol. 11, no. 9, May 2021.

[36] A. Ribeiro, "Cost-effective ROADM architectures for SDM optical networks," *MSc Dissertation in Telecommunications and Computer Engineering*, ISCTE- Instituto Universitário de Lisboa (Iscte–IUL), October 2024.

[37] T. Kuno, Y. Mori, S. Subramaniam, M. Jinno, and H. Hasegawa, "Design and evaluation of a reconfigurable optical add-drop multiplexer with flexible wave-band routing in SDM networks," *Journal of Optical Communications and Networking*, vol. 14, no. 4, pp. 248–256, 2022.

[38] M. Silva, L. Cancela, and J. Rebola, "Cost, power consumption and performance analysis in SDM ROADM architectures for uncoupled spatial channels," *2022 13th International Symposium on Communication Systems, Networks and Digital Signal Processing (CSNDSP)*, Porto, Portugal, July 2022.

[39] S. Sakurai, K. Higashimori, and T. Ohara, "Cost-efficient SDM/BDM network planning based on hierarchical optical cross-connects," *2025 International Conference on Optical Network Design and Modeling (ONDM)*, Pisa, Italy, May 2025.

[40] M. Jinno, "Spatial channel network (SCN): Opportunities and challenges of introducing spatial bypass toward the massive sdm era [invited]," *Journal of Optical Communications and Networking*, vol. 11, no. 3, pp. 1–4, March 2019.

[41] J. O'Ramos, "ROADM architectures for multi-band optical networks," *MSc Dissertation in Telecommunications and Computer Engineering*, ISCTE- Instituto Universitário de Lisboa (Iscte–IUL), 2023.

[42] R. Guerreiro, "GNPy-based planning tool for survivable multi-band optical networks," *MSc Dissertation in Telecommunications and Computer Engineering*, ISCTE-Instituto Universitário de Lisboa (Iscte–IUL), 2024.

[43] ZTE, "Optical cross-connect technology and application," November 2022. [Online]. Available: `https://www.zte.com.cn/global/about/magazine/zte-technologies/2022/6-en/special-topic--intelligent-e-otn/5.html`.

[44] P. Hazarika, H. Buglia, M. Jarmolovičius, E. Sillekens, M. Tan, and A. Donodin, "Multi-band transmission over E-, S-, C- and L-Band with a hybrid raman amplifier," *Journal of Lightwave Technology*, vol. 42, no. 4, pp. 1215–1224, February 2024.

[45] Fibermart, "Semiconductor optical amplifier butterfly package 1550nm 23db gain," February 2025. [Online]. Available: `https://www.fiber-mart.com/`.

[46] M. Radovic, A. Sgambelluri, F. Cugini, and N. Sambo, "Power-aware high-capacity elastic optical networks," *Journal of Optical Communications and Networking*, vol. 16, no. 5, B16–B25, May 2024.

[47] D. Marom, H. Georgopoulos, M. Enrico, A. Blanco, C. Roeloffzen, C. Pineda, B. Saavedra, and S. Ben-Ezra, "Design of multi-granular SDM/UWB optical switch node," *FLEX-SCALE Project Deliverable D3.1, Horizon-JTI-SNS-2022, Grant Agreement*, no. 101096909, May 2023.

[48] C. Papapavlou, K. Moschopoulos, C. Christofidis, D. Uzunidis, K. Paximadis, and D. Marom, "Forthcoming optical x-haul infrastructure supporting 6G mobile network

requirements," *Journal of Optical Communications and Networking*, vol. 17, no. 11, E82–E93, November 2025.

[49] H. Hasegawa, S. Subramaniam, and K. Sato, "Node architecture and design of flexible waveband routing optical networks," *Journal of Optical Communications and Networking*, vol. 8, no. 10, pp. 734–744, October 2016.

[50] R. Jana, A. Mitra, A. Pradhan, K. Grattan, A. Srivastava, and B. Mukherjee, "When is operation over C+L bands more economical than multifiber for capacity upgrade of an optical backbone network?" *2020 European Conference on Optical Communications (ECOC)*, Brussels, Belgium, December 2020.

[51] C. Papapavlou, K. Paximadis, B. Gomez, D. Marom, and I. Tomkos, "Performance analysis of an UWB/SDM optical network node with PIC-based flexible waveband-selective switches," *Conference on Lasers and Electro-Optics, CLEO*, Charlotte, United States, paper SF1L.4, May 2024.

[52] C. Papapavlou, K. Paximadis, D. Marom, and I. Tomkos, "Design and performance insights in backbone node upgrades: From single-band WSS to UWB-based flex-WBSS solutions," *Telecom 2025*, vol. 6, no. 93, December 2025.

[53] A. Anchal and D. Marom, "Impact of joint and independent switching paradigms on switching capacity of contention/-less SDM-ROADM designs," *Journal of Lightwave Technology*, vol. 42, no. 9, pp. 3081–3098, January 2024.

[54] M. Jinno, R. Otowa, Y. Matsuno, D. Soma, R. Sasaki, Y. Hotta, T. Sasaki, K. Komatsu, T. Izumi, K. Maeda, S. Beppu, K. Nakada, S. Takasaka, Y. Wakayama, R. Tahara, N. Yoshikane, T. Tani, Y. Sakurai, R. Sugizaki, and T. Tsuritani, "Spatial channel network (SCN): Implementation and feasibility demonstrations of modular spatial cross-connects using three types of packaged 19-core-fiber-based optical switches," *Journal of Optical Communications and Networking*, vol. 18, no. 7, pp. C1–C12, July 2026.

[This page is intentionally left blank.]

APPENDIX A

Validation of the parameters used in the FLEX-SCALE architecture

This appendix details the computation of the number of components and number of ports used to build the FLEX-SCALE architecture presented in Table 3.1 for three values of D (2, 3, 4) and M=4. The validation of these results is performed with the results reported in [47], [48].

The number of B_{TRxs}, considering $WBSS_{A/D} = 1$, is calculated with [47], [48],

$$N_{BTXs} = N_{BRXs} = 1/4 \times M \times D \tag{A.1}$$

whereas for $WBSS_{A/D} = 2$, is calculated with,

$$N_{BTXs} = N_{BRXs} = 1/2 \times M \times D \tag{A.2}$$

The number of WBSSs, N_{WBSS}, and their port count, P_{WBSS}, are computed with,

$$N_{WBSS} = 2 \times M \times D \tag{A.3}$$

$$P_{WBSS} = M \times (D-1) + WBSS_{A/D} + 1 \tag{A.4}$$

The port count of the inter OXC, $P_{OXC_{INTER}}$, and the port count of the intra OXCs, $P_{OXC_{INTRA_b}}$, are given by,

$$P_{OXC_{INTER}} = [(M \times D \times WBSS_{A/D}) + N_{B_{Tx}} + K_{WSS}] + [(M \times D \times WBSS_{A/D}) + N_{B_{Rx}} + K_{WSS}] \tag{A.5}$$

$$P_{OXC_{INTRA_b}} = 2 \times [(1 + K_{b_{legacy}}) \times N_{WSS_b} \times P_{WSS_b}] \tag{A.6}$$

To calculate the port count of the OXCs, we consider that $K_{b_{legacy}} = 20\%$, $K_C = 0.35$, $K_S = 0.15$, $K_L = 0.25$, $K_{WSS} = N_{WSS_C} + N_{WSS_L} + N_{WSS_S}$, the port count of the WSSs, P_{WSS_b}, is 10 and the number of WSSs per band, N_{WSS_b}, (with b=C, L, S) is given by,

$$N_{WSS_b} = 2 \times K_b \times M \times D \times WBSS_{A/D} \tag{A.7}$$

Table A.1 shows the components dimension for the FLEX-SCALE architecture considering D=2, 3, 5, M=4 and $WBSS_{A/D} = 1$, using the equations described above. Table A.2 shows the same, but for $WBSS_{A/D} = 2$. We have added a column with the values taken from [47] for D=3 and M=4 in Table A.1 and a column with the values taken from [48] for D=5 and M=4 in Table A.2. We observe in Table A.1 that the values taken from [47], for D=3 and M=4, are in agreement with our results. Nevertheless, in Table A.2 the values obtained from [48], for D=5 and M=4, are different, in particular $P_{OXC_{INTER}} = 130$, (we use $P_{OXC_{INTER}} = 220$), and for C-band $P_{OXC_{INTRA_C}} = 720$, (we

use $P_{OXC_{INTRA_C}} = 672$). In [48] the values for K_b are not given and are not the same ones used in [47]. This variable influences K_{WSS} and N_{WSS_b}, which are needed for calculating $P_{OXC_{INTER}}$ and $P_{OXC_{INTRA_b}}$.

TABLE A.1. Component dimensions for the FLEX-SCALE architecture considering D=2, 3, 5, M=4 and $WBSS_{A/D} = 1$.

Port count and number of components	$D = 2$	$D = 3$	$D = 5$	$D = 3$ [47]
P_{WBSS}	6	10	18	10
$N_{BTXs} = N_{BRXs}$	2	3	5	-
$P_{OXC_{INTER}}$	46	68	110	68
N_{WSS_C}	6	9	14	-
N_{WSS_S}	3	4	6	-
N_{WSS_L}	4	6	10	-
K_{WSS}	13	19	30	-
$P_{OXC_{INTRA_C}}$	144	216	336	-
$P_{OXC_{INTRA_S}}$	72	96	144	-
$P_{OXC_{INTRA_L}}$	96	144	240	-

TABLE A.2. Component dimensions for the FLEX-SCALE architecture considering D=2, 3, 5, M=4 and $WBSS_{A/D} = 2$.

Port count and number of components	$D = 2$	$D = 3$	$D = 5$	$D = 5$ [48]
P_{WBSS}	7	11	19	19
$N_{BTXs} = N_{BRXs}$	4	6	10	-
$P_{OXC_{INTER}}$	90	134	220	130
N_{WSS_C}	12	17	28	40
N_{WSS_S}	5	8	12	-
N_{WSS_L}	8	12	20	-
K_{WSS}	25	37	60	-
$P_{OXC_{INTRA_C}}$	288	408	672	720
$P_{OXC_{INTRA_S}}$	120	192	288	-
$P_{OXC_{INTRA_L}}$	192	288	480	-

APPENDIX B

Validation of the network throughput computation for the FLEX-SCALE architecture

To calculate the network throughput, as in [47], [48], a 21 THz bandwidth (BW) (C+L+S band) with a spectral efficiency (SE) of 10 b/s/Hz is used (assuming 64 QAM signals, a channel bandwidth of 150 GHz, a symbol rate of 128 GBaud, so that the $SE = 2 \times 128 \times 6/150 \cong 10$ b/s/Hz). The throughput depends on M and D as follows,

$$Thr_{Node} = M \times D \times BW \times SE \tag{B.1}$$

Figure B.1 shows the node throughput for FLEX-SCALE Layer 1 as a function of D, considering M=2, 4 and 8. For D=4 and M=4 we obtain 3.36 Pbps, whereas for D=5 and M=8 a 8.4 Pbps throughput is obtained. In [48], for D=4 and M=4, a higher throughput is obtained (1.125 times higher, 3.76 Pbps = 3.36×1.125), as well as for D=5 and M=8 (1.125 times higher, 9.4 Pbps = 8.4×1.125).

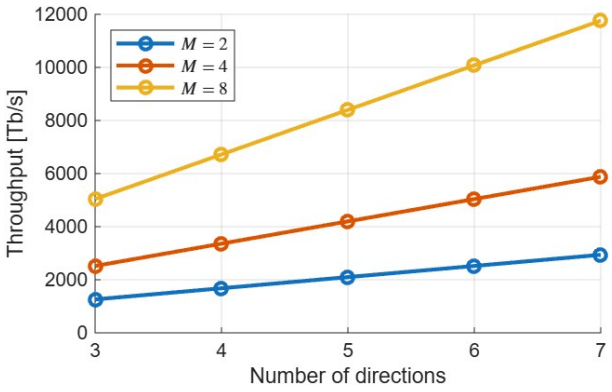


FIGURE B.1. Node throughput for FLEX-SCALE Layer 1 as a function of D, considering M=2, 4, 8.

[This page is intentionally left blank.]

APPENDIX C

Implementation details of large-scale WSSs for MBoSDM architectures

This appendix details the implementation of large-scale WSSs in MBoSDM architectures. Figure C.1 shows the implementation of a WXC in the MBoSDM Baseline architecture considering $M = 4$ and $D = 3$. The A/D is composed of two WSSs 12×209 ($209 = 87 \times 12 \times 0.2$). Figures C.2 to C.4 show the MBoSDM architecture with a S-OXC per band considering $M = 4$, $D = 3$ with $N_C = 0$ (Figure C.2), $N_C = 6$ (Figure C.3) and $N_C = 12$ (Figure C.4). For $N_C = 0$, the A/D is composed of two WSSs 12×209, for $N_C = 6$, the A/D structure is composed of two WSSs 6×105 ($105 = 87 \times 6 \times 0.2$) and finally, for $N_C = 12$, the A/D is composed of two WSSs 1×18 ($18 = 87 \times 0.2$). Figures C.1 to C.4 show only the WSS and A/D structure for the C-band, since for the S and L bands, the A/D structure is implemented in the same way.

Figure C.5 shows the express structure cost for all studied MBoSDM architectures with $D = 3$, $D = 5$ and $D = 7$, considering $M = 4$ and $N_C = 0$. From Figure C.5, we can conclude that, unlike what happened for $N_C = 6$, where the Baseline architecture always had a higher cost, here we see that when D increases, the architectures shown in Figures 3.3 and 3.5 have costs as high as the Baseline architecture. The architecture represented in Figure 3.4 continues to have lower costs than the others, since this architecture has a single MB WXC, which reduces costs. The FLEX-SCALE architecture continues to be the architecture with the lowest costs.

Figure C.6 shows the A/D structure cost for all studied MBoSDM architectures with $D = 3$, $D = 5$ and $D = 7$, considering $M = 4$ and $N_C = 0$. From Figure C.6, we can see that, once again, unlike what happened with $N_C = 6$, where the Baseline architecture had a higher A/D structure cost, this doesn't happen for $N_C = 0$. In this case, all architectures have the same number of transponders and, therefore, the same A/D structure cost, with the exception, once again, of the FLEX-SCALE architecture, which has a lower cost.

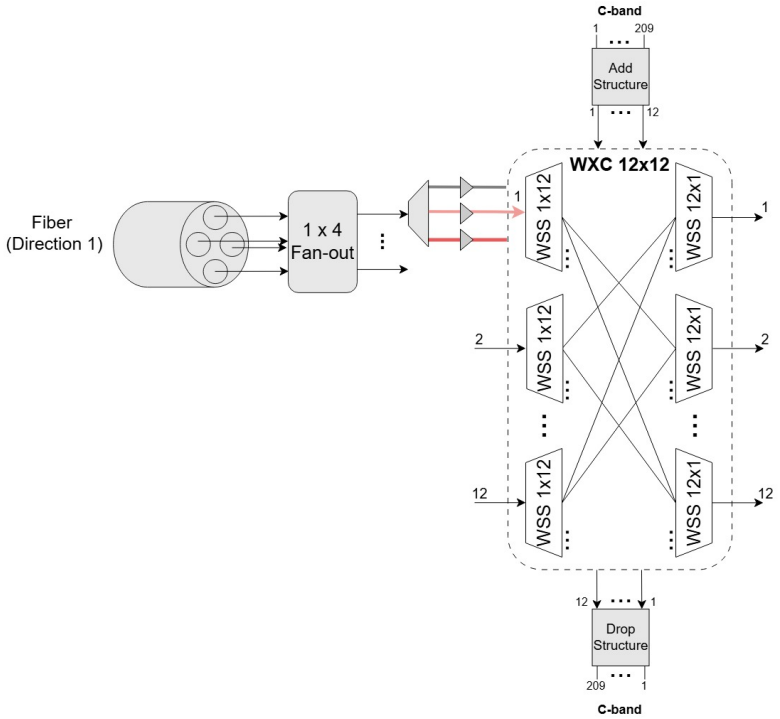


FIGURE C.1. MBoSDM Baseline architecture considering $M = 4$, $D = 3$.

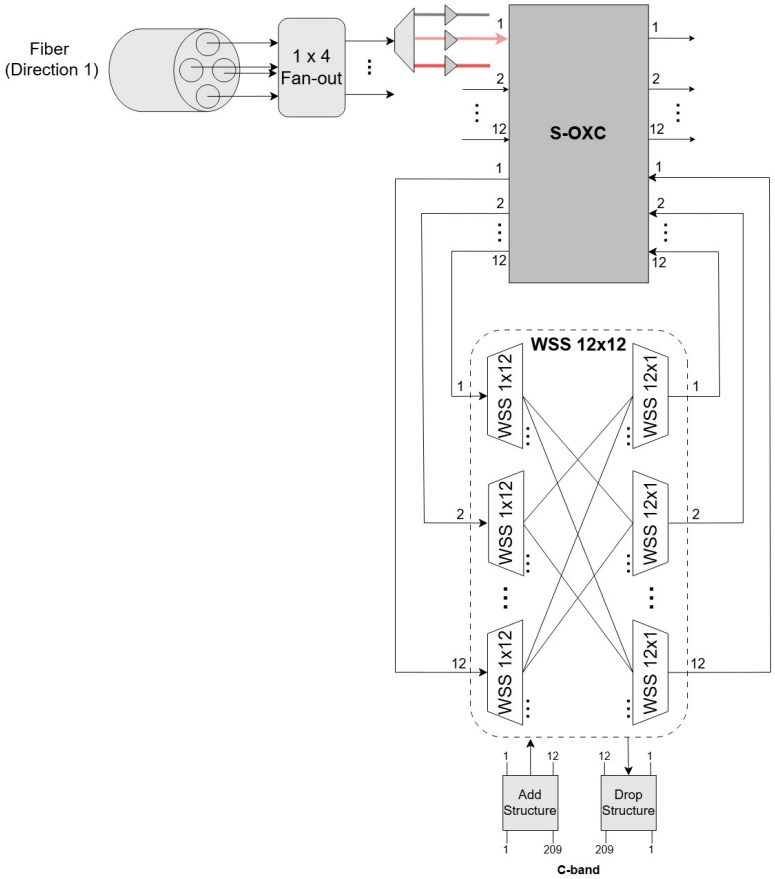


FIGURE C.2. MBoSDM architecture with a S-OXC per band considering $M = 4$, $D = 3$ and $N_C = 0$.

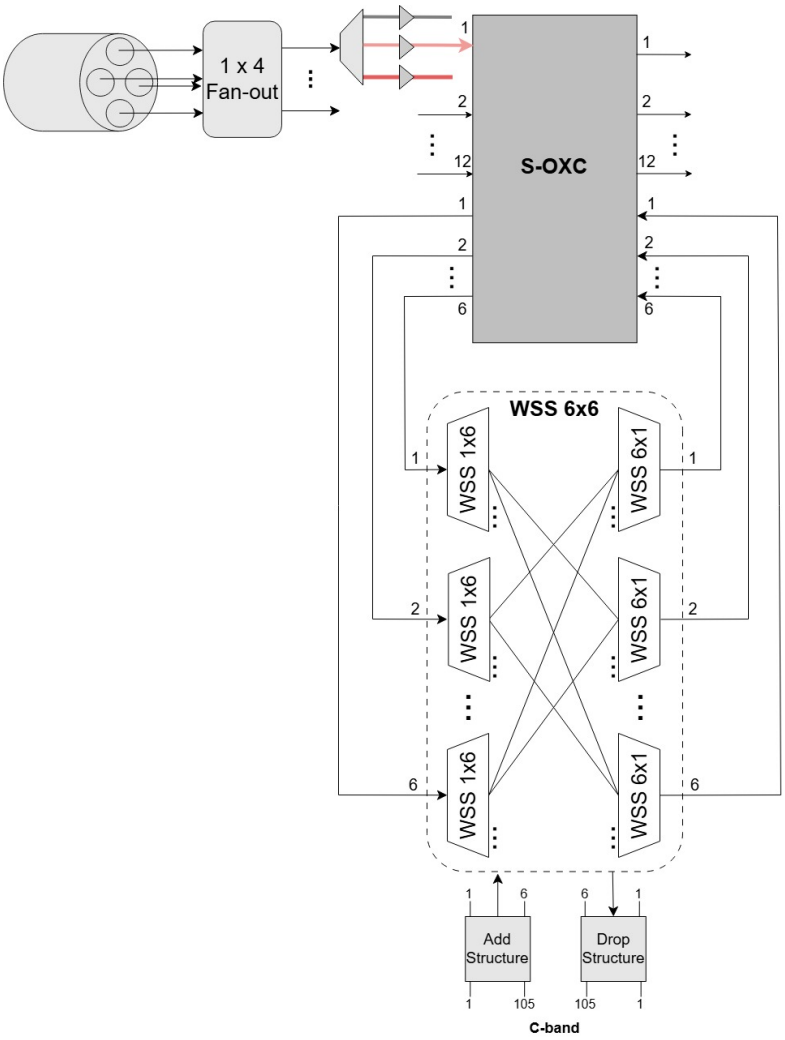


FIGURE C.3. MBoSDM architecture with a S-OXC per band considering $M = 4$, $D = 3$ and $N_C = 6$.

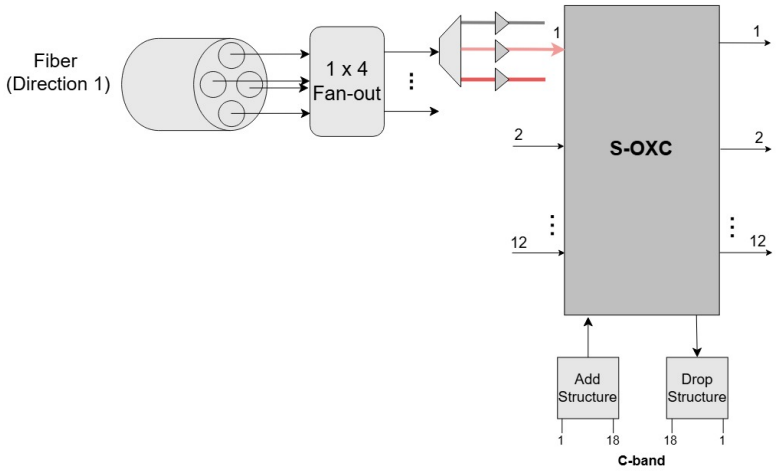


FIGURE C.4. MBoSDM architecture with a S-OXC per band considering $M = 4$, $D = 3$ and $N_C = 12$.

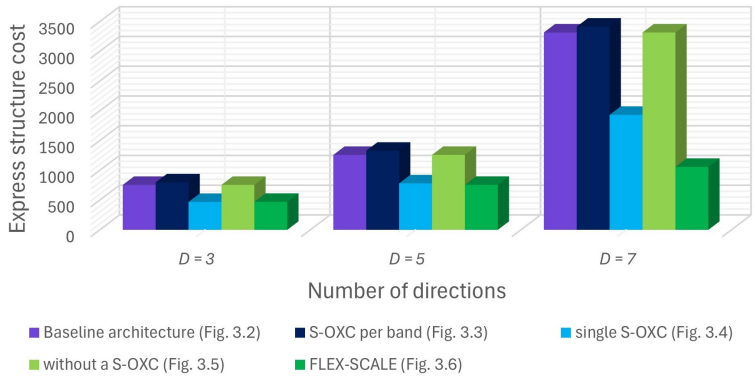


FIGURE C.5. Express structure cost for all studied MBoSDM architectures with $D = 3$, $D = 5$ and $D = 7$, considering $M = 4$ and $N_C = 0$.

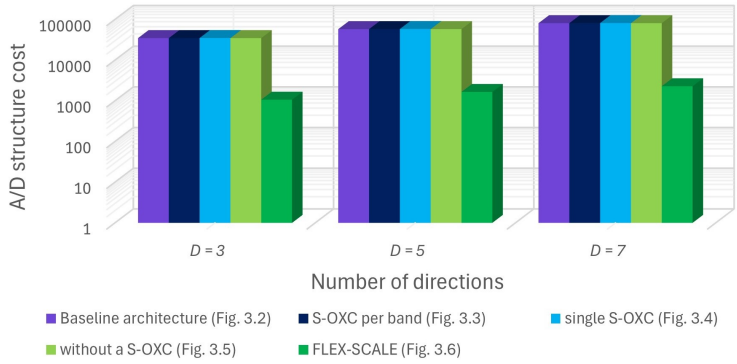


FIGURE C.6. A/D structure cost for all studied MBoSDM architectures with $D = 3$, $D = 5$ and $D = 7$, considering $M = 4$ and $N_C = 0$.